Ion Channel Photoswitch Reveals Crosstalk between Intact and Injured Nociceptive Neurons after Nerve Injury

by
Christian Herold

A dissertation submitted in partial satisfaction of the
requirements for the degree of
Doctor of Philosophy
in

Biophysics

in the
Graduate Division
of the University of California, Berkeley

Committee in Charge:

Professor Dr. Richard H. Kramer, Chair
Professor Dr. Ehud Y. Isacoff
Professor Dr. Daniel E. Feldman
Professor Dr. Diana M. Bautista

Fall 2015

Abstract

Ion Channel Photoswitch Reveals Crosstalk between Intact and Injured Nociceptive Neurons after Nerve Injury

by
Christian Herold

Doctor in Physiology in Biophysics
University of California, Berkeley
Professor Richard H. Kramer, Chair

The development of novel techniques utilizing the advantages of light has created an optical revolution for neuroscience research. Controlling and probing neuronal function with light has provided unprecedented insights by being able to manipulate many neurons simultaneously in intact circuits and living organisms.

In my dissertation research, I used novel optical methods to probe the cellular permeability of sensory neuron populations. Primary nociceptive afferents detect, modulate and integrate many pain-related stimuli. Sensory information is transmitted from the periphery through the dorsal root ganglia along labeled lines coding for sensory modalities and receptive fields. Recently, our understanding of sensory processing has been expanded by the discovery of neuronal interactions both on the level of peripheral nerve endings and in the spinal cord. Here I report a crosstalk between injured and intact neuronal population after peripheral nerve injury. This communication is revealed at the somata of sensory neurons distant from the site of injury and correlates with permeability changes of both injured and intact nociceptor populations after injury. I devised a sensitive probe to measure the activity of nociceptive cells in intact tissue using a photoswitch molecule. Transient Receptor Potential (TRP) ion channel are a major class of molecular sensors detecting painful stimuli. I show that TRPA1, a member of the TRP family, is necessary for this crosstalk which is limited to petidergic, slow conducting C fibers. In addition, electrical activity of nociceptive fibers alone is sufficient to mimic similar permeability changes as nerve injury. Injury induced hyperexcitability of sensory fibers and TRP channel dysfunction have been implicated with conditions of pain hypersensitivity, chronic and neuropathic pain. I therefore propose that this crosstalk might contribute to adaptions of pain signaling in various disease states.

Photoswitch molecules have found many experimental applications in neuroscience research. However, the exact mechanism by which they function remains unclear. Therefore, another part of my research focused on studying interactions of the photoswitchable compound QAQ with the model potassium channel Shaker. I investigated the affinity of both QAQ isomers to the open Shaker channel and surprisingly found that block is not voltage-dependent. Further, I analyzed the effects of use-dependent inhibition and report that QAQ does not associate with closed channels. However, once channels are opened, QAQ does interfere with the kinetics of the gate slowing down the closing of the channel.

To my family.

I. Contents

Table of Figures

List of Tables

Table of Abbreviations

a.u.	Arbitrary units
AAQ	Acrylamine-Azobenzene-Quaternary Ammonium
ACSF	Artificial cerebrospinal fluid solution
AITC	Allyl isothiocyanate
AP-18	4-(4-Chlorophenyl)-3-methyl-3-buten-2-one oxime
ATF3	Activating transcription factor 3
ATP	Adenosine triphosphate
BCTC	N-(4-tertiarybutylphenyl)-4(3-cholorphyridin-2-yl)-tetrahydro-pyrazine1(2H)-carboxamide
BSA	Bovine serum albumine
bzATP	2‘(3‘)-O-(4-Benzoylbenzoyl) adenosine-5‘-triphosphate
CAP	Compound action potential
CFA	Complete Freud‘s Adjuvant
CGRP	Calcitonin-gene-related peptide
DAPI	4‘,6-Diamidin-2-phenylindol
DENAQ	Diethyl-Azobenzene-Quaternary Ammonium
DMA	5-(N,N-Dimethyl) amiloride
DMSO	Dimethyl sulfoxide
DRG	Dorsal root ganglia
EGTA	Ethylene glycol tetraacetic acid
EtOH	Ethanol
HEPES	4-(2-hydroxyethyl)-1-piperazineethanesulfonic acid
IB4	Isolectin-B4
IC50	Half maximal inhibitory concentration
IL	Interleukin
K_V	Voltage-gated potassium channel
L	Lumbar
MW	Molecular weight
N.A.	Numerical Aperture
NGS	Normal goat serum

NTP ..... Nucleoside triphosphate
OCT ..... Optimal Cutting Temperature compound
ORI ..... Oocyte Ringer Solution
P_2X ..... Ionotropic purinergic receptor
PBS ..... Phosphate buffered saline
PCL ..... Photochromic ligand
PFA ..... Paraformaldehyde
PI ..... Photoswitching Index
PKC ..... Protein Kinase C
PTL ..... Photochromic tethered ligand
QA ..... Quaternary ammonium
QAQ ..... Quaternary Ammonium-Azobenzene-Quaternary Ammonium
QENAQ ..... Quaternary Ammonium-Ethylamine-Azobenzene-Quaternary Ammonium
ROI ..... Region of interest
RTX ..... Resiniferatoxin
s.e.m. ..... Standard error of the mean
SNI ..... Spared Nerve Injury
SNL ..... Sciatic Nerve Ligation
SP ..... Substance P
TEA ..... Tetraethylammonium
TFA ..... Trifluoroacetic acid
TNF ..... Tumor necrosis factor
TNP-ATP ..... 2‘, 3‘-O-(2,4,6-Trinitrophenyl) adenosine 5‘-triphosphate
TRP ..... Transient Potential Receptor
TRPA1 ..... Ankyrin Transient Receptor Potential Channel 1
TRPV1 ..... Vanilloid Transient Receptor Potential Channel 1
UV ..... Ultraviolet

Acknowledgment

This dissertation would not have been possible without the generous support and advice of my mentor Dr. Richard Kramer. I want to express my special thanks to him for taking me on in his laboratory and for granting me the academic freedom to venture into an intriguing project. I could follow my scientific interests and the results of this exploration culminated in this work.

I further would like to extend my thank you to all members of the Kramer laboratory for their friendly help, insightful discussions and technical assistance throughout all of my graduate research.

Also, I am very grateful to Dr. Allan Basbaum and his entire lab for a fruitful collaboration, academic mentoring and for introducing me to the exciting field of pain research.

I would like to thank the Howard Hughes Medical Institute for generous financial support of my research project.

Finally and most importantly, I thank my family and friends who encouraged and strengthened me during all the ups and downs along the way. Without their understanding and continued support, this work could not have been completed.

II. Introduction and Background

1. Controlling and Probing Neuronal Function with Light

The amazing capabilities and the vast complexity of mammalian neuronal systems have been a focus of fascination since ancient times when Hippocrates identified the brain as center of intelligence. However, it was not until the late 19^th century when Santiago Ramon y Cajal, the father of modern neuroscience, identified the great variety of building blocks forming the nervous system. Although scientists began to understand the architecture of neuronal circuits, little was known about their function and how sophisticated information was processed to generate all aspects of human intelligence. In the 1950s Hodgkin and Huxley started to reveal the basic components of electrical excitability and complemented by the discovery of chemical neurotransmission by Axelrod, Katz and von Euler, we began to understand the basic underlying mechanisms governing signal transmission and processing in neuronal systems. The emerging scientific field of neurobiology was expanding quickly and the seminal work of Erwin Neher und Bert Sakmann not only highlighted single ion channels as molecular actuators of neuronal processing but also gave neuroscientists a new methodologies to study the nervous system. The patch clamp technique has since become the work horse of modern neuroscience and enabled us to greatly expand our understanding of neuronal signaling. Given the high order complexity of neuronal connections, the vast number of neurons and the even larger number of synaptic connections, invasive electrophysiological recordings are limited in the amount of information they can obtain. Also, electrophysiological techniques are laborious, low-throughput and allow recordings only from a handful of cells at a time.

Advancing technical boundaries, the development and discovery of novel neuroscientific techniques using light as central medium has heralded an optical revolution in neuroscience that transformed the way we study neural circuits and cells.

The utilization of light to control and probe the behavior of neuronal systems or specific proteins like ion channel and receptors entails many advantages. Light intensity can be modulated with very high temporal precision in the femtosecond range and photons can be selectively targeted to subset of cells or even compartments of individual cells with high spatial resolution. Additionally, photons of light carry enough energy to trigger large molecule motions like conformational changes and isomerizations (Fehrentz et al., 2011) [51]. At the same time, modern electronics, cameras, controllers and light sources permit the recording of many optical signals with the same accuracy as light can be controlled itself. The only practical limitations are defined by the physical properties. Spatial precision of light application is confined by diffraction and

scattering phenomena. Light penetration depth is limited by absorption processes when passing through matter. However, light is minimally invasive compared to traditional stimulation and recording techniques and shows minimal artificial side effects when interacting with biological tissue which is sufficiently transparent to achieve sub-μm precision (Wachtveitl and Zumbusch, 2011 [143].

Over the last decade, multiple approaches to use light for control of neuronal function have been developed. The term optogenetics was coined for methods using naturally occurring light sensitive proteins to enable ion transfers across the cell membrane effectively controlling excitability of neurons. Optogenetic tools allow researchers to both activate and inhibit electrical activity of neuronal systems (Fenno et al., 2011; Reiner and Isacoff, 2013) [52][115]. A wide plethora of tools with various properties has been developed for specific applications but heterogeneous expression of those effector proteins in neuronal systems is always required essentially overriding the cell's own ion channel machinery. Optogenetics brought on a revolution for system neuroscience but to understand neuronal circuits on a molecular level other techniques with molecular precision and specificity are needed.

Controlling endogeneous, naturally inherent ion channels and receptors could avoid the issue of overriding existing machinery and instead allow to study the molecular processes that govern cellular excitability. For many decades, classical pharmacology has been providing tools that can manipulate proteins with relatively high selectivity and specificity. However, there are limitations to classical pharmacology that inhibit the discovery of more detailed insights. The application of drugs is generally slow and imprecise as they affect all cells and receptors in a preparation and not only desired target cells. Even technically elaborate local puff perfusions are spatially limited and cannot avoid diffusion of active drugs to adjacent areas. Further, despite enormous efforts to design, screen and test highly specific molecules, this quest is challenging and does not always yield compounds with high selectivity, especially with subunit specific accuracy. Finally, applied drugs remain active in a tissue as long as there are present and wash out might not always be possible or too slow. Classical pharmacology has a slow temporal resolution. Being able to switch molecules from on to off and vice versa with a fast stimulus like light would allow to overcome some of these limitations (Figure 1). In addition, combining light control with genetic targeting allows the selective control of endogenous receptors in a fast, rapidly reversible way to study the functional implication of those receptor in physiological processes (Figure 1).

The building block used for many light sensitive chemicals is an azobenzene group (Figure 2). The geometry of other molecules can modulated in a light dependent way by incorporating an azobenzene that can be photoisomerized from its elongated ground state in *trans* to a bent *cis* isomer. The angle between the two benzyl rings connected by the central nitrogen double bond changes upon isomerization from around 180° to 66° shortening the effective length of the molecule from 9.0Å to 5.5Å. This change in architecture can be used to allow tethered ligands reaching their binding site or sterically enable a molecule to enter the lumen of an ion channel (Figure 2).

An isolated azobenzene group requires near-ultraviolet light (360-395nm) to ultrafast convert azobenzene from its *trans* to a *cis* configuration (Figure 2). Recent advances in chemical

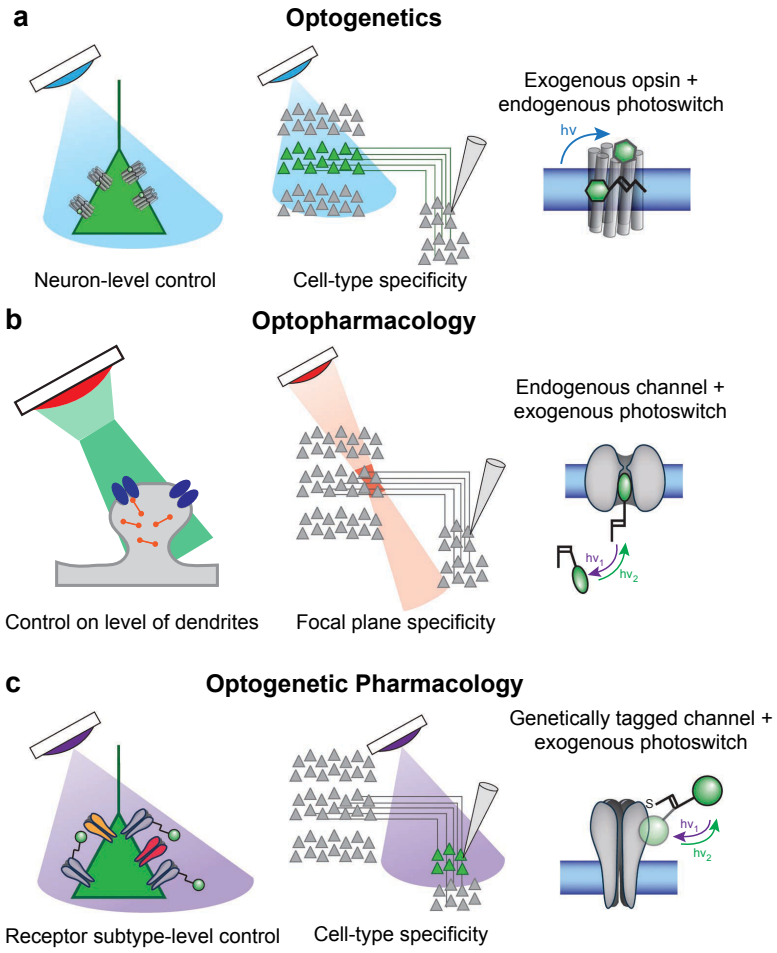

Figure 1.: Different Approaches for the Optical Control of Neuronal Function.
a. Optogenetics means expressing a microbial opsin which can be targeted to cells of choice by genetic means. Those foreign genes incorporate the naturally occurring chromophore retinal to evoke photocurrents across the membrane. Depending on the selectivity of the opsin channel or ion pump, light stimulated neurons become depolarized or hyperpolarized. **b.** In contrast, optopharmacology does not require the expression of external genes but modulates existing, endogenous channels and receptors in a light dependent fashion. **c.** Optogenetic pharmacology combines the advantages of genetic targeting and specific control of selected endogenous receptors in a fast, reversible way.
Adapted from Kramer et al., 2013 [73].

modification modify the electron density of the π electron system to create derivatives which can be operated at longer wavelengths. Return to the *trans* ground state occurs spontaneously by slow thermal relaxation. Back-conversion can be accelerated by illumination with longer wavelengths of light (420-520nm). Under normal light intensity conditions (mW/cm^2), azobenzene is chemically stable, does not photobleach and can be used repeatedly with no impact on function (Kramer et al., 2013) [73]. Phototransitions occur with high quantum yield, are remarkably photostable for isolated azobenzene groups and are little dependent on the local molecular environment (Wachtveitl and Zumbusch, 2011 [143].

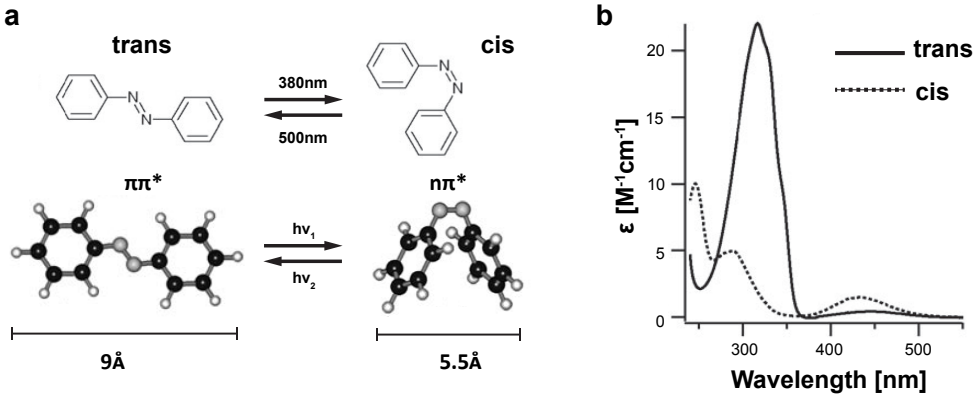

Figure 2.: Chemical Properties of the Azobenzene Group.
a. Chemical structure of the *trans* and *cis* configuration of a azobenzene moiety, two benzyl rings grouped around an azo-nitrogen double bond group. **b.** Absorption spectra of both azobenzene photo isomers.
Adapted from Wachtveitl and Zumbusch, 2011 [143].

Azobenzene based chemistry is also used to control or probe protein function in many other ways (Beharry and Woolley, 2011) [17]. Just to name a few examples, azobenzene switches are used to design light sensitive capsaicin or TRPV1 antagonist derivatives (Stein et al., 2013) [129] or to probe active protein sites with photoswitchable affinity labels (PAL; Harvey and Trauner, 2008) [57].

Besides using light to control neuronal function, other optical methods have been developed that probe electrical or receptor activity. Fluorescent dyes that change their excitation and emission properties when bound to calcium ions have revolutionized how scientists measure neuronal activity of vast neuron ensembles in intact systems and *in vivo*. More recent advances have complemented the tool kit of optical sensors by molecules sensing voltage, neurotransmitter or ionic concentrations.

Taken together, all optical control and detection of neuronal events on both cellular and systems level has dramatically altered modern neuroscience and enabled numerous breakthroughs. As the optical tool kit is constantly being refined and expanded, novel methodologies and sensors allow previously inaccessible systems to be studied and reveal new insights. My dissertation

research employs azobenzene based optical tools to probe and study the activity of specific ion channels and contributes to our understanding how these tools work on a molecular level.

1.1. Photochemical Control of Endogenous Ion Channels

As described in the previous section, photo- or optopharmacology uses light sensitive chemicals to control endogenous ion channels or receptors. This field can be separated into two different approaches: Optogenetic pharmacology permanently links photochromic tethered ligands (PTL) to a genetically engineered protein target. In contrast, photochromic ligands (PCL) do not require genetic manipulation to interact with channels or receptors. PCLs are freely diffusible and therefore less specific. Many PCLs have been designed as open channel blockers.

Optogenetic pharmacology, also sometimes referred to as optochemical genetics (Fehrentz at al., 2012) [50], combines the advantages of fast light switching and precise genetic targeting. This technology provides the means to study the function of native receptors with subunit specificity, cellular precision and temporal accuracy. A point mutation substituting a native amino acid for a cysteine residue close to the intended site of action, e.g. a ligand binding site, chemically attaches the photoswitch compound in the vicinity to that site. For that purpose, a cysteine-reactive group, a maleimide, is engineered to one end of the photoswitch and this maleimide is used to permanently tether the compound to the protein establishing a stable covalent bond. The other end of the central azobenzene group is linked to a ligand of choice, an antagonist or agonist to the protein target. This allows for the ligand to be presented to or withdrawn from the binding site by photo isomerization (Kramer et al., 2013) [73]. Adjusting the position of the cysteine mutation or the length of the photoswitch molecule fine tunes this engineered two-component system. Ideally, to study the function of endogenous receptors free of artefacts all native receptors lacking the cysteine mutation ought to be genetically replaced by an altered variant through gene knock-in substitution techniques.

Many important ion channels and receptors have been engineered in that way. The approach was prototyped by a light-regulated Shaker K^+ channel called SPARK (Banghart et al., 2004; Chambers et al., 2006) [7][30] and other types of potassium channels (Fortin et al., 2011) [54]. Optogenetic pharmacology was later adapted to activate ionotropic glutamate receptors with light, called LiGluRs (Volgraf et al., 2006; Szobota et al., 2007) [142][132], and to modulate the activity of metabotropic glutamate receptors, referred to as LimGluRs (Levitz et al., 2013) [78]. Further developments included light-regulated acetylcholine (Tochitsky, Banghart et al., 2012) [135] and $GABA_A$ receptors (Lin et al., 2014; Lin, Tsai et al., 2015) [83][84].

In summary, optogenetic pharmacology bears the potential to provide insights to neuronal function of specific molecular signaling proteins that is unparalleled by neither optogenetics nor pharmacology. However, the techniques requires both synthetic chemistry, maleimide conjugation on living cells and genetic engineering to be successfully implemented and is therefore technically challenging, especially for *in vivo* applications.

In contrast, photochromic ligands are simpler to use as they do not require genetic manipulation nor chemical linkage. Although they lack specificity, PCLs feature other useful properties.

1.1.1. Photochromic Open Channel Blocker

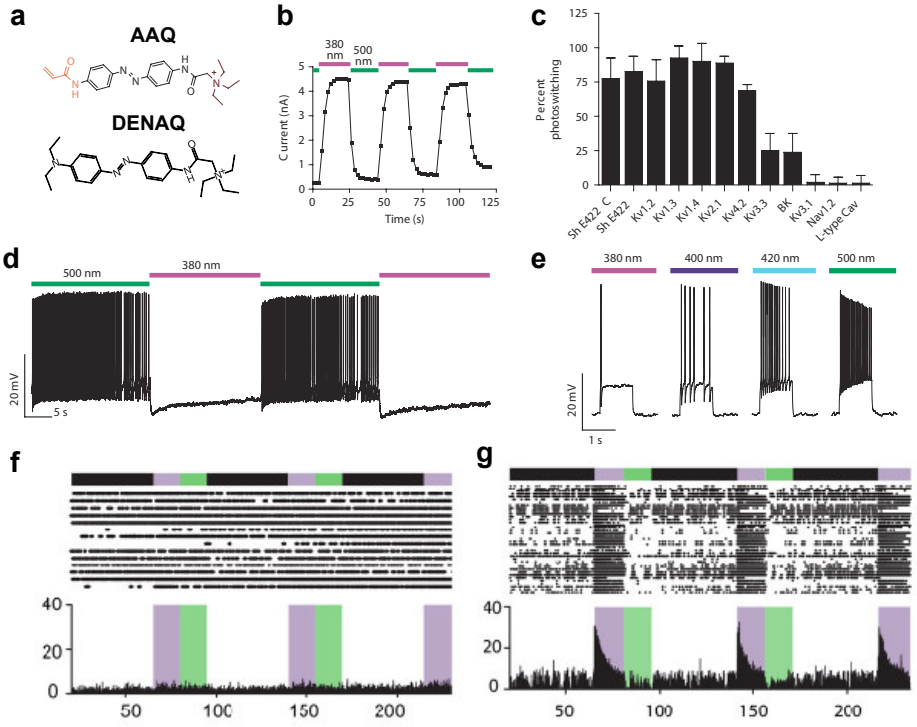

Figure 3.: Photochromic Open Channel Blockers.
a. Chemical Structure of AAQ and DENAQ. **b.** AAQ photosensitizes K^+ currents. **c.** AAQ blocks a variety of voltage-gated potassium channels. **d.** Light dependent modulation of neuronal excitability, blocking K^+ channels with AAQ in green light induces firing while unblocking K^+ channels and restoring potassium currents silences neurons. **e.** The effect of AAQ can be titrated with light using different wavelengths. **c.** AAQ restore photosensitivity to blind retina tissue. Left panel: Before AAQ application, Right panel: After re-animation with AAQ. Spiking raster plots of multi-electrode array recordings of *ex vivo* retina preparations.
Adapted from Fortin et al., 2008 and Polosukhina et al., 2012 [53][113].

Photochromic ligand are freely diffusible molecules whose activity can be switched on and off with light. Although many different types of ligands could be engineered that way, using this approach for open channel blockers appears most obvious as pore blockers are of simpler design (Banghart et al., 2009; Mourot et al., 2013) [106][8]. Photochromic blocker compounds photosensitize endogenous ion channels and inhibit ion conductance when switched by light. Various designs with different properties have been generated and one of the first photoswitches tested was the acrylamine-azobenzene-quaternary ammonium (AAQ, Figure 3) compound. AAQ blocks many types of K^+ channels but does not affect voltage-gated Na^+, Ca^{2+} or neurotransmitter

gated channels (Banghart et al., 2009; Fortin et al., 2008) [8][53]. AAQ in *trans* configuration blocks potassium currents and thus effectively promotes firing. The lack of specificity, both on a channel and cell level, limit AAQ's application as a research tool but widespread photosensitization is beneficial to bestow light sensitivity to blind retinas (Polosukhina et al., 2012) [113]. AAQ requires light in the UV spectrum to be converted but a new generation of red-shifted derivatives overcomes this limitation (Tochitsky et al, 2014) [136]. The activity level of photoswitch molecules can be titrated with light, either by intensity tuning or by illumination with different colors of light as demonstrated at the example of AAQ in Figure 3e.

1.1.2. The Photoswitch Molecule QAQ

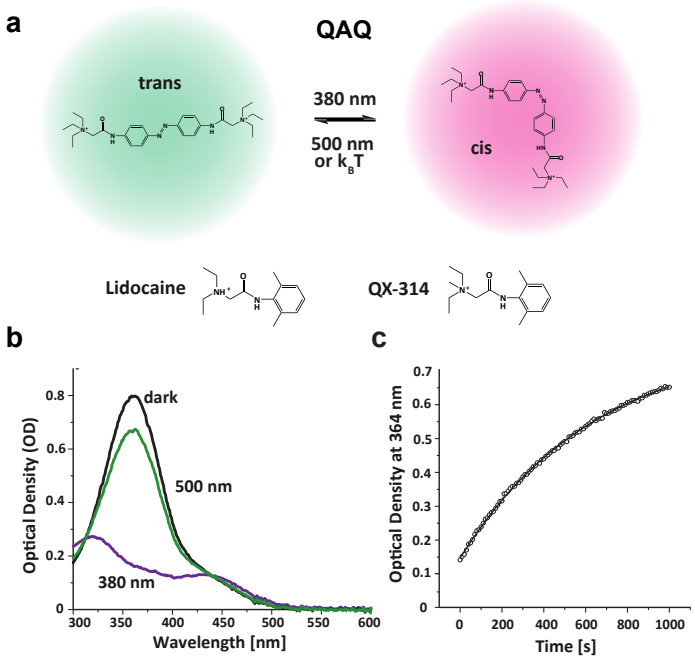

Figure 4.: Chemical Structure and Absorption Properties of QAQ.
a. In contrast to lidocaine and QX-314, a central azobenzene group confers light-dependent conformational changes to QAQ which is symmetrically flanked by two positively charged tetraethylammonium groups. QAQ is bi-stable, 500nm light or slow thermal relaxation (minutes) convert QAQ into its elongated *trans* isomer, 380nm light reverses QAQ into its bent *cis* conformation. K_BT represents thermal energy relaxation with k_B denoting the Boltzmann constant and T denoting temperature. **b.** UV-Vis spectrum of the dark-adapted ground state and both QAQ photo isomers after illumination in saline solution at neutral pH. **c.** Thermal relaxation of QAQ from *cis* to *trans* in the dark and in a probe cuvette. The decay is fitted by a mono-exponential equation yielding a time constant of $t_{1/2}$=449s.
Adapted from Mourot et al., 2012 [104].

The symmetric photochromic ligand QAQ, Quaternary Ammonium-Azobenzene-Quaternary Ammonium (QAQ) combines features that considerably distinguish QAQ from other photoswitch molecules.

QAQ consists of a central azobenzene moiety symmetrically flanked by two, permanently charged quaternary ammonium groups. Similar to other PCLs, illumination with 380 nm light rapidly (milliseconds) converts *trans* QAQ into *cis* QAQ which reverts spontaneously in the dark to *trans* (minutes) but this conversion can be accelerated to a millisecond time frame with 500nm light (Figure 4).

In contrast to AAQ, QAQ photosensitizes many different types of voltage-gated ion channels, Na^+, K^+ and Ca^{2+} channels (Figure 5) when introduced to the cytosol of a cell. However, *trans*-QAQ does not block all K^+ channels as inward-rectifier (K_{ir}) and hyperpolarization-activated cyclic nucleotide-gated (HCN) channels are not affected. Moreover, QAQ also fails to photoregulate N-methyl-D-aspartic acid (NMDA) receptors.

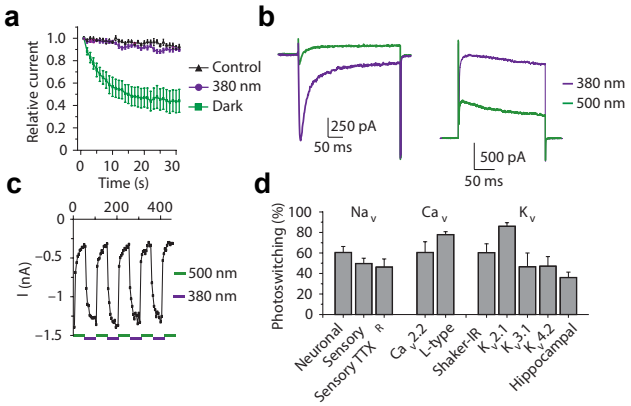

Figure 5.: QAQ Photosensitizes many Voltage-gated Ion Channels.
a. Intracellular QAQ applied through a patch pipette to Na^+ channel expressing cells effectively block sodium currents in a use-dependent manner. **b.** Photoswitching of Na^+ currents is reversible. **c.** Photomodulation of $Ca_V2.2$ currents (left panel) and Shaker K^+ currents (right panel). **e.** Percentage photoswitching of currents through voltage-gated Na^+, Ca^{2+} and K^+ channels. 'Neuronal'describes Na^+ channels from NG108 cells, 'sensory'denotes Na^+ channels rat trigeminal ganglia, TTX^R denotes tetrodotoxin-resistant.
Adapted from Mourot et al., 2012 [104].

Since intracellular QAQ imparts light-sensitive block on voltage-gated sodium channels, QAQ exhibits a strong influence on cellular excitability. *Trans* QAQ potently silences neuronal excitability in a rapidly reversible way (Figure 6b) while *cis* QAQ relieves the block and restores excitability after current injection. Even in 500nm light a single spike at the onset of stimulation can be elicited due to the use-dependent blockade of QAQ (Figure 6a). QAQ affects spiking but has little effect on the resting properties of neuronal cells. Key parameters of neuronal excitability are unchanged in the presence of both QAQ isomers; input resistance, resting membrane potential and firing threshold are unaltered (Figure 6d).

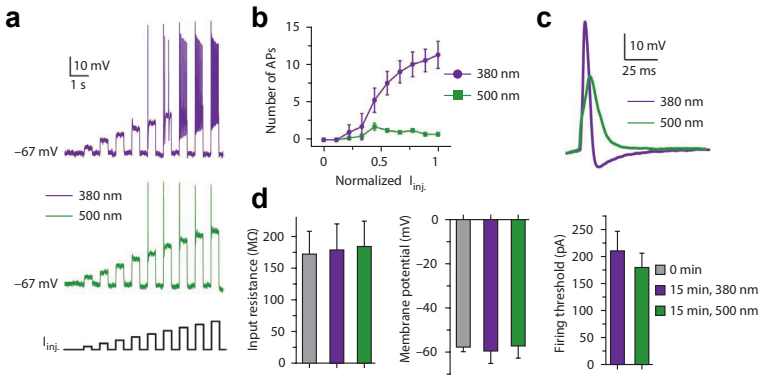

Figure 6.: QAQ as Potent Inhibitor of Neuronal Activity.
a. Elicited action potentials in hippocampal neurons after current injection are potently suppressed with QAQ under 500nm light. **b.** *Trans* QAQ effectively limits the number of triggered spikes with increasing magnitude of injected current (I_{Inj}). **c.** QAQ changes the shape of action potentials in different ways due to its effects on multiple voltage-gated channels. **d.** Properties of neurons at rest are not changed when exposed to QAQ.
Adapted from Mourot et al., 2012 [104].

1.2. Probing Ion Channel and Cellular Permeability

QAQ resembles lidocaine and its derivative QX-314 (Figure 4a) which are local anesthetics that block voltage-gated Na^+, K^+ and Ca^{2+} channels from the cytoplasmic side similar to QAQ (Scholz, 2002; Hille et al., 2001) [125][58]. Lidocaine is a tertiary amine that crosses the membrane uncharged but gets protonated upon entering the cytoplasm (Strichartz, 1973) [131]. Only internal, charged lidocaine can block ion channels. In contrast, the permanently charged derivative QX-314 cannot penetrate cell membranes but blocks channels in similar fashion to lidocaine.

QX-314 has been used for indirect *in vivo* measurements of functional nociceptor expression by application of a QX-314-agonist combinations and evaluating pain thresholds. If functional ion channel were present that can serve as a conduit for cell entry, QX-314 can enter active cells and silence them reducing pain thresholds (Zakir et al., 2012) [149].

Given its permanent, double charged character (Figure 4), QAQ is also membrane impermeant and cannot readily cross the cell membrane. Further, since QAQ imparts light sensitivity to ion channels only from their cytosolic side, it needs to be introduced to the cytoplasm to become active. Bath application of QAQ does not block endogenous ion channels (Figure 7a). Importantly, other ion channels can function as a conduit enabling penetration into the cytosol. These channels need to be active and permeable for large cations to allow QAQ entry into the cytosol. Upon cell entry, QAQ can potently block voltage-gated ion channels in a light regulated, dose dependent manner. We devised an indirect method using a photoswitch compound as a reporter of channel and cellular permeability (Mourot et al., 2012) [104]. Since QAQ exhibits light dependent block of excitation only when intracellular, the amount of conferred light sensitivity of a neuron's excitability serves as a measure of conduit channel activity. The light dependent,

bimodal block of QAQ delivers a highly sensitive way to quantify intracellular QAQ concentration and deduce that information to changes in cell permeability. The degree of conferred light sensitivity hence correlates with the amount of internal QAQ which in turn indirectly correlates with the amount of open ion channels. Therefore, imparted photosensitivity can probe permeability changes of a neuron. In addition, intracellular accumulation of QAQ over time during an incubation period amplifies even small changes in channel open probability enabling the detection of even slight modulations in channel activity.

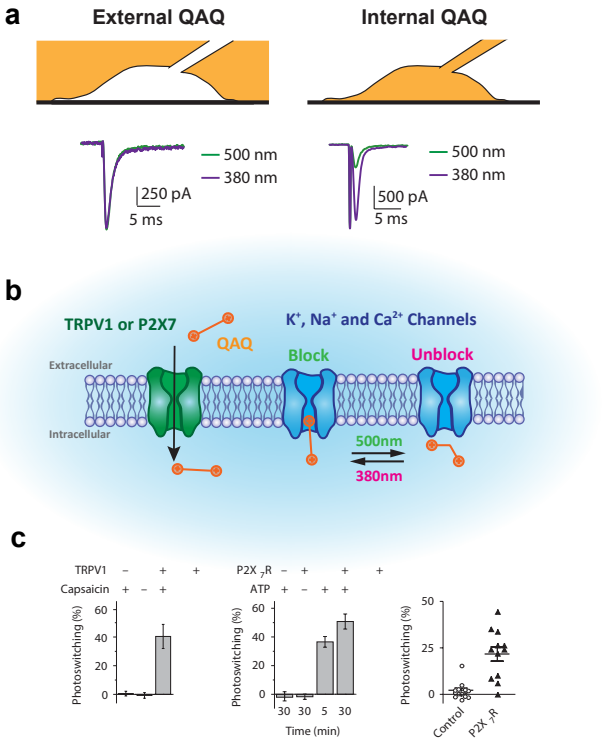

Figure 7.: QAQ is an Internal and Membrane Impermeant Blocker but can Enter Neurons through Nociceptive Ion Channels.
a. External QAQ has no effect on Na^+ currents. In contrast, internal QAQ delivered through the patch pipette enables potent photomodulation of ionic currents. **b.** QAQ can enter cells through active nociceptive ion channels like TRPV1 and P_2X_7. TRPV1 (left panel) and P_2X_7 (right panel) were heterogeneously expressed with a reporter channel. Treatment with QAQ alone did not bestow photosensitivity. However, application of QAQ in concert with respective agonists of TRPV1 and P_2X_7 receptors, capsaicin and adenosine triphosphate (ATP), conferred light regulation.
Adapted from Mourot et al., 2012 [104].

It would be technically very challenging to measure those permeability levels with traditional electrophysiological techniques. Both intra- and extracellular solutions need to be controlled to isolate specific cation currents through the specific ion channels. Further, small changes in open probability but accrued over longer episodes of time could be missed in electrophysiological recordings.

Besides QAQ and QX-314, also other large, cationic molecules can serve as reporters for the permeability change of nociceptive channels. Most prominently, the cationic fluorescent dye Yo-PRO-1 is taken up into the cytosol by active ion channels and therefore functions in a very similar way to QAQ. In analogy, the small styryl dye FM1-43 specifically labels inner ear cells by entering through mechanotransduction, TRPV1 and P_2X_2 receptors when those channels are active and form a dye-permeable low-selectivity pore (Meyers et al., 2003) [96].

While the mechanism of conduction of QAQ is not well understood, we assume this process to work in analogy to activity dependent loading described for the sodium channel blocker QX-314 and the fluorescent dye Yo-PRO-1.

1.3. Activity-dependent Silencing of Nociceptive Neurons with Photoswitch Compounds

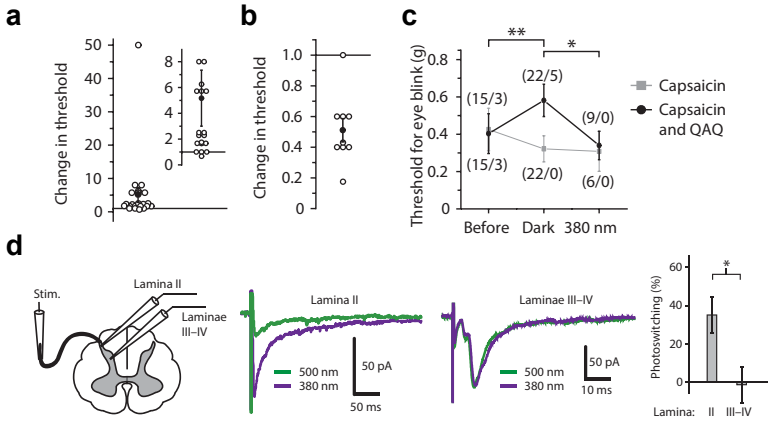

Figure 8.: QAQ as Analgesic *in vivo*.
a Change in blink threshold of a rat eye treated with capsaicin plus QAQ in the dark normalized to blinking threshold in contralateral control eyes treated with capsaicin alone. **b.** Like a but with isomerization of QAQ to *cis*. Relieved block of pain neurons reduces pain threshold. **c.** Group data for eye-blink threshold experiments in rats, pain threshold modulation with light using QAQ. **d.** Photomodulation of nociceptive inputs from primary afferents onto second order neurons in different laminae of the spinal cord.
Adapted from Mourot et al., 2012 [104].

The previous chapter demonstrates how effectively QAQ silences neuronal excitability and potently inhibits action potential firing in neurons (Figure 6). Moreover, the activity-dependent uptake of QAQ targets the molecule only to neurons where certain ion channels are active. As will be described in more detail in later chapters, conduits for QAQ are prominent receptors of pain messages and contribute to signal transduction in the pain perceiving system, the nociceptive system. Anesthetics are drugs that target the nociceptive system effectively suppressing pain sensation. But most of these compounds affect all neurons they are exposed to and their actions

abate slowly (Mourot et al., 2012) [104]. In contrast, QAQ infiltrates pain-sensing neurons activated by noxious stimuli and accumulates intracellularly blocking voltage-gated ion channels. This enables reversible optical silencing of active nociceptive neurons.

By combining activity-dependent uptake and potent silencing, QAQ can effectively modulate pain behavior *in vivo* affecting the pain threshold of the corneal blinking reflex (Mourot et al., 2012) [104]. Similar molecules like QX-314 have been applied for selective, activity-dependent block of nociceptors (Binshtok et al., 2007, 2009 and 2011, Roberson et al., 2011 and 2013; Zhao et al., 2014) [18][20][19][117][118][150] and neuropathic pain (Omana-Zapata et al., 1997) [110].

1.4. Red-shifted Open Channel Blocker PCLs

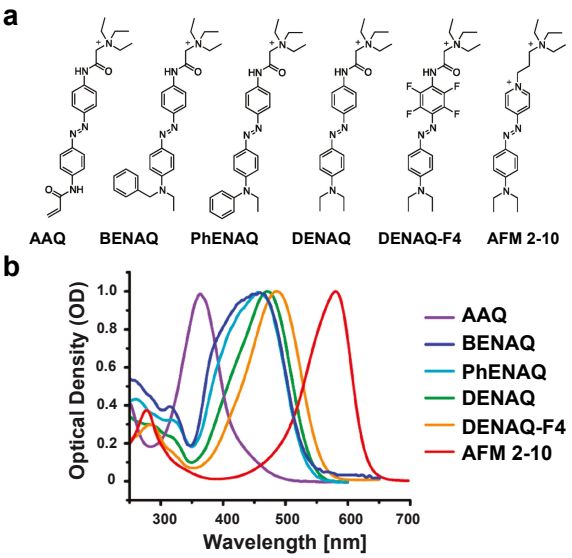

Figure 9.: Toolset of Red-Shifted Photochromic Blockers.
a. Modified photochromic blockers related in design to AAQ. **b.** Absorption spectra of compounds under a.
Adapted from Mourot et al., 2011 [105].

Light of short wavelengths is significantly more scattered when passing through organic tissue than photons of longer wavelengths carrying less energy. The absorption maximum of most PCLs designed to-date lies in the ultraviolet range making targeting the molecule in deeper tissue layers more difficult and requires higher light intensities (Beharry et al., 2011) [16]. Moreover, UV light directly damages proteins and DNA molecules affecting the overall health of neurons. Adapting the chemical design of photoswitch compounds can shift the absorptions maximum toward longer wavelengths by changing the electron density in the conjugated π electron system around the central azobenzene group (Samanta et al., 2013; Wegner, 2012; Dong et al., 2015) [124][145][47]. However, changing electron density affects the stability of the *cis* isomer and

therefore red-shifted derivatives are generally not bi-stable but rather convert back to *trans* very rapidly in the dark. For efficient unblock, light must be continuously applied. On the other hand, these molecules can therefore be practically operated with a single wavelength.

Different chemical designs have been first tested for single charged, open channel PCLs. A slew of tools has been synthesized and the addition or omission of certain chemical groups efficiently modulates absorption behavior (Mourot et al., 2011) [105]. This exemplifies what types of chemical groups in the vicinity of the azobenzene moiety shift absorption characteristics also for other azobenzene based compounds like QAQ.

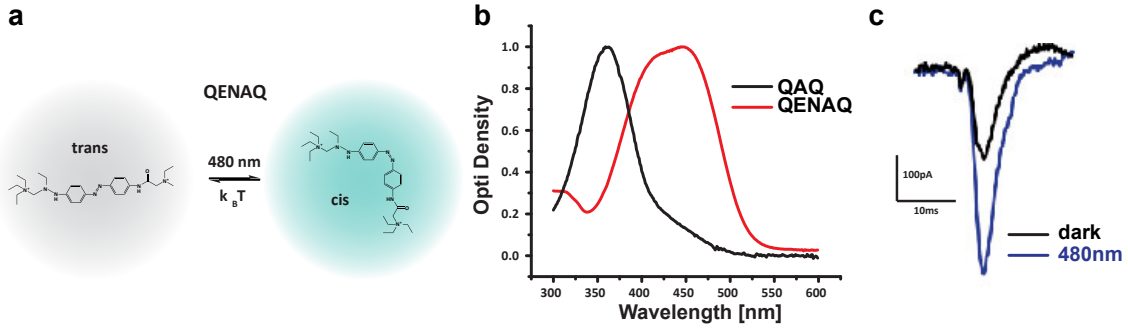

Figure 10.: The Red-shifted QAQ Analogue QENAQ.
a. Chemical structure of the QENAQ. **b.** Absorption spectra of both QENAQ photo isomers. **c.** Control of K^+ currents with QENAQ. Unpublished data, Alexandre Mourot.

The compound Quaternary Ammonium-Ethylamine-Azobenzene-Quaternary Ammonium (QENAQ) has been coined red-QAQ as it combines many characteristics of QAQ with a red-shifted absorption maximum. Conversion of *trans* QENAQ to *cis* can be achieved with visible light around 480nm (Figure 10). However, QENAQ is not thermally stable in *cis* similar to the molecules in Figure 9. QENAQ rapidly and spontaneously reverts to trans in the dark which further differentiates QENAQ from QAQ. Other QAQ derivatives with shifted absorption characteristics have also been synthesized but require further testing (Fehrentz et al., 2012) [50].

2. Interactions of Photoswitch Blockers with Voltage-Gated Channels

Photoswitch molecules are powerful neuroscientific tools controlling and probing neuronal activity from a cellular to a systems level. Specifically, QAQ is utilized in applications of wide scope; to study dendritic integration on a sub cellular level and for restoring light responses to the retina, for instance. Although photoswitch compounds are chemically simple molecules and closely resemble well-studied ion channel blockers (Mourot et al., 2011, 2012, 2013) [103][104][105], the exact mechanism of interaction with and blockade of voltage-gated ion channel targets remains unclear.

In order to study those interactions, we chose to use the Shaker potassium channel as voltage-gated reporter channel for QAQ action. Voltage-dependent potassium channels repolarize action potentials and restore resting membrane potentials. They are crucial for the transmission of electrical signals in the nervous system and are a major target not only for QAQ but for most other photoswitch compounds. We assume that insights obtained from studies of QAQ interaction with potassium channels can be generalized into our understanding of QAQ's mechanism of action in general.

Inside-out patch electrophysiology from *Xenopus laevis* membranes provides an optimal system to study the interaction of blocker molecules with ionic currents and ion channel proteins. Inside-out patch preparations enable direct and rapid control of solutions exposed to the cytosolic side of ion channels, voltage clamp electrophysiology allows for precise control of voltage sensitive channels and light can be readily applied without intensity loss. This minimal experimental system isolates the channels of interest and allows to focus on protein-blocker interaction excluding possible interferences with other components of a cell.

2.1. The K^+ Channel Shaker as Model for the Study of Interactions between a Voltage-gated Ion Channel and Photochromic Blockers

The large superfamily of voltage-gated potassium channels (K_V channels) is evolutionary conserved on a functional and molecular level (Jan and Jan, 2012) [65]. K_V channels consist of four subunits each containing six transmembrane segments, S1-6. The central pore domain is formed by helices S5 and S6 of each of the subunits as well as the P-helix and connecting loops (see Figure 11a). This domain also assembles the selectivity filter and the voltage sensor. The channel gate is controlled by the voltage-sensing domains formed by helix S1 through S4 which surround the pore. All four subunits are subtype-selectively assembled by a N-terminal tetramerization domain that also enables binding of accessory subunits (Tombola et al., 2006) [137]. Those regulating subunits modulate channel gating and contribute to the specificity of neuronal firing patterns (Li et al., 2006) [81]. Ion-conduction occurs on a remarkably high rate of 10^6 to 10^8

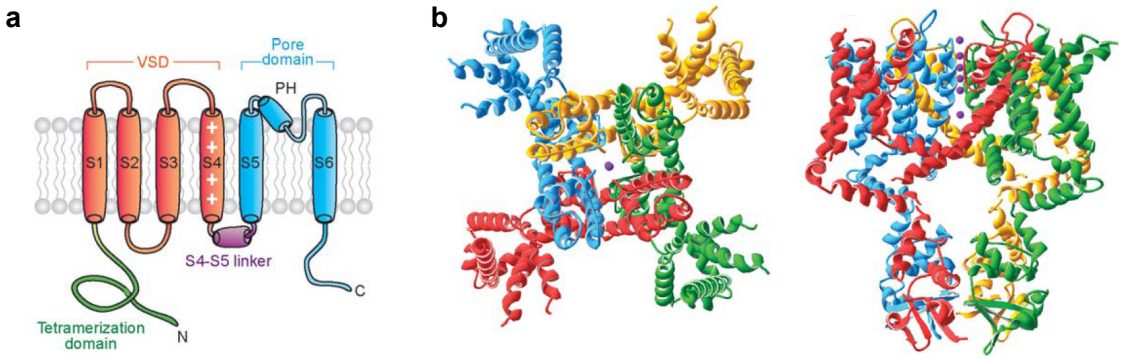

Figure 11.: Structure of the K_V1.2 Potassium Channel.
a. Architecture of a K_V channel subunit. Protein helices are depicted by cylinders, pore domains are colored blue and voltage-sensing domains red. **b.** Top (left panel) and side (right panel) view of the K_V1.2 tetramer three-dimensional structure. K^+ ions are colored purple. Adapted from Tombola et al., 2006 [137] and Long et al., 2005 [86].

ions per second and discriminates between different ion species with very high efficiency. K^+ ion conduction is favored 100 to 1 over Na^+ conduction.

The S4 helix of potassium channels functions as voltage sensor. The gating domain is characterized by positively charged Arginine residues that move through the membrane electric field from inside to outside when the membrane depolarizes moving a net equivalent of 12 to 14 elementary gating charges. Gating happens very rapidly, on the order of 1ms, can be repeated very frequently, up to 1000Hz, and is sensitive to changes in membrane voltage, in range of a few mV. The membrane electrical field performs work on the gate to alter the channel's conformation within the membrane. This process can be hindered and delayed by molecules blocking the movement of the gate effectively propping the channel open.

One of the best-studied members of the K_V1 ion channel family is the fast-inactivating, homo-tetrameric, voltage-gated potassium channel Shaker from the fruit fly *Drosophila melanogaster*. In the fly, Shaker channel mutants show aberrant, uncontrolled leg movements which is caused by increased action potential firing in muscles and elevated transmitter release. Shaker channels are type A potassium channels responsible for repolarization of the membrane potential after firing and therefore regulating fire frequency and threshold.

The crystal structures of the mammalian Shaker family K^+ channel K_V1.2 (Long et al., 2005; Figure 11) [86], the open K_V1.2-2.1 chimera in native lipid environment (Long et al., 2007) [87] and the bacterial Shaker analog KcsA (Sokolova et al., 2001) [128] significantly contributed to our understanding linking structural insights to channel function.

The Shaker channel can be activated be depolarizing membrane potential with half activation around -45mV. Native Shaker contains a ball-and-chain domain that provides fast N-type inactivation (Molina et al., 2008) [101]. The ball peptide has a high affinity for the pore and rapidly blocks ion conduction once the channel is opened. Besides fast inactivation, Shaker also

shows slow C-type inactivation that can be modulated by small molecules like open channel blockers.

Shaker is considered an archetypical potassium channel, has been extensively studied (Molina et al., 1998) [100] and experimental handling is easy and convenient. Shaker has been utilized as a general K^+ channel paradigm and we therefore also chose Shaker as a model for studying interactions of photoswitch molecules with voltage-gated potassium channels.

2.2. Properties of Previously Studied Open Channel Blockers of Shaker

Decades ago it has been shown that quaternary ammonium (QA) compounds block K^+ channels once opened. Quaternary ammonium derivatives are for example tetraethylammononium (TEA), decyltriethylammonium, QX-222, QX-314 and lidocaine which is also used as local anesthetic. Those small organic compounds function as open channel blocker, can enter the channel vestibule only when opened and need to dissociate before the channel can close again. Some channel mutants (Holmgren et al., 1997) [60] can force the channel to close with the QA still associated essentially trapping the molecule. Further, most larger QAs prevent the channel from closing and affect gating by slowing down channel opening and closing (Armstrong, 1969 and 1971) [4][5]. In wildtype Shaker channels, external TEA blockade is voltage-sensitive and TEA further decelerates slow C-type inactivation (Molina et al., 1997) [99]. Mutations in Shaker‘s pore region (T449, D447) however, can render external TEA block voltage-insensitive, abolish TEA‘s effect on inactivation and, if mutated to charged residues, diminish TEA block altogether suggesting that interaction with those mutated residues provide critical coordination for TEA function (Molina et al., 1997) [99]. TEA and external cations compete for an inactivation site that needs to empty before the channel can close by a foot-in-the-door mechanism.

Research on sodium channels has shown that open channel blockers specifically bind certain residues within the lumen and those binding sites are located in the internal pore and can modulate affinity dramatically (Yamagishi et al., 12009) [148]. The interaction of internal TEA with Shaker has been considered well-understood proposing TEA being coordinated by four specific residues (Choi et al., 1993) [35] and interference with slow inactivation via a foot-in-the-door mechanism. However, more recent studies established that TEA is localized in a more external location of the outer vestibule and does not require specific coordination with outer-vestibule residues (Andalib et al., 2004) [2].

Finally, it has been proposed that QA compounds could access the channel via two alternative routes: a slow hydrophobic route accessible in all channel states and a rapid hydrophilic route only accessible when the channel is in its open state (Tikhonov, 2008; Bruhova, 2008) [134] [25].

For QAQ specifically, we have so far shown that internal QAQ blocks Shaker currents but no further experiments focused on more detailed interactions were previously conducted (Mourot et al., 2012 and 2013) [104] [103].

3. Nociceptive Ion Channels and the Perception of Pain

Sensory information are essential for all organisms to interact with the environment. In higher organisms, the peripheral sensory nervous system is specialized to detect external and internal mechanical, thermal and chemical stimuli and transform them into electrical signals. Environmental stimuli are gradual in nature ranging from innocuous to intense, potentially harmful or noxious levels. This observation led to the development of the Intensity Theory attributing the capability of detecting pain to all sensory neurons in an intensity dependent way.

In contrast to the Intensity Theory, Charles Sherrington proposed in 1898 the existence of specialized cells for sensing pain within the peripheral nervous system and this concept was later refined by Ed Perl (Mason, 2007) [92]. Pain is an essential physiological function providing protection from injury. The perception of acute or potentially tissue damaging stimuli is an important characteristic for an organism's wellbeing in order to stop further damage, avoid potential hazards or protect injuries. Acute pain alerts organisms to noxious and potentially harmful or tissue damaging stimuli and triggers appropriate responses to protect the organism. People that do not experience pain often succumb to medical problems that go unnoticed and untreated. Pain is a vaguely defined type of sensory perception. Mechanical and thermal stimuli can be painless at low intensities but become painful over prolonged exposure or increased force or energy level. In addition, the distinction between innocuous and noxious stimuli is highly dependent on the subjective state of an individual; the line between painless and painful perception is blurry.

In mammals, the actual emotion of pain is generated as result of the association of various brain areas and constitutes a complex sensation under the control of many dynamic regulation mechanisms. The neural representation of pain is eventually formed in the neocortex. In general, pain is defined as an unpleasant sensory and emotional experience associated with actual or potential tissue damage, or described in terms of such damage (Loeser and Treede, 2008) [85]. 'Pain experience'includes concepts from molecular and cellular to cognitive and emotional processes.

When studying pain in animals it becomes even harder to assess pain levels and hence pain behavior serves as a measure for pain sensations. All this complicates the study of pain detection and perception. The mechanisms sensing pain in the periphery are also referred to as nociception.

Historically, pain was understood as a byproduct of physical damage that alerts of harmful impact but is tightly coupled to that external input. We now know that pain itself can be a disease. Chronic or neuropathic pain syndromes create lasting sensations of pain that are generated within the nervous system without external stimulation. Those disease states might originate from an initial traumata but become an independent diseases over time.

Chronic and neuropathic pain is a serious health concerns and afflicts over 20% of the worldwide population, especially older people, according to the International Association for the Study of Pain.

3.1. Anatomy and Physiology of the Nociceptive System

The nociceptive system in physiologically divided into cells transmitting signals from cutaneous and deep structures like muscles, joints and viscera. Since 95 to 98% of all nociceptors innervate the skin and most studies have been conducted on that class, I will be focusing on cutaneous nociceptor signaling. Afferents signaling from deep tissues are mostly C or Aδ fibers, contain peptides, participate in neurogenic inflammation and create dull, poorly localized, diffuse pain.

The first detection of noxious stimuli in the periphery is mediated by a defined set of molecular sensors, mostly ion channels, which recognize external or internal stimuli and convert them into electrical signals through the influx of sodium and calcium ions. Those sensors are collectively called transducer channels and they create a generator potential. Propagating channels like voltage-sensitive sodium channels amplify detected signal and send them to the dorsal horn of the spinal cord where messages are modulated and finally transmitted to the brain (Figure 12). Some sodium channel sub-types are selectively expressed in DRGs, e.g. $Na_V1.7$ and 1.8, which makes them attractive targets for pain therapeutics. Sensitizing channels like the TNF-α Receptor 1 or the IL-6 Receptor can modulate pain message while being transmitted to the central nervous system.

Cells converting nociceptive, noxious and potentially tissue damaging stimuli are called pain neurons or nociceptors and their somata are located in the trigeminal and dorsal root ganglia (DRG) along with cell bodies of other sensory neurons. Nociceptors account for roughly 45% of all DRG neurons and are mostly small in cell diameter. The spinal cord is bilaterally symmetrical and incompletely divided into a right and left halve by the ventral median fissure. Therefore, both DRGs on the left and right side are considered equal. Each dorsal root (also named posterior root, radix posterior, radix dorsalis or radix sensoria) is attached to the dorsolateral sulcus of the spinal cord by a series of rootlets arranged in a line, the dorsal root entry zone. Dorsal roots are large and contain more fibers than ventral roots (Watson, 2012) [31]. Some adjacent DRGs are fused or in some cases both dorsal and ventral root enter a DRG. All sensory cells show a distinct pseudo unipolar geometry sensing stimuli in the periphery innervating the skin and inner organs, transducing this information through peripheral fiber tracks and relaying them to the dorsal horn through their central terminal, the site of neurotransmitter release (Figure 12). Nociceptors innervate the periphery with free nerve endings and they lack the impressive structural specialization observed in Pacinian, Meisner‘s or Ruffini‘s corpuscles. Second-order neurons in the spinal cord are activated by glutamate and substance P neurotransmitters. Sensory axons can be well over 1m in length in humans and show a characteristic T junction branching access to the cell bodies. DRGs are located in the vertebral column immediately adjacent to the spinal cord. Each sensory neurons has one axon fiber relaying information from the periphery to the central nervous system. This architecture stipulated the concept of labeled lines assuming that each fiber senses a distinct type of stimuli and transmits this specific sensation hardwired into the nervous system. However, this notion has been recently challenged as will be explained in more detail in a separate section.

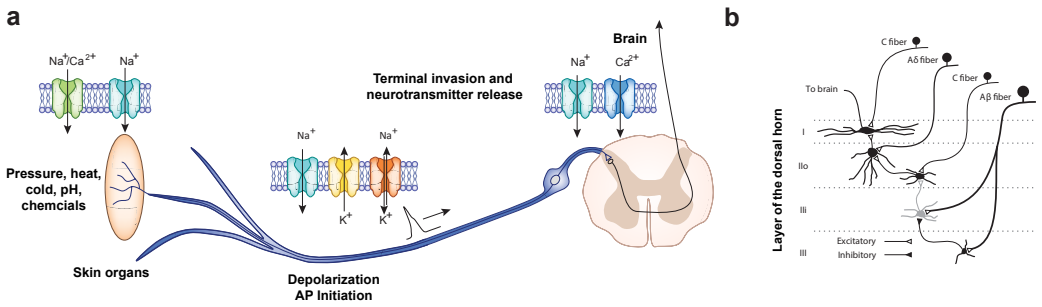

Figure 12.: The Mammalian Nociceptive System.
a. Schematics of the nociceptive system detecting stimuli in the periphery and relaying information to the central nervous system in the spinal cord. Adapted from Waxman and Zamponi, 2014 [144]. **b.** Projections of different sensory fiber types onto second-order neurons in the dorsal horn of the spinal cord. Interneurons (grey) mediate crosstalk between different inputs. Adapted from Prescott et al., 2014 [114].

Nociceptors are a subgroup of sensory neurons that response to noxious stimuli but are unresponsive to innocuous stimuli. Sensory neurons are remarkably diverse (Lumpkin et al., 2007) [88] and one way to classify them is by their degree of myelination, thus their conduction velocity (Kandel, 2012) [68]. By anatomical and functional criteria, nociceptors can be classified into three main groups: large diameter, myelinated, rapidly conducting Aα and β primary sensory fibers, thinly myelinated, more rapidly conducting Aδ fibers and small to medium diameter, unmyelinated, slowly conducting C fibers (Table 1).

Another way of grouping nociceptors is by their neurochemistry which subdivides cells into peptide-containing and non-peptidergic cells. Peptides expressed are generally calcitonin-gene-related peptide (CGRP) (Eberhardt et al., 2008) [48], neuropeptide Y (Shi et al., 2006) [127], neurotensin (Matthew et al, 1993) [93], substance P (Ruscheweyh et al., 2007) [122], tyrosine hydroxylase (Brumovsky et al., 2006) [26] or somatostatin (Matthew et al, 1993) [93]. Non-peptidergic neurons are predominantly identified by expression of the plant lectin isolectin-B4 (IB4) (Fang et al., 2006; Zwick et al., 2002) [49][153].

Yet another way of distinction is based on staining properties of nociceptors in light microscopy which classifies into two broad groups: large, light cells rich in neurofilament (Aα, Aβ, and Aδ mechanoreceptors) and small, dark cells which are poor in filament (C and Aδ fibers).

Besides difference in morphology, nociceptors can also be grouped according to their sensory modality and stimulus intensity (Kandel, 2012) [68]. Somatosensory neurons forming the peripheral nervous system detect a wide range of external and internal stimuli including physical conditions like temperature and pressure as well as environmental irritants and endogenous inflammatory agents. Thermoreceptors respond to changes in temperature, touch receptors to pressure, stretch or hair movement. Many nociceptors are activated by multiple types of stimuli and therefore are polymodal in their response. In addition, many sensors are co-expressed in peripheral terminals rendering respective nociceptors polymodal as well on both molecular and

Fiber Type	Cell Size	Myelin	Conduction Velocity	Nociceptor Types
Aα-β	6-20μm	yes	35-120m/s	Muscle spindle receptors, proprioceptive information, Golgi tendon organs, all mechanoreceptors
Aδ	1-5μm	thin	3-30m/s	Free nerve endings of touch and pressure
C	0.2-1.5μm	no	0.5-2m/s	Cold and warm thermosensors

Table 1.: Peripheral Fiber Types.

cellular level. Especially C fibers are predominantly polymodal responding to multiple painful stimuli and internal signaling molecules.

Aβ fibers detect innocuous stimuli affecting skin, joints, muscle and inner organs and do not contribute to pain sensations. Aδ fibers can be classified in type I and II differentiated by their response to intense heat and tissue injury. Both groups of A fibers send their central terminals into the superficial dorsal horn of lamina 1 and 2 and 70% of all A fibers show a large cell body diameter.

Lumbar spinal nerves are named after vertebrae below which they emerge and mice have 5 or 6 paired lumbar DRGs. The mouse shows a considerable variability in the number of vertebrae segments both between and within strains (Green, 1941) [56] but C57BL/6J mice have mostly 6 lumbar vertebrae (Rigaud et al., 2008) [116]. There are 15 dorsal and 15 ventral rootlets on every side of each segment. Each rootlet coalesces to form dorsal and ventral roots, respectively. All spinal nerves leave the vertebral column trough the intervertebral foraminae and intermingle in plexuses forming peripheral nerves that each bundle axons from different DRGs. Roots L2 through L6 form the lumbar plexus. For most strains, the murine sciatic nerve is primarily composed of fibers originated from L3 and L4 DRGs (Laedermann et al., 2004; Rigaud et al., 2008) [76][116]. In contrast, the sciatic nerves of rats mostly contain axons from DRGs L4 and L5. There is an estimated number of 7,100 neurons residing in DRG L3 with 2,650 myelinated and 4,550 unmyelinated fibers (Biscoe et al, 1982) [21]. In contrast, there are only roughly 12,000 cell in a L5 ganglion (Shi et al., 2001) [126].

Unmyelinated C fibers terminate in laminae 1-2 of the spinal cord whereas Aδ fibers mostly from cutaneous mechanoreceptors innervate laminae 3-5. Afferents from hair follicles descend onto laminae 4-5 through laminae 1-3. Myelinated Aβ and Aδ fibers also terminate throughout the superficial dorsal horn of laminae 1-2, 70% of all large-diameter axons are myelinated. There are no efferent fibers in the dorsal root but only afferent fibers of the somatosensory system.

3.2. Communication between Nociceptive Neurons

Traditionally, DRG cell bodies were considered to be merely passive relays stations mainly responsible for protein translation and energy production. Recently, many findings challenge this view uncovering the importance of action potentials entering DRG cell bodies transforming our understanding of DRGs from dead ends to dynamic modulators of pain signaling.

An example of inter-DRG communication is the DRG sandwich synapse connecting two sensory cells through glia cell signaling which modulates sensory processing (Rozanski et al., 2012 and 2013) [119][121][120].

Many studies have reported peripheral mechanisms of crosstalk resulting in cross-activation of nerve endings by pro-inflammatory mediators through adjacent tissue damage. In contrast, some types of mechancial allodynia after peripheral damage are in part regulated by the central circuitry of the dorsal horn. Interneuons mediate crosstalk between different dorsal horn layers, establishing interconnections between separate sensory pathways (Figure 12) and subsequently generating pain hypersensitivity (Prescott et al., 2014) [114].

Satellite cells and gap junction coupling are thought to also play an important role in interneuron communication within the DRG (Huang et al., 2010) [62] but exact contributions to nociceptive processing are still unknown. The potential importance of satellite cells is suggested by their high number within the DRG accounting for 5.5 times the number of neurons (Watson, 2012; Ledda et al., 2004) [31][77].

Moreover, studies have shown that the expression of nociceptive channels changes in both injured and intact neuronal population after peripheral trauma at the DRG cell bodies which could be interpreted as evidence for neuronal communication (Hudson et al., 2001) [63]. Further, Substance P (SP), an important contributor to nociceptive processing, is released at the cell bodies after injury indicating a possible autocrine or paracrine signaling mechanism. Studies suggest that uninjured primary afferents are functionally important for the maintenance of chronic pain (Ali et al., 1999; Li et al., 2000) [1] [80]. TRPV1 expression in injured cells after partial nerve injury is reported to decrease while neighboring intact cells express more TRPV1 (Hudson et al., 2001) [63]. These effects has been observed in multiple pain models: Seltzer sciatic nerve ligation, spinal nerve ligation and chronic constriction injury. On the other hand, the expression of TRPA1 and TRPM8 is increased after nerve injury (Frederick et al., 2007) [55]. However, mechanical hyperalgesia is not abolished in TRPA1 mutant mice (Kwan et al., 2006) [74].

3.3. Pathophysiology of Pain Perception

Pain in the absence of noxious stimuli is debilitating. Besides peripheral mechanisms, this pathological disruption of information processing is also controlled by emotional and cognitive factors (Bushnell et al., 2013) [27] which contribute to chronic and neuropathic conditions.

The sensation of acute pain is an important protective mechanism to avoid or reduce tissue damage. Once an injury occurred, transient hypersensitivity to noxious and innocuous stimuli supports regeneration and healing. However, pain that persist in the absence of external stimuli and after full recovery of an injury becomes pathological with profound consequences for the quality of life of millions affected by chronic or neuropathic pain conditions. While symptoms are diverse and manifold, two main types of hypersensitivity have been described. Allodynia occurs when normally innocuous stimuli evoke pain where in contrast, hyperalgesia describes the increased sensitivity to painful stimuli. The molecular and cellular mechanisms of the transition from acute to chronic pain have been focus of extensive research and both peripheral and central mechanism have been proposed contributing to a complex, multi-stage development of the disease (Basbaum et al., 2009) [12]. In addition, nociceptive and itch producing pathways can be altered by many different signaling pathways engaged during injury or inflammation. These maladaptive changes can alter nociceptive responses and cause hyperexcitability of sensory fibers.

3.4. Sensitization Mechanisms of Nociceptive Receptors

Nerve and tissue damage sensitizes nociceptors. Cell damage spills a wide array of signaling molecules into the tissue space triggering inflammation which leads to the further release of inflammatory mediators collectively called the 'inflammatory soup'(Julius and Basbaum, 2001) [67]. Those chemical can lead to nociceptors becoming more excitable and active, or 'sensitized'. This phenomena is termed 'axon- or neurogenic reflex'and describes the local inflammation of nociceptive terminals. Studies have shown that sensitizing receptors are crucial for peripheral hyperalgesia (Cunha et al., 2005) [41]. Predominately, three major pro-inflammatory cytokines modifying pain receptors have been identified underlining the complexity of nervous and immune system interactions: interleukin 1β (IL-1β), tumor necrosis factor (TNF-α) and interleukin 6 (IL-6). These signaling molecules either directly act on nociceptive receptors or indirectly promote the release of other inflammatory reagents like prostaglandins.

3.5. Molecular Sensors of Pain: Transient Receptor Potential Ion Channels

Research over the last two decades identified a vast repertoire of sensing molecules mediating sensory perception. In the periphery, the Transient Potential Receptor (TRP) ion channel superfamily is the major class of diverse sensors and transducers for nociceptive messages. TRP channels are calcium permeable, non-selective, cation channels that produce an excitatory generator potentials upon detection of external or internal stimuli. Most TRP channels can be polymodally activated by many chemical and physical stimuli. Since their discovery, TRP channels have been implicated not only with the transmission of acute pain signals but also with changes occurring during pathophysiological conditions. In addition, inflammatory molecules and many regulatory protein cascades have been shown to modulate TRP channel signaling.

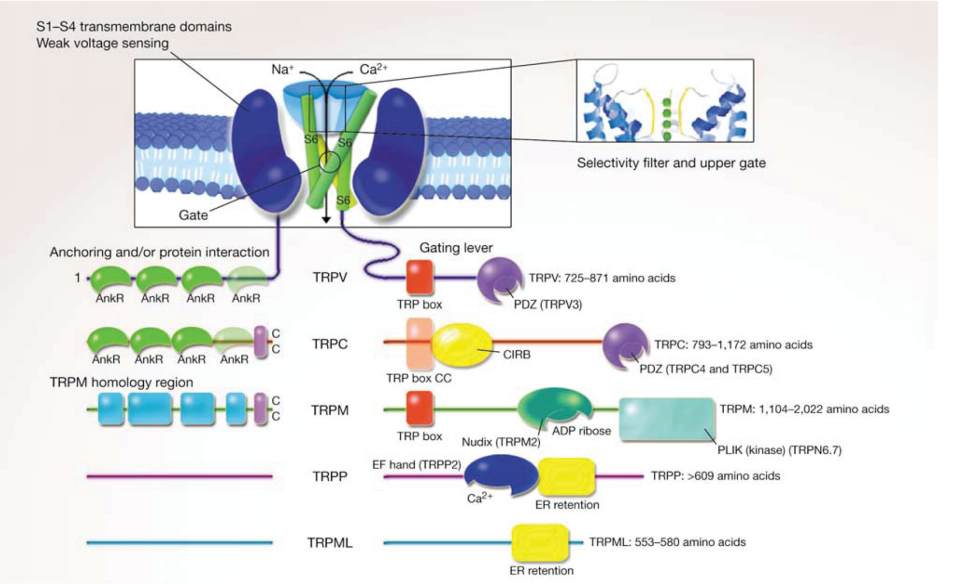

Figure 13.: TRP Channel Architecture.
Most TRP channels are nonselective cation channels with $P_Ca/P_Na < 10$, the monovalent-selective TRPM4 and TRPM5, and the Ca^{2+} selective TRPV5 and TRPV6 are exceptions. TRP channels are weakly voltage-sensitive. The helices S5 and S6 form the pore and there is considerable diversity in the structure of cytoplasmic domains which act as linkers for gating modulators.
Adapted from Clapham 2003 [38].

TRP channels can be found in many organisms but were first discovered in the fruitfly *Drosophila melanogaster*. Members of the TRP family show very distinct structure-function relationships. Notably, extensive N- and C-terminal domains contain many interaction sites for regulatory proteins and signaling molecules transforming TRP channels in complex signal integrators. TRP channels form mostly homomeric tetramers each consisting of 6 transmembrane domains with both cytosolic N and C termini (Figure 13). The TRP superfamily consists of 6 subfamilies with a total of 28 currently identified members which differ considerably in the conduction of divalent ions. The superfamily is divided into the canonical (TRPC), vanilloid (TRPV), ankyrin (TRPA), melastatin (TRPM), polycystin (TRPP) and mucolipin (TRPML) subfamily (Mickle et al., 2015) [97]. Many of the subfamily members just recently have been discovered and little is known about their function and expression. However, a highly conserved 6-mer segment near the channel pore, named the TRP box, seems to be a common structural element involved in gating although exact function remains unknown (Valente et al., 2008) [139]. To date, members of the TRPV, TRPA and TRPM subfamilies have been implicated with sensory transduction and nociception.

TRPAs, TRPCs, and TRPVs contain ankyrin repeat domains which are involved in channel assembly and function. Ankyrin domains serve as adapters to ankyrin proteins that in turn mediate attachment to spectrin-actin based elements of the membrane cytoskeleton maintaining

membrane integrity and anchoring membrane proteins (Mickle et al., 2015) [97]. Most prominently, TRP channel are linked to the sensation of temperature: TRPV1 responses to more than 42°C, TRPV2 to more than 53°C, TRPV3 to more than 32°C and TRPV4 to more than 33°C. In contrast, TRPA1 (<10-15°C) and TRPM8 (<25°C) are activated by temperature below body temperature. Studies found that temperature sensitivity to the family of heat-sensitive TRP channels is conferred by a common C terminal domain (Dhaka et al., 2006) [46].

Two prominent members of this family, the heat and capsaicin receptor TRPV1 and the wasabi receptor TRPA1, have also been established as key integrators of pain-related messages and modulators of pain hypersensitivity.

Besides TRP channels, ionotropic purinergic receptors (P_2X receptors) contribute to the detection and modulation of nociceptive messages (Chizh and Illes, 2001) [34]. P_2X receptors are cation selective ion channels activated by ATP. They are involved in various physiological processes like the modulation of cardiac rhythm and vascular tone as well as macrophage activation and apoptosis. P_2X receptors can form homo- and heteromers from 7 different subunit and all receptor subtypes have specific expression patterns and cellular functions. For example, mice lacking the receptor subtype P_2X_3 show reduced responses to subcutaneous ATP injection (Cockayne et al., 2000) [39].

3.5.1. The TRPA1 Receptor

TRPA1 is unique among mammalian TRP channels as is has a large number of N-terminal ankyrin repeats that provide binding sites for many signaling molecules (Montell, 2005) [102]. TRPA1 orthologues are found in many diverse species (Clapham et al., 2003) [37] and TRPA1 can be activated and modulated by a wide range of chemical and physical stimuli. Besides the pungent ingredient of mustard oil or wasabi, allyl isothiocyanate (AITC, Bandell et al., 2004; Jordt et al., 2004) [6][66], TRPA1 is activated by allicin, the pungent ingredient of garlic (Bautista et al., 2005; Macpherson et al., 2005) [90][15]. More importantly, TRPA1 displays a crucial sensitivity to a range of environmental irritants like tobacco smoke as well as endogenously produced proalgesic agents (Bautista et al., 2006) [14], mediators generated after tissue damage. TRPA1 senses chemical damage (Macpherson et al., 2007) [91], is directly activated by formalin and mediates formalin induced pain (McNamara et al., 2007) [94]. TRPA1 is also triggered by noxious cold temperature drops (below 15°C) (Story et al., 2003) [130] although TRPA1 is not required for sensing cold (Karashima et al., 2009) [70] since TRPM8 is the main cold sensor in mice (Dhaka et al., 2007 and 2008) [44][43]. Further, the wasabi receptor is activated by reversible chemical alteration (Hinman et al., 2006) [59], conformational changes are induced by covalent modification of accessible cysteines (Macpherson et al., 2007) [89].

Moreover, TRPA1 lacking mice exhibit pronounced deficits in bradykinin evoked nociceptor excitation and pain hypersensitivity (Bautista et al., 2006; Bandell et al., 2004; Kwan et al., 2006) [14][6][74]. Bradykinin is an endogenous inflammatory peptide whose release can lead to hyperalgesia. Studies showed that TRPA1 also contributes to allodynia (Caspani et al., 2009)

[29] and enduring pain after nerve injury where mRNA levels are up regulated (Obata et al., 2005; Katsura et al., 2006) [109][71]. Additionally, selective blockade of TRPA1 attenuates pathological pain (Chen et al., 2011) [32]. TRPA1 also modulates mechanotransduction in cutaneous sensory cells (Kwan et al., 2009) [75].

TRPA1 is co-expressed with calcitonin-gene-related peptide (GCRP) (Story et al., 2003) [130] and mostly TRPV1. TRPA1 knock-out studies in mice (Bautista et al., 2006; Kwan et al., 2006) [14][74] highlight the crucial role of TRPA1 in nociception and establish TRPA1 as a significant drug target (Chen et al., 2011) [32].

3.5.2. The TRPV1 Receptor

The cation channel TRPV1 has been identified as one of the molecular receptors involved in sensing noxious heat (temperatures above 43°C). Besides sensitivity to heat and a weak susceptibility to changes in voltage, TRPV1 can be triggered by both low and high pH conditions (Dhaka et al., 2009) [45], by various chemical stimuli like capsaicin, the pungent component of chili peppers, other vanilliods like resiniferatoxin, or ethanol. Additionally, TRPV1 signaling is highly regulated by a variety of inflammatory agents and its gating is modulated by modifications including phosphorylation through Protein Kinase C (PKC), a keystone in cellular signal regulation. TRPV1 is mainly expressed in subsets of both slow, unmyelinated C and faster conducting, myelinated A nociceptive fibers. TRPA1 is mostly co-localized with TRPV1 although a small population of TRPA1+/TRPV1- cells has been recently identified (Braz et al., 2010) [23]. Protonation or TRPV1 shifts the temperature sensitivity curve toward lower temperature allowing the channel to be opened at body temperature in an inflammatory environment. A high-resolution cryo-EM structure of TRPV1 recently revealed insights into structure-function relationships and regulator binding sites (Liao et al., 2013; Cao et al., 2013) [82], [28]. TRPV1 knock-out studies in mice showed that the receptor is not necessary for normal heat detection but mutant mice show reduced thermal hyperalgesia.

3.5.3. The Phenomena of Pore Dilation

Recent studies revealed that unlike most ion channels TRP channels can undergo a dynamic change in ionic selectivity under certain conditions of prolonged and strong stimulation as it was first observed in the neuronal P_2X receptors P_2X_2 and P_2X_4 (Virginio et al., 1999; Khakh et al., 1999) [141][72]. While the exact mechanism remains unknown, this activity has been widely referred to as pore dilation. Not only a significant increase in cation permeability but also an induced conductivity to large cations (up to 900Da) like the dye YO-PRO-1 was observed which suggested the conception of a channel pore dilation process. These findings were unexpected and challenged the notion that selectivity would be like a fingerprint to a specific channel given by a rigid pore structure. Subsequent studies further revealed that intensive and prolonged capsaicin stimulation causes similar alterations in ion selectivity for TRPV1 (Chung et al., 2008) [36] with a parallel increase of calcium permeability by five-fold. Although heat and low external

pH alone do not suffice to trigger pore dilation in cell culture, both stimuli enhance selectivity changes when simultaneously applied with capsaicin. Given the central role of calcium in cell signaling in general and specifically in synaptic plasticity, this finding highly suggests a specific physiological function pointing to dynamic adaptation mechanisms. A near atomic resolution cryo-EM structure of TRPV1 revealed a possible dynamic flexibility of the selectivity filter region which could structurally explain a pore dilation phenomena (Liao et al., 2013; Cao et al., 2013) [82][28]. Pore dilation of TRPV1 has been so far only shown *in vitro* (Chung et al., 2008) [36] and can be modulated by N-glycolisation (Veldhuis et al., 2012) [140].

Similar behavior has been also reported for TRPA1 (Banke et al., 2010) [9] in DRG cell cultures despite controversial reports (Nakagawa et al. 2013) [107] which could be explained by the sensitivity of pore dilated activity to various experimental conditions. At higher extracellular calcium (2mM), about 17% of TRPA1 conductivity is carried by calcium, the pore diameter is dynamically adapting from about 11Å at restricted opening and 3Å in the dilated state after mustard oil stimulation (Karashima et al., 2010) [69]. In contrast, TRPM8 does not seem to show pore dilation (Chen et al., 2009) [33].

Following the discovery of ionic selectivity it has been speculated (Bautista et al., 2008) [13] that this mechanism might contribute to mechanisms of pain hypersensitivity. However, it is poorly understood whether pore dilation occurs in intact tissue and physiological implications are unknown. Indeed, there is still considerable argument about the pore dilation phenomena in general. One alternative explanations hypothesizes the activation of adjacent, secondary channels with a native high permeability like pannexin. Other studies develop a different model to explain permeability changes. Li et al. postulate that ion depletion processes create an apparent shift in selectivity for P_2X receptors although not the channel permeability but rather the available ions for conductance change (Li et al., 2015) [79].

3.6. Experimental Models for the Study of Chronic Pain

As mentioned before, assessing pain in animals is especially complex since they cannot verbalize the amount of pain they are experiencing. Therefore, only pain associated behavior can be observed, standardized and used as a proxy for the amount of pain experienced.

The Spared Nerve Injury (SNI) surgery has become a standard model for studying neuropathic pain related to peripheral injury. In contrast to inflammatory, crush or ligation models, SNI is a simple procedure but produces robust and reliable long-lasting pain-like behavior without excessive inflammation (Pertin et al., 2012) [112]. In addition, it allows to study both injured and intact neuron population and communication between then within the same ganglia. Inflammation based models like injections of Complete Freud's Adjuvant (CFA) are less specific in their effects, less robust and affect an unknown number of fibers within a given DRG.

The activating transcription factor 3 (ATF3) is a marker for axotomized neurons with a very high signal to noise ratio (Tsujino et al., 2000) [138]. Co-staining for ATF3 can distinguish injured and intact populations.

4. Objective of Research

4.1. Probing Nociceptive Activity in Intact DRGs

Nociceptive neurons and circuits detect and dynamically modulate pain signals generating both acute and persistent pain. Adaptation of pain sensitivity is beneficial when it facilitates protective measures but can be disadvantageous if persistent pain is transformed into pain hypersensitivity or chronic and neuropathic pain. These alterations can happen in the periphery after nerve damage or in the central nervous system in form of plastic changes of the circuitry. Nociceptor signaling is regulated by a variety of inflammatory agents released after cell death and nerve injury. These factors substantially modulate nociceptor activity by increased spontaneous firing, amplified transmitter release and enhanced excitability. Finally, the ion channels TRPA1 and TRPV1 have been shown to play a key role as polymodal integrators of multiple inflammatory mediators. In addition, recent studies have reported that the cellular permeability of nociceptive neurons is altered in a TRP channel dependent way.

My dissertation research aims to understand activation and functional implications of dynamic changes in permeability of nociceptive neurons. Modulation of the activity of pain neurons is critically involved in mechanisms leading to pain hypersensitivity. I therefore hypothesize that dynamic changes in permeability occur during nerve injury and play a role for the induction of hypersensitivity. Further, my research focusses on the interaction between different neuronal populations. Specifically, I want to elucidate if injury induced permeability contributes to crosstalk between injured and intact nociceptors.

I study permeability changes in intact dorsal root ganglia with a photoswitch compound recording from many cells at once with a multi-electrode array.

4.2. Interactions between Photoswitch Compounds and Voltage-gated Ion Channels

The photoswitch QAQ has been utilized for many different applications in neuroscience research. However, designing tailored experiments and correctly interpreting results require a sound knowledge and understanding of QAQ. Without detailed insights on QAQ‘s behavior inside neuronal cells, effects of QAQ block could be misunderstood and yield misled conclusions. Researchers apply QAQ for any type of experiment need to be equipped with further information to use this tool correctly.

In my thesis, I therefore want to understand more about QAQ‘s mechanism of action and study the interactions of QAQ with a well-known model for a voltage-gated ion channel.

Specifically, I strive to answer some of the following questions:

What is the affinity of *trans* and *cis* QAQ to the Shaker K^+ channel? Is there an optimal intracellular concentration with maximal block in *trans* and minimal current perturbation in cis at reasonable light intensities? Can *cis* QAQ block ion channels? Can QAQ bind to the closed channel? Further, we hypothesize that QAQ, like other quaternary ammonium compounds, interferes with gating of the channel and thus stabilizes the ion channel in either the open or closed conformation. Where in the outer or inner vestibule of the channel does QAQ reside during block? Is coordination with specific residues within the vestibule required for optimal block? Does the voltage across the membrane influence blocking properties? Does QAQ interact with the mouth of the selectivity filter? Moreover, could QAQ become trapped within the lumen once the channel closes? If QAQ is retained within the closed channel, can it photo-isomerize? Does QAQ interfere with the inactivation behavior of the channel? Moreover, how does QAQ compete with the ball peptide or other quaternary ammonium compounds?

All this information can help other scientists designing experiments more accurately and interpret results more insightful.

I want to answer those questions using inside-out patch electrophysiology from *Xenopus laevis* oocyte membranes. In addition, I am utilizing *in silico* molecular docking of QAQ into the lumen of various K^+ channels to estimate sterical flexibility of QAQ molecules within the channel and derive suggestions about a feasible mechanism of block.

III. Materials and Methods

1. Preparation of Photoswitch Compounds

Throughout all presented studies the orange colored Trifluoroacetic acid (TFA) salt of QAQ has been used which has a total molecular weight (MW) of 722.72 with the MW of QAQ itself accounting for 481.37. The di-formate salt (MW 586.72) and di-chloride salt (MW 552.27), both of black color, were tested as well but for consistency purposes not used. Using TFA is of advantage as it is physiologically inert and shows no known interactions with neuronal tissue. Furthermore, QAQ-TFA is more soluble in water than other QAQ salts.

For all photoswitch compounds, stock solutions were prepared from powder at concentrations of around 20mM in dd H_2O and stored in aliquots at -20° C to minimize the number of freeze-thaw cycles. No dimethyl sulfoxide (DMSO) or ethanol was used to dissolve stock solutions. Exact final concentrations were determined by spectroscopic means. A test sample was diluted to a μM range to ensure measurement in the linear range of the detector and concentrations were concluded from the absorption maxima at λ=362nm following the Beer-Lambert Law:

$$C_\lambda = \frac{E}{\epsilon_\lambda \cdot E \cdot d}$$

with E denoting total sample extinction (without unit), ϵ_λ denoting the compound specific chemical extinction coefficient in $\frac{l}{mol \cdot cm}$ at wavelength λ, d equals cuvette length in cm and c describes compound concentration in $\frac{mol}{l}$. ϵ_{362nm} was experimentally determined by a dilution series and linear regression of E values at λ_{362nm} over a linear range. The slope equals ϵ and takes a value of 29,000 $\frac{l}{mol \cdot cm}$ for QAQ-TFA solutions in water.

On the day of experiment, an aliquot stock solution was thawed and diluted to a final concentration of 300μM in artificial cerebrospinal fluid solution (ACSF) or oocyte ringer solution (ORI) depending on the experimental setting. Final concentrations were again confirmed spectroscopically.

The extinction coefficient for QAQ derivative compounds is very similar to QAQ and thus ϵ for QAQ was used throughout. Further, for testing of the QENAQ compound its TFA salt (MW 738.79) was dissolved and the chloride salt for DENAQ (MW 455.59) was used for testing this compound on DRG tissue.

Individual photoswitch batches were synthesized either in-house by Michael Kienzler and Wan-Chen Lin (UC Berkeley) or by an external contractor (Jubilant Chemsys, India).

2. Extracellular Recordings from Intact Mouse Dorsal Root Ganglia

In order to read out permeability changes in an intact nociceptor population, we employed multi-electrode arrays to record from intact dorsal root ganglia tissue. Multi-electrode arrays enable extracellular recordings from many cells as once in intact nociceptive DRG tissue delivering high-throughput read-outs from many cells at once on a population level (Figure 14). This way the native geometry of peripheral and central axons as well as somata architecture within the DRG are preserved and other DRG culturing artefacts can be avoided (Zimmermann et al., 2009) [151]. Given the absence of spontaneous activity, action potential firing was elicited using either a suction electrode enclosing the peripheral nerve bundle or wires forming a simple cuff stimulation electrode (Figure 14).

Light sensitivity of elicited action potentials served as readout of QAQ entry which correlates to nociceptor permeability. Higher levels of conferred photosensitivity correspond to higher conferred cellular permeability levels.

2.1. Animals

Male wild type mice (C57BL/6J strain, Jackson Laboratory), homozygous TRPV1-/- mice and homozygous double knock outs TRPV1-/-, TRPA1-/- (gift of Diana Bautista, UC Berkeley), 2-6 months old were used in all experiments. At least 2-3 different animals were used for each experiment, multiple tissue samples were collected from one mouse. All animal use procedures were approved by the UC Berkeley and UC San Francisco Institutional Animal Care and Use Committee and were conducted in accordance with the NIH Guide for the Care and Use of Laboratory Animals and the policies of the International Association for the Study of Pain.

2.2. Preparation of Intact Dorsal Root Ganglia (DRG) Tissue from Adult Mouse

Adult mice were deeply anesthetized with isoflurane (Piramal Healthcare, India) and quickly sacrificed by cervical dislocation. The skin covering the dorsal side of the mouse was removed and the peripheral sciatic nerves were isolated from the surrounding muscle. Fibers were transected about 5mm distal to the sciatic plexus preserving about 2.5-3cm of total nerve fiber. Following transection the spinal column from the upper cervical vertebrae to the lower lumbar region was carefully detached from the rest of the mouse and placed in cold (4° C) artificial cerebrospinal fluid

solution (ACSF, buffered at pH 7.4, in mM: 124 NaCl, 4 KCl, 2 $MgCl_2$, 2 $CaCl_2$, 26 $NaHCO_3$, 20 D-glucose, 2 Na Pyruvate, 0.4 Ascorbic Acid), constantly equilibrated with 95% O_2 and 5% CO_2 gas (Bio-Blend Mix, Praxair, USA) to stabilize pH and ensured oxygenation. $CaCl_2$ was added after oxygenation to avoid precipitation. A laminectomy from the thorax to the sacrum revealed the spinal column which was subsequently removed and severed from the peripheral nervous system exposing the DRGs. The tissue was dissected while being submerged in cold, oxygenated ACSF. Finally, bone structures of the spinal column were gently opened to take out the lumbar L3 to L6 DRG segments. Only the most outer layer of the epineurium was removed, leaving the tissue intact otherwise. After dissection, DRG preparations were placed on a floating nitrocellulose membrane (Sartorius Stedim Biotech, USA) in an oxygenation chamber keeping the tissue at the air-solution interface of equilibrated ACSF at room temperature (18-20° C) to recover for 30-60 min before the start of recordings.

All solutions used during dissection and recording were prepared fresh or stored no more than 3 days at 4° C. Before the start of an experiment, all solutions were filter sterilized (0.22μm) as well as temperature (on ice for dissection, 37° C for recording) and pH equilibrated.

2.3. Multi Electrode Array Recordings from Intact Dorsal Root Ganglia

Intact DRG tissue was mounted onto a multi electrode array (MEA) chip (MEA60-200 3D GND, Qwane Bioscience, Switzerland) consisting of 60 3D-shaped platinum electrodes penetrating 60μm into the tissue spaced at 200μm (Figure 14). The tissue was secured in place to ensure optimal contact using a 'harp'made from dialysis membrane stretched over thick platinum wire and bonded with super glue; the wire was U-shaped to allow the nerve to exit without being crushed. The MEA chip was mounted on an MEA1060-UP-BC amplifier (Multi Channel Systems, Germany) and placed on the stage of an upright microscope (Labophot-2, Nikon, Japan). Peripheral nerves were electrically stimulated using either a suction electrode or hook wire electrodes (Figure 14) driven by an external, battery driven DS2 stimulus isolator (Digitimer, United Kingdom). Both stimulation methods have distinct advantages which are listed in Figure 14.

In the suction electrode setup, the nerve bundle was gently led into a manipulator-mounted glass suction electrode of appropriate size. Far distal nerve branches were selectively stimulated by guiding a fiber bundle over two closely spaced chlorinated silver hook electrodes immersed in mineral oil and electrically isolated by a grease seal. Stimulation mode (constant current vs. constant voltage), blanking time of the amplifier (200-2,000μs), stimulus pulse length (20-600μs) and stimulation strength were optimized to yield extracellular responses with maximal response amplitude while minimizing electrical artifacts at the beginning of a stimulation episode. DRGs were checked for response to stimulation at 1Hz prior to recording. Evoked responses were recorded at 20kHz sampling rate with MC-Rack v4.5.12 software (Multi Channel Systems, Germany). Raw voltage traces were filtered with a second order Butterworth high pass filter using a cut-off frequency of 300Hz and hard wired amplifier low pass filter of 10kHz. Recordings after stimulation with hook electrodes were filtered with a second order Butterworth band pass filter isolating the frequency interval between 300Hz and 1kHz. Illumination was provided by a

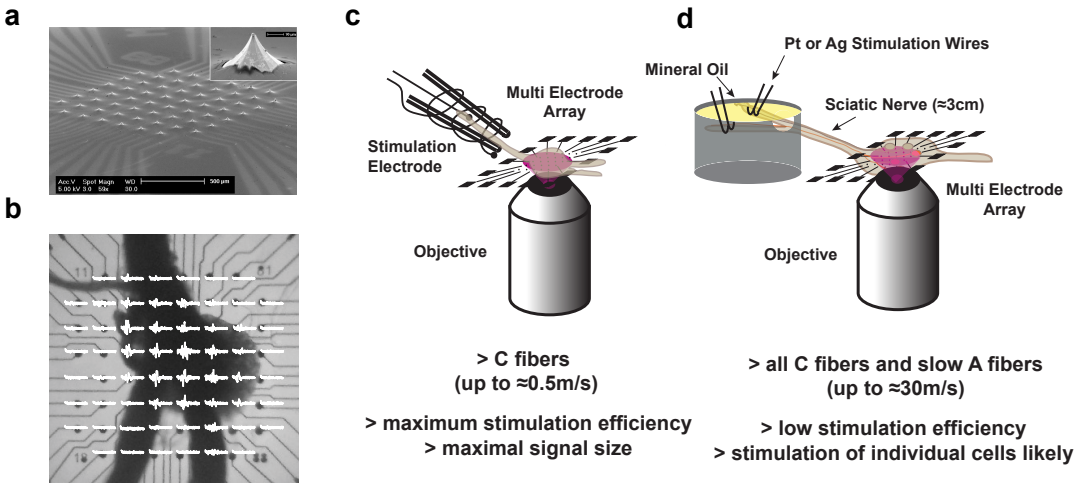

Figure 14.: Multi-electrode Recordings from Intact DRG Tissue.
a. Multi-electrode array chip for extracellular recordings with close-up of a tip-shaped Pt electrode protruding into the tissue (Metz et al., 2001) [123]. **b.** Intact DRG tissue mounted onto a transparent MEA chip. **c.** Schematic presentation of a suction electrode setup: peripheral nerve bundle is tightly inserted into the electrode to optimize stimulation efficiency. Due to the vicinity of stimulation and recording electrode, the stimulation artefact is masking any other fibers than C fibers in the recording. **d.** Schematic presentation of a wire electrode setup: a peripheral nerve fiber bundle is guided over to parallel, chlorinated silver or platinum hook electrode and submerged in mineral oil to reduce artefacts and increase stimulation efficiency. Up to 3cm distance between site of stimulation and recording allow temporal separation of both C and slow Aδ fibers from the stimulation artefact.

Spectra-LCR-3X-A2 LED light source (Lumencor, United States) routed through a 4x objective, resulting in intensities of 22mW/cm^2 for 542nm and 9.3mW/cm^2 for 390nm light, respectively. White light exposure for QENAQ and DENAQ experiments was provided by a Nikon IR-filtered 100W Mercury Lamp at light intensities of around 15mW/mm^2 for wavelengths between 300 and 700nm. Stimulator, recording software and light source were centrally controlled by a custom made Matlab (MathWorks, United States) program triggering TTL pulses through a BNC-2110 I/O card (National Instruments, United States). The MEA chamber was continuously perfused with oxygenated ACSF at about 3ml/min and recordings were performed at constant 37° C. Unless otherwise noted, the QAQ photoswitch compound was incubated at 300μM solution in ACSF for 5 min. QAQ concentration was confirmed using a photo spectrometer measuring absorbance at 362nm as described above. When using blockers, the DRG was pre-incubated with the blocker for 5min before the application of QAQ with the blocker. The DRG was always washed with ACSF for 10min after incubation before recording to ensure complete removal of extracellular photoswitch. Recordings were done at a stimulation rate of 10Hz for a 5s period while illuminating the DRG with 380nm or 500nm light, respectively (Figure 15). For hook electrode recordings, fibers were probed at 2Hz. The start of recordings was synchronize to the onset of the stimulus pulse and recordings lasted 50 to 90ms for each stimulation sweep. Each experiment consisted of 5 cycles of 30s under 380nm light followed by 30s under 500nm light

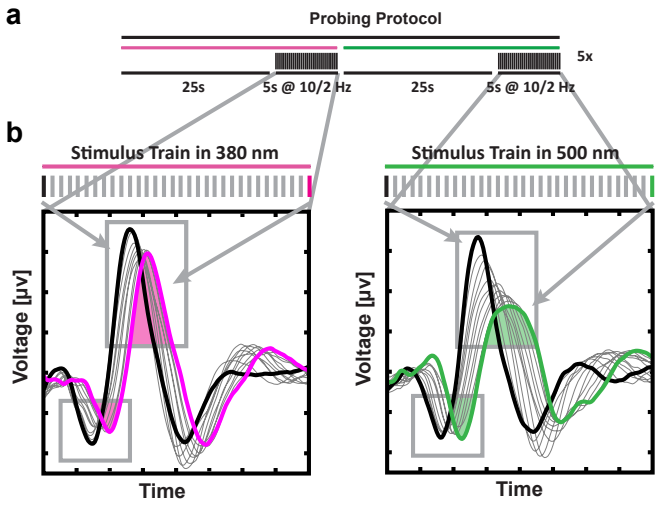

Figure 15.: Extracellular MEA Signals with QAQ Blocking and Unblocking.
a. Representation of a standard probing protocol: 25s illumination in one wavelength of light are followed by a 5s of 10Hz electrical stimulation train. The entire protocol is repeated 5 times. **b.** Example signal traces of compound action potentials in 380nm (left panel) and 500nm (right panel) light, respectively.

(Figure 15). The DRG was stimulated for the last 5s under each wavelength of light, allowing 25s to recover from adaptation in between stimulation episodes. For recordings using silver wire hooks as stimulation electrodes the detection threshold was conservatively set to 3.5 times of the standard deviation of a noise recording.

2.4. Analysis of MEA Data

Given the synchronous triggering of spikes in multiple units, recorded signals at individual electrodes are non-linearly integrated from multiple source and the resulting signal can be described as extracellular compound action potentials (CAP) (Figure 15). Therefore, CAP shape and size fluctuates considerably and a categorization is not feasible. However, since the individual components of those complex signals are derived from units that are either light-sensitive or not, the resulting non-linear combination also shows light dependence in some aspects. To explore this phenomena further and to quantify imparted photosensitivity, we developed a custom-made data handling and analysis program.

2.4.1. Data Processing

Multi electrode data was recorded in the mcd file format (Multi Channel Systems, Germany) and data was imported into Matlab using the import functionality of the FIND program bundle

(University of Freiburg, Germany) (Meier et al., 2007, http://find.bccn.uni-freiburg.de) [95]. Subsequent analysis was performed by a custom made Matlab program package.

While blanking the recording electrodes during stimulation and optimizing stimulus conditions minimize the stimulation artifact, in most recordings such an artifact could not be completely avoided. This artifact was excluded from the analysis and evoked signals were detected by a threshold manually set beyond the noise level. For hook electrode recordings, a dynamic threshold of 3.5 times above the standard deviation of a manually defined baseline noise region was used as the signals are significantly smaller compared to suction electrode stimulations. Overall responses were divided in negative and positive deflections and each deflection was analyzed separately, considered as one signal. A Matlab algorithm extracted 18 parameter values for each signal detected and performed standardized quality control conservatively excluding small and/or irregular signals.

2.4.2. Statistical Analysis

Signal parameters were averaged over five recording cycles in each wavelength and different measures of photosensitivity were determined. Since QAQ functions as an open channel blocker the last 1.5s of the 5s stimulation episode were used to calculate normalized photosensitization (or Photoswitching Index, PI) which is defined as:

$$PI = \frac{signal_{380nm} - signal_{500nm}}{signal_{380nm} - signal_{500nm}}$$

PI ratios were pooled by condition from multiple animals and compared using non-parametric significance tests like the Mann-Whitney/Wilcoxon u test and the Kruskal-Wallis test with Dunn‘s post hoc analysis.

3. Pharmacology

Various pharmacological reagents were used to selectively block certain ion channels or receptors. Mostly, comprehensive cocktails of multiple blockers were used to achieve universal inhibition for different activation mechanisms. Unless otherwise stated, all blockers were prepared fresh from their respective stock solutions und diluted to working concentration in ACSF. Blocker mixes were applied during QAQ incubation and preceding QAQ exposure.

The following abbreviations were used in Table 2: EtOH is ethanol; DMA is 5-(N,N-Dimethyl) amiloride; BCTC is N-(4-tertiarybutylphenyl)-4 (3-cholorphyridin-2-yl) â€“ tetrahydropyrazine1(2H)-carboxamide; TNP-ATP: 2‘,3‘-O-(2,4,6-Trinitrophenyl) adenosine 5‘-triphosphate.

Agonist	**Description**	**Solvent**	$\mathbf{c}_{final}$	**Supplier**
HC030031	Selective TRPA1 antagonist blocking AITC and formalin induced activation	DMSO	100μM	Tocris Bioscience
AP-18	Reversible TRPA1 antagonist blocking Yo-PRO uptake	DMSO	100μM	Tocris Bioscience
DMA	TRPA1 antagonist blocking pore dilation	H_2O	100μM	Sigma-Aldrich
BCTC	Competitive TRPV1 antagonist blocking acid and Capsaicin activation	DMSO	10μM	Tocris Bioscience
AMG 9810	TRPV1 antagonist inhibiting capsaicin-, proton-, heat- and endogenous ligand-induced activation	EtOH	10μM	Tocris Bioscience
Capsazepine	Selective vanilloid receptor antagonist	EtOH	100μM	Tocris Bioscience
TNP-ATP	Competitive antagonists of different P2X receptors	EtOH	100μM	Tocris Bioscience

Table 2.: Table of Antagonist Reagents Used for DRG Recordings.

To antagonize TRPA1 channel opening, we used a blocking cocktail consisting of HC030031, AP-18 and DMA (for details see Table 2). DMA has been shown to block both regular and pore-dilated TRPA1 activity (Banke et al., 2011) [10]. In addition, Ap-18 has been shown to block Yo-PRO-1 uptake (Chen et al., 2009) [33]. Unless otherwise noted, TRPV1 antagonist mixtures included BCTC, AMG and capsazepine (for details see Table 2).

To selectively activate receptors, common agonist at previously reported concentrations were used as listed in the following overview:

Agonist	**Description**	**Solvent**	$\mathbf{c}_{final}$	**Supplier**
Capsaicin	TRPV1 agonist	EtOH	1μM	Sigma-Aldrich
AITC	TRPA1 agonist	DMSO	30μM	Tocris Bioscience
Menthol	TRPM8 agonist	EtOH	100μM	Sigma-Aldrich
bzATP	$P2X_7$ agonist	H_2O	250μM	Sigma-Aldrich

Table 3.: Table of Agonist Reagents Used for DRG Recordings.

4. Experimental Pain Models: Spared Nerve Injury and Sciatic Nerve Ligation

Under isoflurane anesthesia, the terminal branches of tibial and peroneal nerves but not the sural nerve were transected for Spared Nerve Injury (SNI). In contrast, all branches of the sciatic nerve were affected for the Sciatic Nerve Ligation (SNL) procedure. Recordings were performed 1 or 7 days post-surgery as described above.

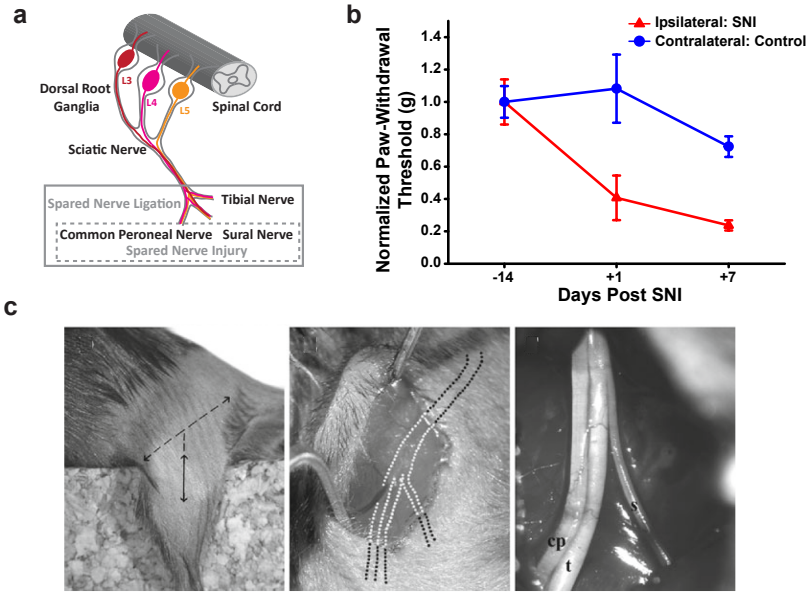

Figure 16.: Surgical Procedures for SNI and SNL.
a. Illustration of used surgery models. Incision of the skin on the lateral side of the left thigh reveals the three major sciatic nerve branches. In the Spared Nerve Injury model (SNI), both the tibial and the common peroneal nerve are injured through transection while leaving the sural nerve in intact. In contrast, during Sciatic Nerve Ligation (SNL) no sciatic branches are spared. For each animal the contralateral side served as sham control where the skin was opened but no nerves severed. **b.** Von Frey test for mechanical hyperalgesia. SNI induces pain hypersensitivity 24 hours after surgery at the ipsilateral hind paw while the contralateral sham surgery leg is not affected. **c.** Photographs of SNI surgery of a mouse. Dashed lines indicates incision and dotted lines display position of sciatic bifurcation. cp abbreviates common peroneal, t tibial and s sural nerve. Adapted from Pertin et al., 2012 [112].

5. Resiniferatoxin Treatment

Resiniferatoxin (RTX, Sigma-Aldrich, United States) was intraperitoneally administered in increasing doses once a day (30 μg/kg (day 1), 70 μg/kg (day 2), 100 μg/kg (day 3), 200 μg/kg (day 4) and 200 μg/kg (day 14)) at least 1 week prior to dissection and recording. The effect of

RTX treatment was confirmed by negative responses to the heat plate behavioral test at normally noxious temperatures.

6. Behavioral Pain Assays

Quantifying pain in animals is challenging. Typical pain behaviors are used to serve as a correlate for perceived pain in a mouse. To measure mechanical hypersensitivity the Von Frey Test has been historically used. The rodent hind paw is probed with calibrated filaments (Von Frey hairs) of increasing stiffness. The mechanical force at which the mouse withdraws its paw is considered the pain threshold. The animal is placed on an elevated mesh, left for 1h to be acquainted with the new environment and then probed with the filaments from below the animal. Multiple sessions are needed to establish a stable withdrawal response.

After SNI, pain behavior was verified with the Von Frey tests to check if the phenotype of mechanical allodynia indeed was induced (Figure 16b). This was done for a first set of mice only as it is reasonable to assume that constant surgical techniques produced reliable phenotypes in subsequent animals.

To verify successful RTX treatment and systemic loss of TRPV1 expressing cells, treated mice were subjected to a hot plate test. Animals were placed onto a heated surface unable to escape. The temperature is increased gradually and pain behavior like licking of paws, vocalization and attempts to escape are used to determine the detection of heat and associated pain.

7. Imaging of Dye Uptake

7.1. Dye Loading into *Ex Vivo* DRGs

For dye loading experiments, adult mice were anesthetized with sodium pentobarbatol and DRG tissue was removed as described above. **Ex vivo** DRGs were incubated with 100nM Yo-PRO-1 solution (containing 0.0001% DMSO, Yo-PRO-1 iodide at stock concentration of 1mM from Life Technologies, United States) in equilibrated ACSF for 15min at room temperature. The incubation solution also contained 1:2000 4‘,6-diamidin-2-phenylindol (DAPI), a nuclear marker, to identify all individual cells for counting.

7.2. Immunohistochemical Staining of DRG Tissue

Extracellular Yo-PRO-1 was washed away for 5 min, fixed with 4% paraformaldehyde (PFA) in phosphate buffered saline (PBS) at room temperature for 1h and cryoprotected in 30% sucrose for 4h. Whole DRGs were frozen in Optimal Cutting Temperature (OCT) compound on dry ice.

During the entire process tissue samples were kept covered and protected from light to preserve maximal fluorescence. Sections of 12μm thickness were cut on a cryostat. After incubation for 1h at room temperature in PBS with 10% normal goat serum (NGS) and 0.3% Triton X-100 (blocking buffer), sections were immunolabeled for 2 days at 4° C in 1% NGS + 1% Bovine Serum Albumine (BSA) in PBS with the following antibodies and concentrations: guinea pig anti TRPV1 (gift of David Julius, UCSF) at 1:10,000, mouse anti N52 (Sigma, United Sates) at 1:10,000, rabbit anti ATF3 (activating transcription factor 3) at 1:1,000, and streptavidin-conjugated IB4 (isolectin B4) at 1:1,000. Sections were washed 3x with PBS and then incubated with Alexa 594 and 647 conjugated secondary antibodies at 1:600 in 1% NGS + 1% BSA in PBS at room temperature for 2h. After washing, the sections were mounted on slides using Fluoromount-G (Southern Biotech, United States) and protected with glass coverslips.

7.3. Confocal Fluorescence Microscopy and Imaging Analysis

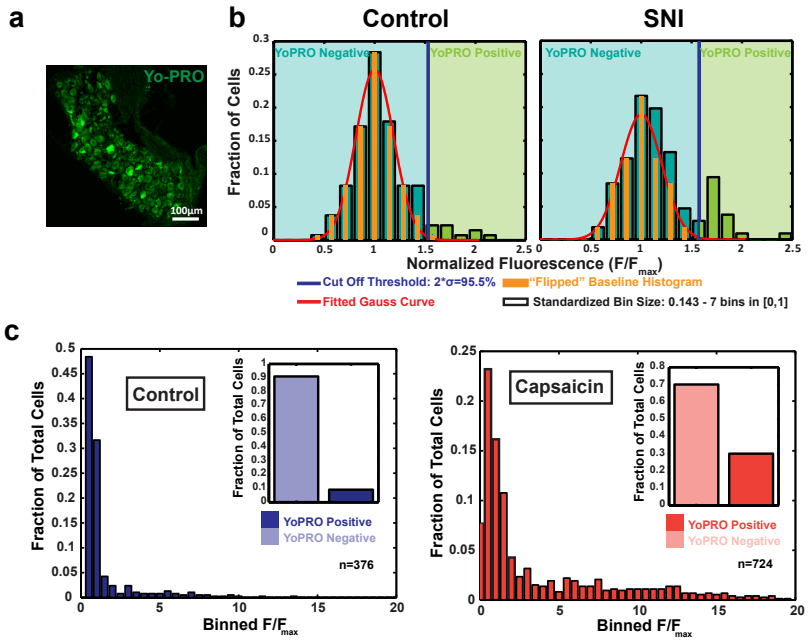

Figure 17.: Analysis of Yo-PRO-1 Uptake.
a. Example fluorescence image of a Yo-PRO-1 labeled cryo-scetion. **b.** Histogram of fluorescence distribution of individual cells within one example image for a control (left panel) and SNI (right panel) DRG. **c.** Cell fluorescence distribution for life cell counting. In the absence of cryo-sectioning artefacts, Yo-PRO-1 positive cells are easier to identify. Histograms were fitted to Gauss curves as described to determine cut-off for separation into positive and negative cells.

After staining, DRG sections were examined by confocal fluorescence microscopy (Zeiss LSM 780 NLO AxioExaminer, Germany) imaging Yo-PRO-1 separately and the remaining three fluorescent channels simultaneously ('blue'for DAPI: 405nm excitation, 410-473nm emission capture,

'green'for Yo-PRO-1: 488nm excitation, 499-578nm emission capture, 'yellow'for ATF3: 561nm excitation, 586-648nm emission capture, 'red'for either IB4, TRPV1 or N52: 633nm excitation, 665-750nm emission capture). For each section, a z-stack of 20 slides at 0.54μm thickness was imaged with a 2048 x 2049 pixel (20x objective, 607.28μm x 607.28μm) resolution and average intensity projections were used for further analysis.

The outer contour of individual cells with visible nucleus was marked and average fluorescence intensity per channel was measured using Image J imaging software (FiJi package version 1.49b, NIH). For each individual section with a sufficient cell number (more than 40 cells), the distribution of Yo-PRO-1 fluorescence signals was normalized to the bin with maximal cell count at a standardized bin size of 0.143 a.u. (arbitrary units) bringing the histogram to align with 1 on a F/F_{max} scale. Subsequently, the histogram values below 1 were mirrored to the range above 1 to extract an assumed 'baseline signal'. The resulting symmetric distribution was fitted using a simple Gauss model and a cut-off fluorescence signal of twice the standard deviation of the fitted curve was defined. All cells with intensities greater than the cut-off were considered as 'Yo-PRO-1 positive', all other cells as 'Yo-PRO-1 negative'(Figure 17). For the analysis of antibody labels a simple threshold for fluorescence was assumed to assign positive and negative cells, respectively.

Sensory cells are gradually myelinated and thus, N52 labeling is gradual as well. For simplification purposes, a categorization in myelinated and unmyelinated neurons is helpful. To determine a reasonable cut-off separating both populations, the N52 signal was plotted over cell size. This curve shows a characteristic double-sigmoid shape as myelination increases with cell size (Figure 18). The first turning point is consistently used as general separation marker between myelinated and unmyelinated populations.

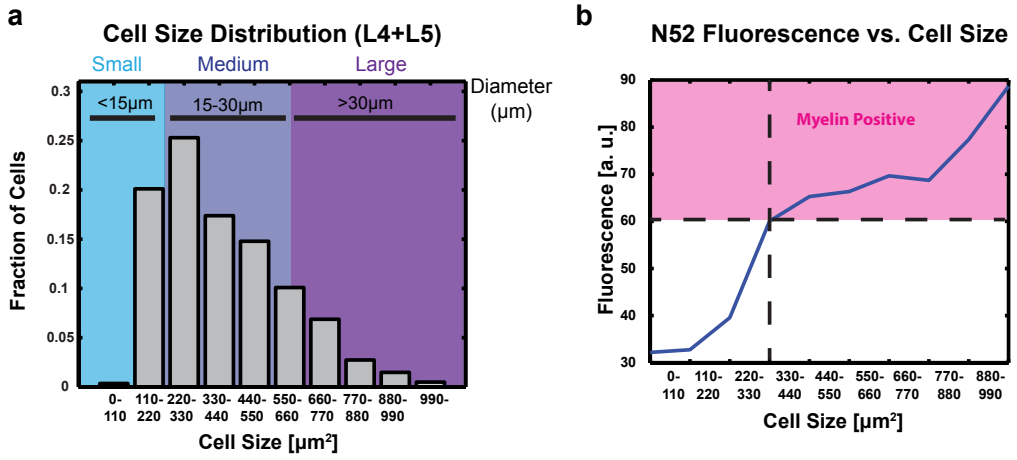

Figure 18.: Analysis of Myelin Immunohistochemical Labeling.
a. Size distribution of cells after cryo-sectioning and staining. **b.**N52 signal distribution over cell size used to determine threshold for categorization of cells into myelinated and unmyelianted.

8. Preparation of *Xenopus* Oocytes

8.1. Harvesting and Handeling of Oocytes from *Xenopus laevis*

In full compliance with approved procedures by the UC Berkeley Institutional Animal Care and Use Committee, oocytes of maturation stage I to IV from *Xenopus leavis* frogs were surgically removed from female adults by laparotomy. The animals were anesthetized by tricaine methane-sulfonate (MS-222, Western Chemical, United States) at neutral pH and individual frogs were used up to 6 times to harvest eggs. Removed oocytes were pre-digested with 1-2 mg/ml collagenase (Sigma, United Sates) to support defolliculation and the connective membranes were manually removed to isolate individual cells. Oocytes with their vitelline membrane intact were then kept at 16° C in Oocyte Ringer solution (ORI, in mM: 96 NaCl, 2 KCl, 1$MgCl_2$, 1.8 $CaCl_2$, 5 4-(2-hydroxyethyl)-1-piperazineethanesulfonic acid (HEPES), adjusted to pH 7.4 with NaOH) until the experiment.

8.2. Expression of Ion Channel Proteins in *Xenopus* Oocytes

To efficiently express ion channel proteins in oocytes membranes, mRNA fragments encoding for respective genes were injected into cells for direct translation. All procedures involving RNA were carried out with extra care and pre-treatment of bench spaces and tools with RNAase (RNAse Away, Molecular Bioproducts, United Sates). RNA constructs were synthesized from linearized DNA plasmids containing the target gene, e.g. Shaker (IR), a promoter sequence and a T7 site as previously described (Smart and Krishek, 1995) [133]. Shaker constructs were cloned into a PBS KS(+) bluescript backbone vector. For plasmid linearization, 10μg DNA were incubated with an appropriate restriction enzyme in a 30μ total reaction volume for 1 h at 37° C. After DNA purification using a PCR purification kit (Qiagen, United States), 0.5μg linearized DNA at a minimum concentration of 170ngμl were transcribed *in vitro* supplemented by 5μl of mixed nucleoside triphosphate (NTP) with the mMessage mMachine T7 kit (Applied Biosystems, United States). The reaction was stopped by adding 15μl nuclease-free water and 15μl LiCl for RNA precipitation during chilling at -20° C for at least 30min. Precipitated RNA was concentrated by centrifugation for 15min at 4° C at maximum speed. Supernatant was carefully removed and the pellet was washed with ice cold 70% ethanol, air dried and re-suspended in 12μl nuclease free water. Finally, RNA concentration was determined using spectroscopy and stored at -80° C until injection.

RNA injection took place 12 to 48 hours after oocyte harvest with a Nanoinject II microinjector (Drummond Scientific, United States) and injected oocytes were stored in ORI for 2-3 days at 16° C at regular atmosphere before recording. Injection pipettes were pulled from borsillicate capillaries (Microcaps with inner diameter of 0.70mm and an outer diameter of 0.97mm, Drummond Scientific, United States) with a micropipette puller (P-97, Sutter Instruments, United States). Tips were broken over a tissue cloth to have an approximate tip diameter of 15μm,

backfilled with colored mineral oil and loaded with RNA solution. RNA was diluted in ORI to a final concentration of 0.05-1ng/nl and 25-50nl were injected totaling 2.5-5ng of RNA. For optimal expression and oocyte health, RNA was injected at the midline, the equatorial band, between animal and vegetal pole (Smart and Krishek, 1995) of stage IV oocytes sized around 1-1.2mm [133], see Figure 19.

After injection, storage at 4 ° C slows protein expression and was sometimes used to allow good recordings from oocytes 3-4 days after injection. As some oocytes die after injection and contaminate the storage solution, ORI buffer was replaced every day.

9. Electrophysiological Recordings from Inside-Out Membrane Patches

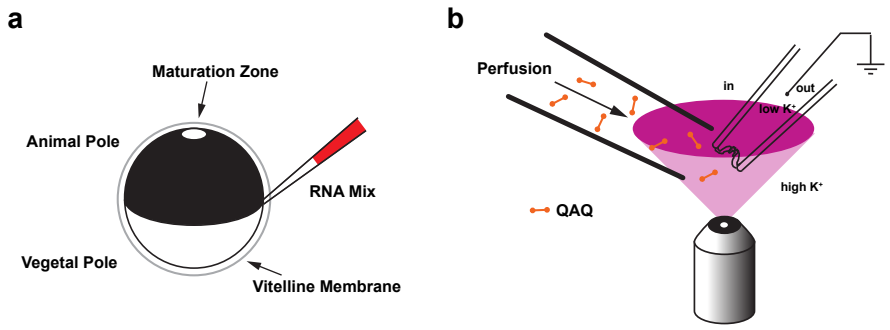

Figure 19.: Electrophysiology on *Xenopus* Oocytes.
a. Diagram of a *Xenopus laevis* mature oocyte of stage IV. **b.** Schematic representation of an inside-out patch recording setup with fast application perfusion tube.

Filamented borsillicate glass pipettes (Warner Instruments, United States; outer diameter 1.5mm, inner diameter 1.17mm) were pulled suing a micropipette puller (P-97, Sutter Instruments, United States). After pulling, heat polishing was used to shape pipette tips and optimize resistance in solution. Pipettes had resistances between 1-2MΩ with an opening of 2-4μm and were filled with pipette solution mimicking extracellular ion composition (in mM: 150 NaCl, 10 KCl, 10 HEPES, 1 $MgCl_2$, 3 $Cacl_2$, adjusted to pH 7.4 with NaOH, filtered 0.2μ m, aliquoted and frozen at -20° C).

A chloride coated silver wire electrically connects the pipette to the amplifier after mounting the pipette onto the amplifier‘s head stage. Pipette and reference electrode were chlorinated freshly by dipping into highly concentrated hydro chlorite solution for 10min prior to each experiments. An air-tight pressure system was used to apply negative or positive suction to the pipette. The entire setup was placed on an air cushioned stabilization table and shielded by a Faraday cage to minimize electrical noise.

9.1. Pulling of Inside-Out Membrane Patches

To remove the outer vitelline membrane, an oocyte was placed in hypertonic stripping solution (in mM: 200 K^+ asparate, 20 KCl, 1 MgCl, 10 ethylene glycol tetraacetic acid (EGTA), 10 HEPES, pH 7.4) for a few minutes to shrink the cell volume and help detach the vitelline membrane from the oocyte (Brown et al., 2008) [24]. Alternatively, the outer membrane was carefully peeled off directly with fine forceps without damaging the cell membrane.

After removal of the vitelline membrane, oocytes were transferred into the recording chamber filled with bath solution (in mM: 160 KCl, 0.5 $MgCl_2$, 1 EGTA, 10 10 HEPES, adjusted pH 7.4 with KOH). Bath solution mimics intracellular ion compositions and all electrophysiology experiments were conducted at room temperature.

A high resistance seal (GΩ seal) between the pipette and the cell membrane was established before the pipette was retracted rapidly ripping out a piece of membrane which covers the opening of the pipette forming an inside-out patch.

9.2. Voltage Clamp Recordings

Electrophysiological signals were amplified by a Patch Clamp PC-501A amplifier (Warner Instruments, United States), low-pass filtered at 1kHz, digitized at 5kHz by a Digidata 1322A converter (Molecular Devices, USA), and acquired with Clampex 10 software (Molecular Devices, USA).

A gravity driven perfusion system with a self-made line connector was used to quickly apply different solutions to the membrane patch. For that purpose, the pipette tip was guided into a polyethylene tube ending of the perfusion system. With minimal dead volume compounds can directly presented to the patch with relatively short time delay (Figure 19).

Electrical current through Shaker K^+ channels was stimulated by depolarizing the membrane voltage from -60mV to +40mV (Δ 100mV driving force initiating an outward current) during a 200ms time window. For regular recordings, currents were probed at 0.5-1Hz frequency. Currents showed mild slow inactivation over time which was corrected by linear modeling of current decrease over the period of the experiment.

Prior to the probing pulse, a seal test stepping from -60 to -80mV for 50ms was performed to ensure the stability of the recording and possibly correct for leak in post analysis.

9.3. Light Application

Illumination of membrane patches and QAQ photoswitching was provided by a Lambda-LS xenon lamp (Sutter Instruments, United States) with 379$\pm$ 17nm and 500$\pm$ 8nm band pass filters and a 125W light source. The light beam was led through a 20x objective (Nikon Fluor, Japan, Numerical Aperture (N.A.) 0.75). Measured at the objective aperture using a handheld optical

power meter (1918-C, Newport, United States), this light source yielded intensities of 500μW/cm^2 for 500nm and 3.85mW/cm^2 for 380nm light, respectively.

9.4. Analysis of Electrophysiological Data

Electrophysiological data was recorded with Clampex data acquisition software (Molecular Devices, United States) and stored in abf format. A custom-made Matlab program (Mathworks, United States) was used to convert, concatenate and analyze abf files. The steady state currents from repeatedly probing Shaker were determined and displayed as time series.

Dose-response curves were created utilizing the following model equations:

$$I_c = A_1 + \frac{(A_1 - A_2)}{(1+10^{log(x_0 - c)\cdot p})}$$

where I_c=current at concentration c, p=Hill coefficient, 10^{logc_0} = IC 50, A1=bottom and A2=top asymptote.

10. Molecular Docking *In Silico*

Molecular models of the three-dimensional structure of the open channel Kv1.2-2.1 chimera (Long et al., 2007) [87] were used to dock *cis* and *trans* QAQ molecules into the lumen of the channel. Molecular docking was carried out in Glide 5.7 implemented in Maestro 9.2 (Schr$\acute{}$odinger Inc, United States). The x-ray structure was used to create a grid after the addition of hydrogen atoms and the removal of non-protein moieties. A QAQ 3D structure was docked ito this grid using the Standard Precision algorithm. A maximum of 100 poses were listed but likelihood scores of the first hits were very similar. The top hit was plotted.

IV. Results

1. Probing Nociceptive Activity in Intact DRGs

1.1. Optimization of Multi Electrode Data Analysis

Extracellular electrodes record electrical signals from an unknown number of cells in their vicinity. External stimulation synchronizes spiking and signals are integrated from multiple units in a non-linear fashion. In addition, QAQ changes the shape of action potentials in different ways due to its effects on multiple voltage-gated channels (Figure 6). This contributes to the complexity of recorded signal.

Those factors make it impossible to assign recorded potentials to individual units effectively masking single cell information. Hence, spike sorting techniques like principal component analysis cannot be applied. In order to boost sensitivity of QAQ detection under these circumstances, we devised a tailored analysis protocol that evaluates signal deflections of compound potentials individually without any assumption of signal origin (Figure 20). It is reasonable to assume that individual components of complex signals are differentially influenced by individual signal sources which might or might not exhibit photosensitivity.

Figure 20 outlines the basic steps converting extracellular signals into an abstract measure of conferred photosensitivity, called Photoswitching Index (PI). The PI value is defined as the normalized difference between signal strength in 380nm and 500nm light, hence the difference between uninhibited and blocked response (see Methods for more details). Eventually, individual PI values can be correlated with permeability levels, higher PI implies a higher permeability.

This optimized analysis flow presents a few advantages compared to previously applied analysis protocols and takes some key properties of QAQ action into account. Sorting complex voltage signals into deflections crossing a certain threshold does not bias the analysis as both negative and positive deflections are equally frequent and show similar levels of photosensitivity (Figure 21a). Further, QAQ is a use-dependent open channel blocker and thus, full blocking effect is reached just after ion channels have been opened for some time. Therefore, QAQ block increases and stabilizes toward the end of a stimulus train if QAQ is present in the cytosol. If QAQ was unable to enter a cell, the signal will only slightly desensitize during stimulation but this effect is not light-sensitive. Focusing further analysis on the last episodes of stimulation therefore increases QAQ detection sensitivity, see Figure 21b.

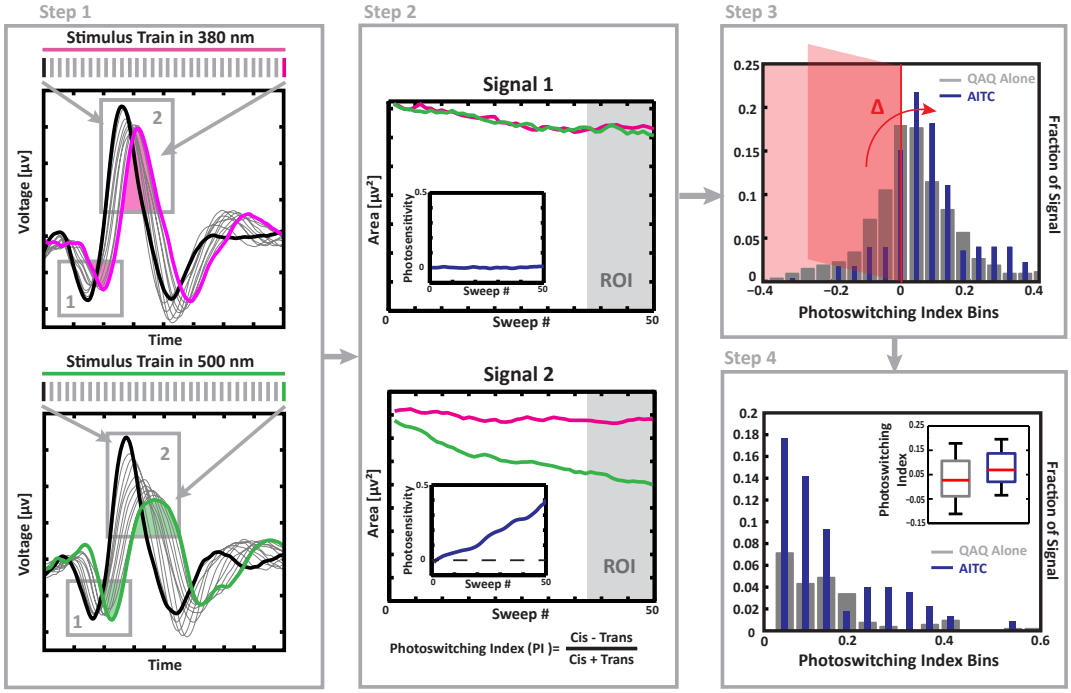

Figure 20.: Optimized Analysis Flow Converting Multi Electrode Raw Data to a Quantification of Conferred Photosensitivity.

Step 1: Schematic of a typical signal during a stimulus train in 500nm and 380nm light. Given QAQ's use-dependent block, photosensitization is most efficient toward the end of a stimulus train. Each electrode records synchronized activity of multiple cells in the vicinity and electrical signals from individual neurons integrate in a non-linear way to the overall recorded signal. To achieve maximal sensitivity, we devised an analysis method that separates complex signals into individual deflections in the voltage trace. **Step 2:** In order to determine photosensitivity of individual deflections the area under the signal is measured. To account for use-dependence, the parameter value toward the end of a stimulus train are used to calculate a Photoswitching Index (PI) as further described in Methods. **Step 3:** PI values of individual deflections from many recordings are pooled to assess the overall distribution of photosensitivity. **Step 4:** Photosensitive effects are masked and blurred by the biological variability of signal responses. To reveal the net contribution of positive PI signals, we subtracted the negative parts of the normalized distribution from the positive part which can be interpreted as approximate net photosensitivity imparted to the system.

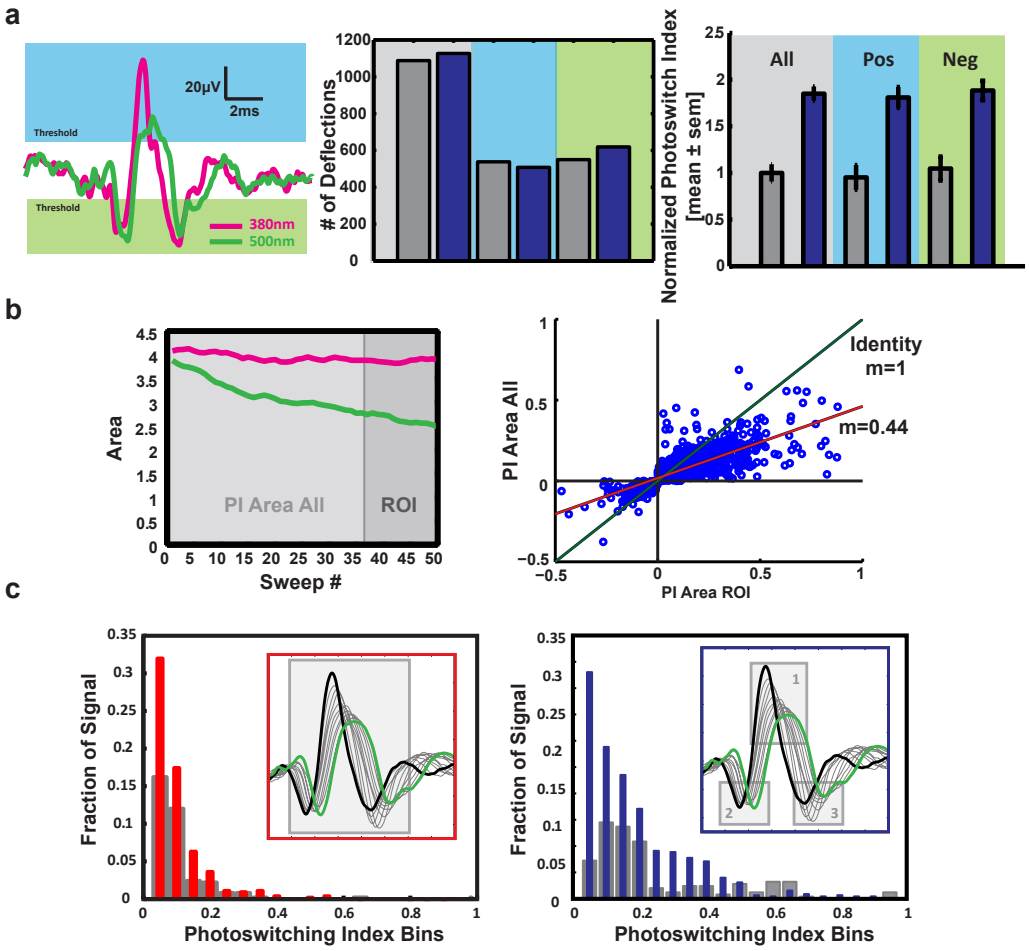

Figure 21.: Optimized Analysis Increases the Sensitivity of Detecting Changes in Photosensitivity. **a.** Representation of an example signal (left panel). Positive and negative defections are equally likely (middle panel) and show equal amounts of conferred photosensitivity (right panel). Hence, separate evaluation is not biased. **b.** Given QAQ's property as open channel blocker, evaluating the later episodes of a stimulus trains (left panel) more accurately represents maximal QAQ block (right panel). **c.** Comparison of analysis methods. Pooling all deflections within one electrode (left panel) loses information. In comparison, separate evaluation of individual deflections preserves photosensitivity information and yields a more detailed and accurate representation (right panel).

1.2. QAQ is a Sensitive Reporter for Permeability Changes of Various Nociceptive Channels in Intact DRGs

We have previously shown that capsaicin, a potent and selective agonist of TRPV1, can induce permeability changes in intact DRGs (Mourot et al., 2012) [104]. We next asked whether other nociceptive ion channels can be selectively activated in a similar way. We applied several potent pharmacological activators of important molecular pain sensors to intact DRG tissue while probing permeability changes with co-incubation of QAQ. Both ally isothiocyanate (AITC), a selective activator of TRPA1, menthol, an agonist to TRPM8, as well as (4-benzoyl) benzoyl ATP (bzATP), an ATP analog specific to activating P_2X_7 receptors, induce enhanced permeability to the photoswitch QAQ (Figure 22). We therefore assume that most nociceptive channels can change their permeability in intact tissue and that QAQ uptake is an efficient and sensitive quantitative correlate to detect those changes. In the absence of QAQ, UV light alone is sufficient to introduce a small bias of signal magnitude as neuronal firing is increased under UV light. However, this effect is significantly smaller in comparison to QAQ induced photosensitivity (Figure 22).

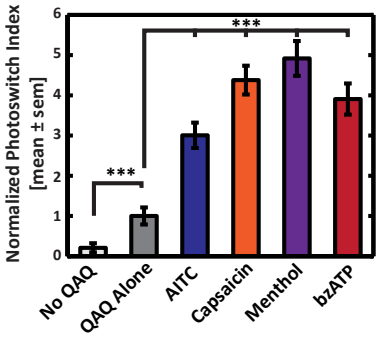

Figure 22.: QAQ is a Sensitive Reporter for Permeability Changes of Various Nociceptive Channels in Intact DRGs.
Selective activation of nociceptive ion channels leads to QAQ uptake. QAQ can enter sensory neurons to a small extend in the absence of any stimuli under physiological conditions (37°C, pH 7.4) indicating a basal activity of nociceptive channels. In contrast, treatment with 30μM AITC (300±31%, n=7 DRGs, 226 signals), 1μM capsaicin (438±36%, n=20 DRGs, 388 signals), 100μM menthol (492±43%, n=5 DRGs, 330 signals) and 250μM bzATP (391±39%, n=7 DRGs, 469 signals), confers enhanced light sensitivity to intact DRGs. In the absence of QAQ, UV light alone marginally enhances excitability (20±11%, n=14 DRGs, 459 signals). All data is normalized to mean PI of control QAQ alone (100±21%, n=21 DRGs, 533 signals). Statistics: Kruskal-Wallis test for non-parametric distributions with Dunn's post hoc test: *** denotes a significance level of $p<0.001$.

In all following figures, the average PI values for different conditions are consistently normalized to the mean PI of wildtype control DRGs for comparison to baseline permeability levels.

2. Probing Nociceptive Activity after Peripheral Injury

2.1. Spared Nerve Injury does not Affect all DRGs Equally

SNI surgery does not affect all sensory cells within a DRG. Further, SNI has differential effects on different DRGs. The cell bodies of most axotomized fibers are located within the L3, L4 and L5 DRGs (Rigaud et al., 2008) [116]. Labelling for ATF3 revealed that after SNI surgery about 40% of all cells within DRGs L4 and L5 are axotomized as the damage marker ATF3 is expressed (Figure 23a). In contrast, no cells show expression of ATF3 in control DRGs.

The anatomy varies between different mouse strains and genetic models. Therefore, we compare the number of injured cells in L4 and L5 DRGs and found that L4 is more affected by SNI than L5 (Figure 23b). This results confirms similar studies in C57BL/6J mice (Laedermann et al., 2004) [76].

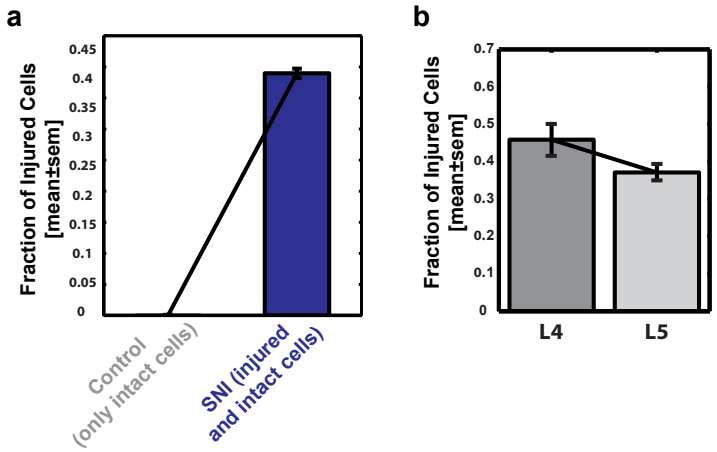

Figure 23.: SNI Surgery affects Lumbar DRGs Differently.
a. Number of axotomized sensory neurons in contralateral control and ipsilateral SNI DRGs. ATF3 labelling reveals cell bodies. Control: 4/5414 cells, 0.07±0.004%, SNI: 1650/4234 cells, 39.6±1.9%. **b.** Given the anatomy of the peripheral nervous system, SNI surgery affects more cells in L4 (45.9±4.2%) than L5 DRGs (37.1±1.9%).

2.2. Peripheral Nerve Injury Chronically Enhances Photoswitch Permeability in Nociceptive Neurons

We having shown that selective activation of different nociceptive ion channels can induce changes in photoswitch permeability. Given the importance of those channels for the regulation of chronic and neuropathic pain, we hypothesized that peripheral nerve injury could be sufficient to trigger similar changes in nociceptive neurons. We chose an established and well-characterized murine model for chronic and neuropathic pain, the Spared Nerve Injury (SNI), to measure QAQ uptake after injury (Figure 24a). SNI surgery leads to mechanical hyperalgesia of the respective hind paw lasting for many days (Pertin et al., 2012) [112] and the cell bodies of most affected, axotomized fibers are located within the L3, L4 and L5 DRGs (Rigaud et al., 2008) [116]. We found that QAQ uptake is increased in DRGs ipsilateral to the surgery one day after SNI in contrast to contralateral sham control DRGs of the same animals (Figure 24b). Seven days after inducing this chronic pain condition, the effect observed in ipsilateral DRGs is still chronically elevated compared to contralateral control DRGs (Figure 24c). Given the anatomy of the mouse peripheral nervous system, different lumbar DRGs contain different proportion of injured cells. There are considerable differences in sciatic nerve anatomy between different mouse strains but a recent study has established that SNI surgery preferably affects L3 and L4 fibers with minor contributions from L5 (Rigaud et al., 2008) [116]. In analogy, we find that L3 and L4 DRGs show larger differential increases in permeability than L5 (Figure 24e) further supporting the hypothesis that permeability changes for a DRG population is correlated with the number of directly axotomized cells within that population.

While SNI surgery directly affects only a subset of sensory neurons within each DRG, another subset is not directly injured by the procedure. We therefore asked if increasing the number of directly axotomized neurons will increase overall permeability. To test this hypothesis, we deployed another mouse model of chronic injury that affects all sciatic fibers, the Sciatic Nerve Ligation (SNL) model. Mice undergoing SNL show pronounced hypersensitivity to mechanical stimuli, mechanical allodynia, cold allodynia, thermal hyperalgesia, and spontaneous pain develop within 24-48 hours and persist for approximately 10-16 weeks (Jaggi et al., 2011) [64]. We probed photoswitch permeability one and seven days after SNL and noticed larger permeability changes compared to SNI (Figure 25b). Since we increased the proportion of injured cells, we conclude that a pronounced increase in permeability after SNL is correlated to the presence of more injured cells.

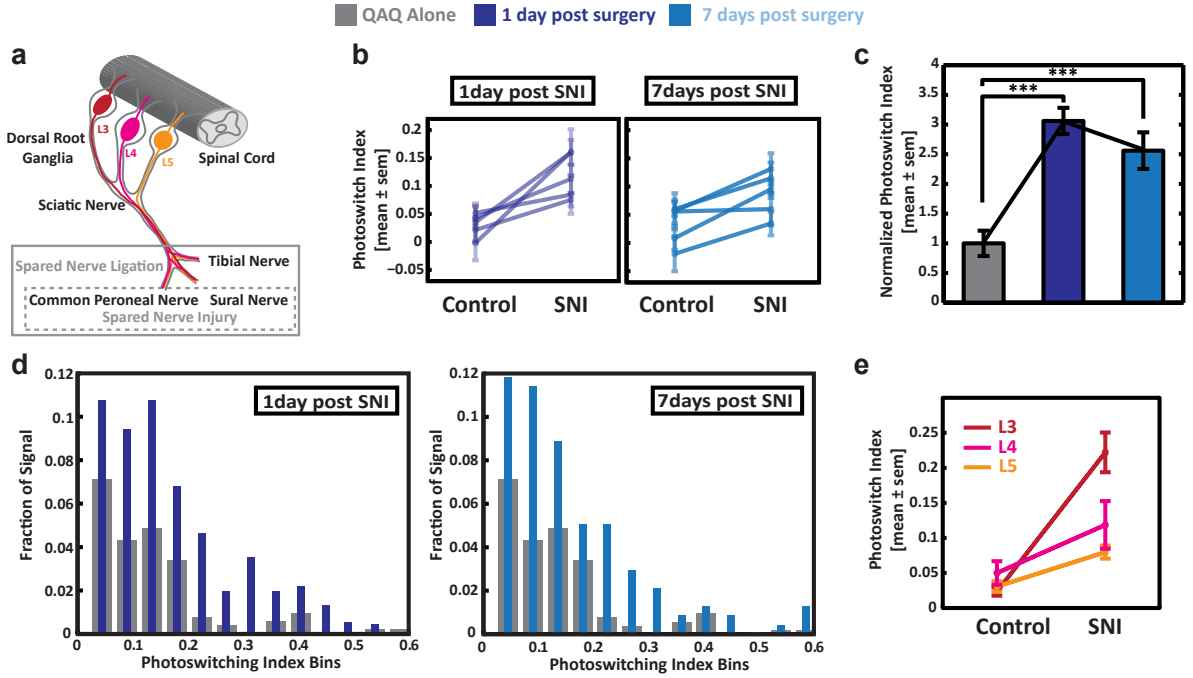

Figure 24.: Peripheral Nerve Injury Chronically Enhances the Permeability of Photoswitch Molecules in Intact DRGs.

a. Illustration of used surgery models. Incision of the skin on the lateral side of the left thigh reveals the three major sciatic nerve branches. In the Spared Nerve Injury model (SNI), both the tibial and the common peroneal nerve are injured through transection while leaving the sural nerve intact. In contrast, during Sciatic Nerve Ligation (SNL) no sciatic branches are spared. For each animal the contralateral side served as sham control where the skin was opened but no nerves severed. **b.** Direct Comparison between ipsilateral surgery and contralateral control DRGs for individual animals after SNI. For each time point, 5 animals and 2-3 DRGs each were recorded. **c.** Nerve injury induces enhanced QAQ permeability. Nerve injury induces enhanced QAQ permeability. Average PI values in surgery DRGs are normalized to mean PI of sham control DRGs (100±21%, n=21 DRGs, 533 signals). Permeability enhances one day after SNI (306±22%, n=17 DRGs, 456 signals) and remains chronically elevated seven days after SNI (256±30%, n=8 DRGs, 237 signals). Statistics: Kruskal-Wallis test for non-parametric distributions with Dunn's post hoc test, *** denotes a significance level of $p<0.001$. **d.** Distribution histogram for the net contribution of positive PI values one day (left panel) and seven days after SNI (right panel). Higher PI values correlate with higher permeability levels and control DRGs are displayed in grey. **e.** Permeability levels correlate with the number of affected cells within different lumbar DRGs. L3 (Control: average PI 0.023±0.005, n=4 DRGs, 220 signals; SNI: average PI 0.221±0.029, n=3 DRGs, 55 signals) shows a stronger increase in photosensitivity than L4 (Control: average PI 0.031± 0.007, n=7 DRGs, 267 signals; SNI: average PI 0.080±0.009, n=3 DRGs, 157 signals) and L5 (Control: average PI 0.049±0.016, n=5 DRGs, 140 signals; SNI: average PI 0.118±0.034, n=3 DRGs, 38 signals). Statistics: Rank sum test for non-parametric distributions, *** denotes a significance level of $p<0.001$.

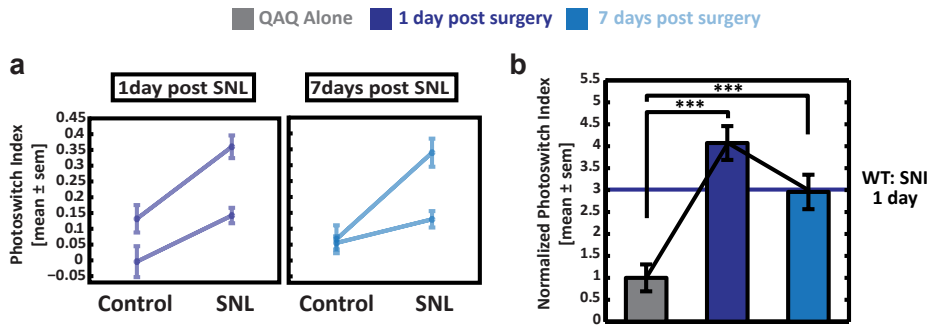

Figure 25.: Peripheral Nerve Injury Chronically Enhances the Permeability of Photoswitch Molecules in Intact DRGs after Sciatic Nerve Ligation.
a. Direct Comparison between ipsilateral surgery and contralateral sham control for individual animals after SNL. For each time point, 2 animals and 2-3 DRGs each were recorded. **b.** SNL affects more sensory neurons and induces higher permeability levels than SNI. DRG tissue one day post SNL-surgery (100±30%, n=6 DRGs, 137 signals) shows significantly higher levels of permeability (407±38%, n=4 DRGs, 118 signals) than tissue at the same time after SNI ($p<0.05$). The time course of permeability, however, is comparable to SNI injury (7 days post SNL: 295±39%, n=4 DRGs, 74 signals). Statistics: Kruskal-Wallis test for non-parametric distributions with Dunn's post hoc test: *** denotes a significance level of $p<0.001$.

2.3. TRPA1, but not TRPV1, is Necessary for Increased Permeability after Nerve Injury

We next asked which nociceptive ion channels contribute to the observed increase in permeability after nerve injury. TRPV1 has been shown to play a key role in nociception and is involved in the induction of chronic pain states like mechanical hyperalgesia. We therefore tested genetically modified animal model lacking any functional TRPV1 protein to elucidate if TRPV1 is necessary to mediate observed permeability increases after SNI surgery. While the absence of TRPV1 reduces permeability in control DRGs (Figure 26a), we found that injury induced permeability changes are still present in DRG tissue from TRPV1 knock-out mice one day after injury (Figure 26a). Moreover, permeability levels continue to rise seven days after surgery in contrast to animals after SNI with functional TRPV1 (Figure 26a). These results indicate that TRPV1 is both not necessary for injury induced shift in activity and the lack of TRPV1 seems to potentiate the permeability of other nociceptive channels over a lasting period after the injury.

Previous studies have also found that the lack of TRPV1 increases thermal hyperalgesia rather than abolishing it indicating compensation mechanisms in genetic knock out models that possibly could account for the observed effects.

We next asked whether TRPA1 might contribute to the observed increase in nociceptive permeability and tested of a mix of acutely applied TRPA1 antagonists (see Methods) is able to abolish injury induced loading. Co-application of blockers with QAQ reduced QAQ uptake (Figure 26d) indicating an involvement of TRPA1. Removing all functional TRPA1 protein, we

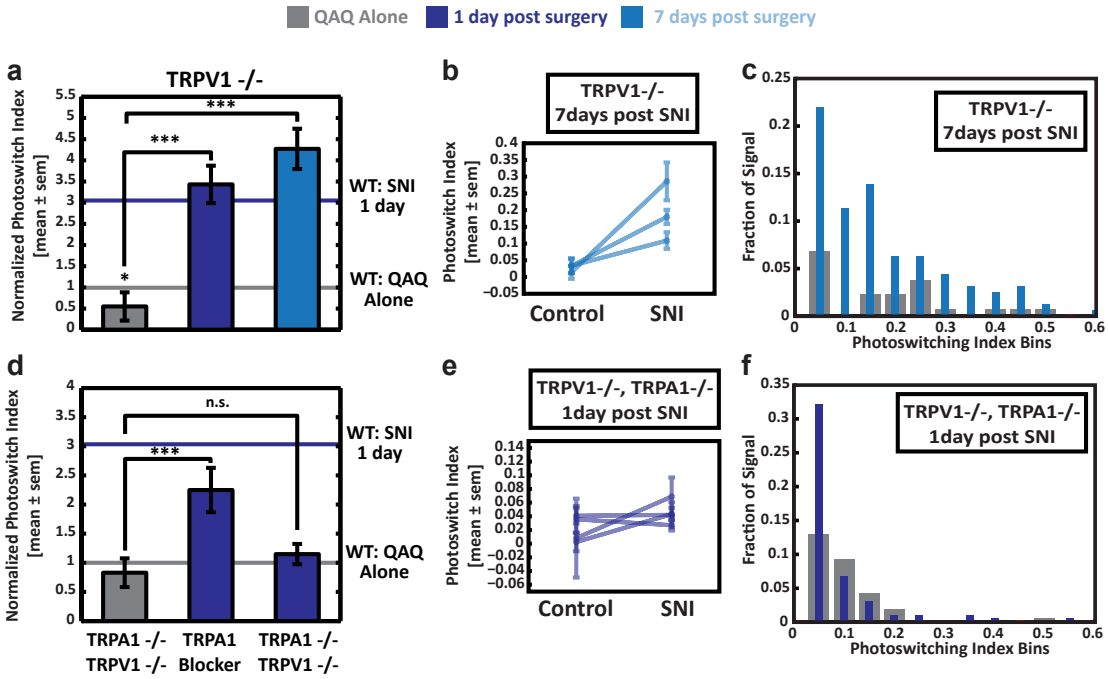

Figure 26.: TRPA1, but not TRPV1, is Necessary for Increased Nociceptive Permeability after Injury.

a. SNI injury in mice lacking TRPV1 potentiates increases in permeability. Average PI values are normalized to mean PI of wildtype control DRGs. Activity in contralateral DRGs is reduced (55±33%, n=8 DRGs, 131 signals) to baseline activity in wildtype. However, activity one day after SNI is increased (343±44%, n=5 DRGs, 90 signals) and continues to rise seven days post SNI (427±47%, n=9 DRGs, 159 signals). **b.** Direct Comparison between ipsilateral surgery and contralateral control DRGs for individual TRPV1 knock-out animals 7 days after SNI. 3 animals and 2-3 DRGs each were recorded. **c.** Distribution histogram for the net contribution of positive PI values seven days after SNI in TRPV1 -/- animals. Higher PI values correlate with higher permeability levels and control DRGs are displayed in grey. **d.** TRPA1 is necessary for nerve injury induced permeability. Average PI values are normalized to mean PI of wildtype control DRGs. Acute block of TRPA1 reduces permeability (224±38%, n= 4 DRGs, 81 signals) compared to wildtype DRGs after SNI without blockers but levels remain elevated compared to no-injury control. Permeability in contralateral DRGs of TRPA1/TRPV1 double knock out animals is reduced (82±24%, n=8 DRGs, 163 signals) to baseline activity in wildtype and SNI does not significantly increase activity (114±17%, n=8 DRGs, 193 signals). **e.** Direct Comparison between ipsilateral surgery and contralateral control DRGs for individual TRPV1/TRPA1 knock-out animals one days after SNI. 4 animals and 2-3 DRGs each were recorded. **f.** Distribution histogram for the net contribution of positive PI values one day after SNI in TRPV1 -/-, TRPA1 -/- mice.

next tested injury induced permeability in TRPA1/TRPV1 double knock-out animals and found that no permeability change can be detected (Figure 26d and e). Since the number of available SNI mice is limited we forewent testing the effects of TRPV1 blocker on wildtype DRGs after surgery.

In analogy to the results for wildtype mice after SNI, we also found the highest increase in permeability levels for L3 DRGs of TRPV1 lacking animals (Figure 27a). In contrast, animals lacking TRPA1 show no increase in permeability for any DRG (Figure 27b).

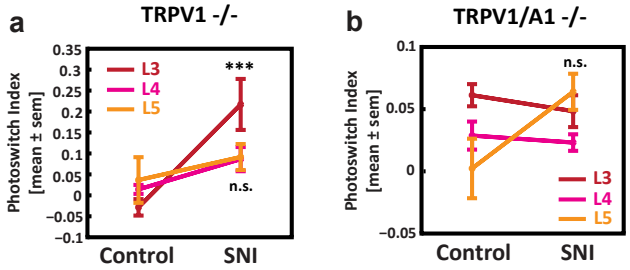

Figure 27.: Permeability of Lumbar DRGs of TRPV-/- and TRPV1-A1-/- Mice.
a. Permeability levels of individual lumbar DRGs of TRPV1 knock-out animals. L3 (Control: PI -0.028±0.019, n=2 DRGs, 45 signals; SNI: PI 0.217±0.061, n=2 DRGs, 36 signals) shows the higher increase in photosensitivity than L4 (Control: PI 0.014± 0.011, n=3 DRGs, 70 signals; SNI: PI 0.086±0.029, n=2 DRGs, 34 signals) and L5 (Control: PI 0.037±0.054, n=2 DRGs, 28 signals; SNI: PI 0.091± 0.031, n=3 DRGs, 50 signals). **b.** Permeability levels of individual lumbar DRGs of TRPV1/A1 double knock-out animals. L3 (Control: PI 0.061±0.008, n=4 DRGs, 146 signals; SNI: PI 0.048±0.013, n=3 DRGs, 56 signals) shows the higher increase in photosensitivity than L4 (Control: PI 0.028±0.011, n=5 DRGs, 101 signals; SNI: PI 0.023±0.006, n=2 DRGs, 96 signals) and L5 (Control: PI 0.002±0.024, n=3 DRGs, 21 signals; SNI: PI 0.064±0.014, n=3 DRGs, 41 signals).
Statistics: Wilcoxon Rank sum test non-parametric distributions: *** denotes a significance level of $p<0.001$, n.s. describes not significant.

2.4. Peripheral Injury Affects TRPV1 Expressing Cells

Multiple studies show that TRPA1 is highly correlated with TRPV1 expression and TRPA1 positive cells are a full subset of TRPV1 nociceptors (Pecze et al., 2009; Neubert et al., 2008) [111] [108]. However, this finding has been challenged suggesting a small population of TRPA1 expressing, TRPV1 lacking sensory neurons (Braz et al., 2010) [23]. While genetic ablation of TRPV1 increases activity, we wondered how the complete removal of TRPV1 expressing cells would affect observed permeability levels. Systemic treatment with resiniferatoxin (RTX), an ultrapotent capsaicin analog, results in thermal hypoalgesia through the permanent loss of TRPV1 expressing fibers following calcium excytotoxicity. In contrast to peripheral treatment like in capsaicin ointments, TRPV1 nociceptors will not recover (Mitchell et al., 2010) [98]. The effectiveness of RTX treatment was confirmed using the hot plate test and levels of permeability are decreased compared to wiltype controls after SNI surgery (Figure 28a). Surprisingly, baseline QAQ uptake after RTX treatment was only marginally reduced (Figure 28)a.

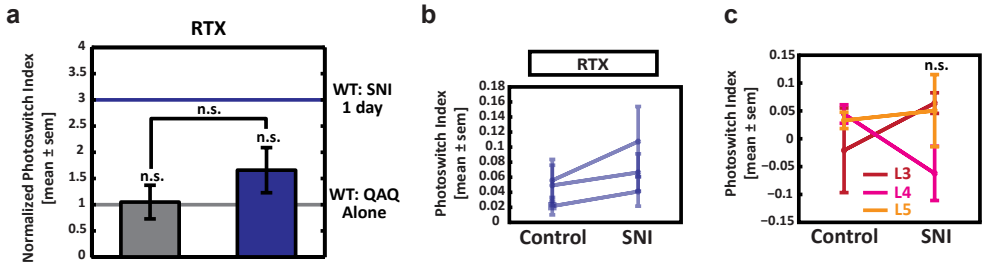

Figure 28.: Peripheral Injury Affect TRPV1 Expressing Cells.
a. TRPV1 expressing cells contribute to nerve injury induced permeability. Control treatment with RTX does not significantly lower baseline permeability (105±32%, n= 9 DRGs, 121 signals). However, nerve injury fails to significantly increase permeability in RTX treated animals (165±43%, n=7 DRGs, 92 signals). Statistics: Kruskal-Wallis test for non-parametric distributions with Dunn's post hoc test: n.s. describes not significant. **b.** Direct Comparison between ipsilateral surgery and contralateral control DRGs for individual RTX treated animals one days after SNI. 4 animals and 2-3 DRGs each were recorded. **c.** Permeability levels of individual lumbar DRGs for RTX treated mice. L3 (Control: PI -0.020±0.075, n=2 DRGs, 25 signals; SNI: PI 0.064±0.018, n=2 DRGs, 58 signals), L4 (Control: PI 0.044±0.016, n=2 DRGs, 53 signals; SNI: PI -0.062±0.048, n=2 DRGs, 27 signals) and L5 (Control: PI 0.033±0.014, n=5 DRGs, 63 signals; SNI: PI 0.050±0.064, n=2 DRGs, 28 signals) show no significant increase in permeability. Statistics: Wilcoxon rank sum test for non-parametric distributions: n.s. describes not significant.

Taken together, our data suggests that TRPA1 is necessary for increased cellular permeability after nerve injury. In contrast, TRPV1 is not necessary but might contribute in a permeability modulating way. This notion is further supported by recent studies that present evidence for molecular interactions between TRPV1 and TRPA1 and proposing that the lack of TRPV1 disinhibits TRPA1 activity (Weng et al., 2015; Weyer and Stucky, 2015) [146] [147].

3. Activity Dependent Long-term Potentiation of Photoswitch Permeability

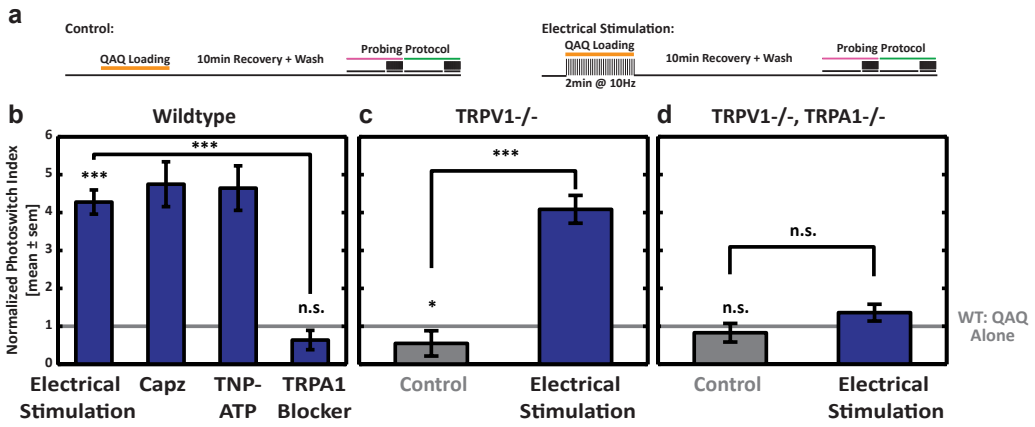

Figure 29.: Activity Dependent Long-term Potentiation of Photoswitch Permeation.
a. Schematic displaying protocols for QAQ loading during electrical stimulation and control, respectively. **b.** Electrical stimulation increases photoswitch permeability of DRG tissue. 2min exposure to a 10Hz stimulus train is sufficient to increase QAQ uptake to 427±32% (n=8 DRGs, 219 signals) compared to control. Permeability changes are not blocked by 1mM Capzasepine (Capz, 474±59%, n=4 DRGs, 94 signals), a TRPV1 antagonist, or 100μM TNP-ATP (464±58%, n=6 DRGs, 79 signals), a blocker of P_2X receptors. However, simultaneous treatment with TRPA1 blockers (see Methods) significantly reduces QAQ uptake (64±26%, n=5 DRGs, 128 signals). **c.** Genetic absence of TRPV1 does not abolish increased permeation. Electrical stimulation of DRG tissue from TRPV1-/- knock out animals still leads to increased QAQ uptake (409±37%, n=5 DRGs, 149 signals). **d.** TRPA1 is necessary for activity dependent permeability changes. TRPA1/TRPV1 double knockout mice show no increased QAQ uptake after electrical stimulation (136±22%, n=4 DRGs, 169 signals).

SNI surgery damages axons of sensory neurons in the periphery far away in from their respective cell bodies. We therefore wondered how the information of nerve injury is conveyed to the DRG somata where changes in cell permeability occur. One possible hypothesis involves retrograde transport of signaling molecules along the axons of injured cells. Alternatively, injury induced hyperexcitability and increased firing, both sensory triggered and spontaneous, could be mediating the effect of peripheral injury to the cell bodies. To test this hypothesis, we inquired whether electrical stimulation of the peripheral nerve fibers *in vitro* could trigger similar permeability changes in nociceptive cells than injury. In the absence of any other stimulants, we found that a two minute long electrical stimulus burst alone is sufficient to drive cell entry of QAQ (Figure 29b). Since extended firing of sensory neurons might affect the permeability of various nociceptive channels, we used pharmacology to identify what nociceptive channels contribute to this effect. Both capzasepine, a potent TRPV1 antagonists, and TNP-ATP, a selective blocker of P_2X receptor opening, do not abolish firing induced QAQ uptake (Figure 29b). In contrast, treatment with TRPA1 antagonists (see Methods) effectively inhibits firing induced uptake of QAQ (Figure 29b). DRGs lacking TRPV1 receptor show increased photoswitch permeability

when exposed to electrical stimulation (Figure 29c) similar to naive tissue. In contrast, identical same stimulation conditions in a TRPV1/TRPA1 double knock-out do not increase permeability of sensory neurons (Figure 29d). Together these results suggest that TRPA1 in the DRG cell bodies is necessary for activity dependent QAQ uptake and thus permeability changes at the DRG somata level.

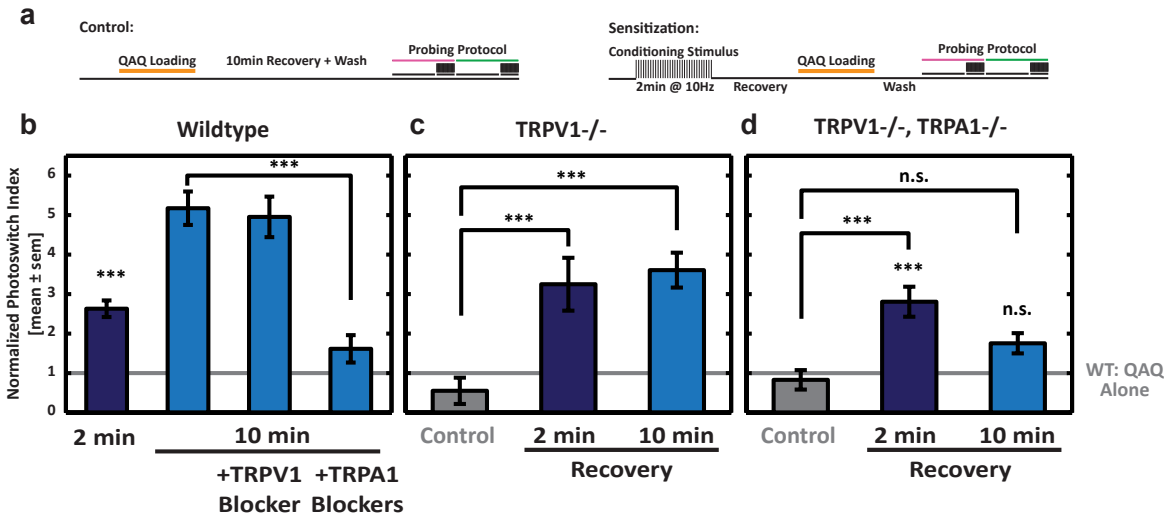

Figure 30.: Activity Dependent Long-term Sensitization of Photoswitch Permeation.
a. Schematic displaying protocols for conditioning DRG tissue with electrical stimulation and controls, respectively. **b.** Photoswitch permeability induced by electrical stimulation is not transient. DRG tissue from wildtype mice was exposed to a conditioning stimulus of electrical activity decoupled from QAQ exposure which occurred after a recovery period in the absence of any further stimulants. Permeability remains increase after 2 min (263±21%, n=6 DRGs, 322 signals) and continues to increase 10 min after stimulation (517±43%, n=9 DRGs, 240 signals). TRPV1 blockers (see Methods) fail to block permeability changes (495±51%, n=9 DRGs, 208 signals) while TRPA1 blockers significantly inhibit QAQ uptake 10 min after conditioning (161±35%, n=4 DRGs, 143 signals). **c.** Genetic lack of TRPV1 does not abolish increased permeation. TRPV1 receptors are not necessary for activity dependent potentiation (2 min after conditioning: 325±67%, n=6 DRGs, 58 signals; 10 min after conditioning: 360±44%, n=6 DRGs, 146 signals). **d.** TRPA1 is necessary to mediate permeability changes over longer periods of time. Sensitization of DRG tissue lacking TRPA1 and TRPV1 receptors does not lead to significantly increased permeability changes 10 min after conditioning (175±26%, n=5 DRGs, 179 signals) but increased permeability in 2 min after conditioning is still persists (281±38%, n=4 DRGs, 103 signals).

The previous results suggest that firing directly modulate permeability in a TRPA1 dependent and relatively fast way as QAQ incubation and electrical stimulation happened simultaneously and QAQ was washed away right after the stimulus. We now wondered how long this increased activity level would persist after the activity stimulus had eased. We therefore designed a conditioning protocol separating the episode of electrical activity from probing permeability. In tissue form wildtype mice we found that with increasing time between conditioning and probing enhanced levels of permeability appear (Figure 30b) suggesting that permeability changes are not directly

linked to cell depolarization but rather are modulated in a firing dependent manner through unknown signaling cascades. Genetic ablation of TRPV1 does not prevent increased permeability levels (Figure 30c) but in tissue lacking both functional TRPA1 and TRPV1 permeability changes are greatly reduced indicating that TRPA1 is necessary for this effect. This observation if further supported by the finding that co-application of TRPA1 blockers during activity probing prevents permeability changes (Figure 30).

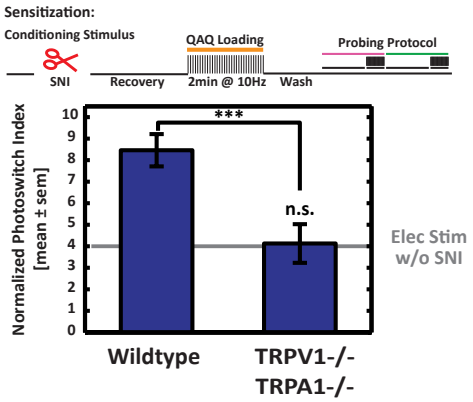

Figure 31.: Nerve Injury Sensitizes DRG Tissue to Electrical Stimulation.
DRG tissue after peripheral nerve injury is more sensitive to electrical stimulation than DRGs after sham surgery (846±75%, n=5 DRGs, 76 signals). However, lack of TRPA1 and TRPV1 significantly reduce this sensitization but fail to abolish the effect totally (413±89%, n=4 DRGs, 39 signals).
Statistics: Kruskal-Wallis test for non-parametric distributions with Dunn's post hoc test: *** $p<0.001$, ** $p<0.01$, * $p<0.05$, n.s. describes not significant.

Furthermore, nerve injury sensitizes DRG tissue's susceptibility to electrical stimulation and QAQ uptake in tissue after SNI surgery is potentiated many fold in both wildtype mice and animals lacking TRPA1 (Figure 31) which suggests that other mechanisms play a role as well.

In summary, action potential firing effectively mimics the effects of nerve injury and peripheral damage potentiates the permeability of sensory neurons.

4. Peripheral Injury also Chronically Enhances the Permeability of Fluorescent Dye Molecules

In order to visualize permeability changes and enable identification of affected cell types, we performed loading studies using the fluorescent dye molecule Yo-PRO1 that has been previously utilized to probe permeability changes in sensory neurons (Meyers et al., 2003) [96]. Yo-PRO-1 is a double charged cation, in similar size and geometry than QAQ (molecular weight (MW) of QAQ: 722, MW of Yo-PRO-1: 629). In analogy to QAQ, Yo-PRO-1 is membrane impermeable and requires open ion channel to function as conduits to be delivered into the cytosol. Intracellular Yo-PRO-1 thus serves as evidence for increased cellular permeability. We incubated 100nM Yo-PRO-1 with acute preparations of DRG tissue one day after SNI surgery and fluorescently imaged cytosolic dye uptake in life cells. DRG tissue affected by SNI surgery shows an increased number of Yo-PRO-1 positive cells compared to control DRGs (Figure 32). Similarly, exposure of DRG tissue to Yo-PRO-1 dye while stimulating spiking leads to an increased number of labelled sensory cells (Figure 32b).

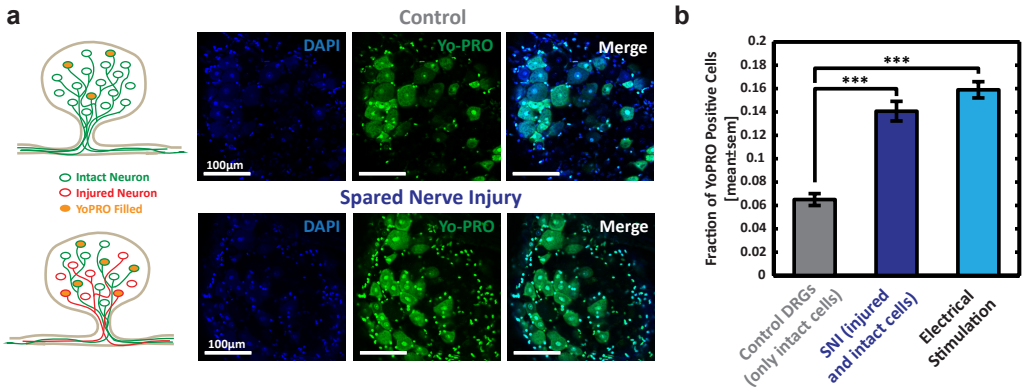

Figure 32.: Peripheral Nerve Injury chronically Enhances the Permeability of Dye Molecules in Intact DRGs.

a. Enhanced Yo-PRO-1 uptake after SNI injury and electrical stimulation. Example fluorescent images of life, pre-fix DRG samples after incubation with Yo-PRO-1 one day after surgery. **b.** Quantification of Yo-PRO1- positive cells. Number of Yo-PRO-1 positive cells after SNI (14.1±0.8%, n=211/1500 cells) and challenge with an electrical stimulus (15.9±0.7%, n=380/2391 cells), respectively. Cell numbers are compared to control DRGs (6.5±0.5%, n=142/2183 cells). Statistics: Fisher's exact test, *** denote significance level $p<0.001$.

5. Nerve Injury affects both Intact and Injured Populations of Nociceptive Neurons

Sensory neurons have been characterized with the concept of labelled lines where individual fibers transmit specific sensory information independently from adjacent fibers and where DRG cell bodies merely serve as a signal relay stations. However, recent research is challenging this notion of the sensory system and we were wondering if nociceptive permeability changes too were not limited to the fibers directly affect by nerve injury. Stimulation close to the DRG cell bodies cannot distinguish between intact and injured cells since both fiber population are bundled and equally activated. We therefore decided to stimulate individual nerve fibers with silver wire electrodes after they branch at the sciatic plexus in the periphery. This way we can distinguish between the tibial, sural and common peroneal nerves, respectively. In the absence of noticeable spontaneous activity, separate stimulation ensures that recorded signals at the cell bodies originate from the stimulated fibers (Figure 33a). When we selectively stimulated and recorded from both spared and injured nerve fibers after SNI, we surprisingly found that both neuron populations became photosensitized. We thus conclude that permeability changes are not limited to directly axotomized neurons (Figure 33b) and that some kind of crosstalk is taking place between both neuron populations. This crosstalk communicates the signal of nerve injury form directly affected to not directly affected sensory cells.

An additional advantage of stimulating far in the periphery is that longer fibers enable us to record from faster conduction Aδ fibers since they become separated from the stimulation artefact (Figure 33a). Grouping of fiber responses by conduction velocity reveals that only slow conducting C fiber seems to take up QAQ while faster Aδ fibers do not contribute to any crosstalk nor change permeability when directly affected by nerve damage (Figure 33d).

We next asked whether we could combine visualization of sensory cells showing permeability changes with immunohistochemical labeling. We devised a protocol that involves loading of Yo-PRO-1 into live DRG tissue and preservation of dye signal throughout the preparation process for immunohistochemical labeling. Yo-PRO-1 is a small, easily diffusible molecule affected by wash-out effects during fixation and staining. Moreover, fluorescent read-out is relatively insensitive compared to photosensitivity measurements. Therefore, we assume that Yo-PRO-1 labeling after cryo-sectioning underestimates the number of cells which actually undergo permeability changes. We further postulate that only cells with the largest permeability differential compared to control baseline will become clearly distinguishable (Figure 17 in Methods). However, the fraction of positive Yo-PRO-1 identified cells after immunohistochemsirty is comparable to results obtained from life imaging (compare to Figure 32). We first inquired whether co-staining for the transcription factor ATF3, which labels the nuclei of axotomized cells (Tsujino et al., 2000) [138], can confirm our previous results that permeability changes are not limited to injured cell populations. Indeed, co-labelling revealed that both ATF3 positive and negative cells take up significantly more Yo-PRO-1 after SNI compared to control DRGs that only contain intact neurons (Figure 34d).

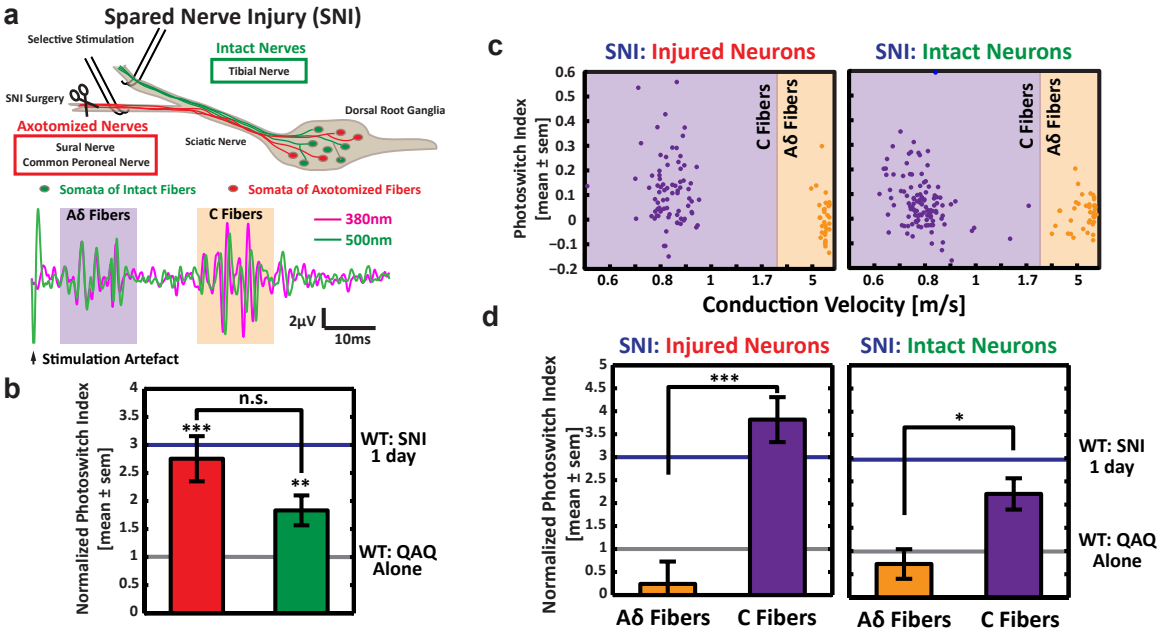

Figure 33.: Nerve Injury affects both Intact and Injured Populations of Nociceptive Neurons.
a. Selective activation of injured and intact nerve fibers and example recording using silver hook electrodes. Fibers of the tibial nerve were spared during surgery and selective activation of those fibers isolates electrical responses from the population of intact neurons. **b.** Both axotomized and intact sensory fibers are affected by nerve injury. The overall photosensitivity of both injured and spared nerve fibers is increased after SNI. Injured fibers show an increased mean PI of 275±40% (n=5 DRGs, 111 signals) while intact nerve bundles average to a PI of 183±27% (n=11 DRGs, 152 signals). Mean PI value are normalized to contralateral control DRGs that did not undergo surgery. **c.** Photosensitivity of individual signals sorted by conduction velocity. Distant stimulation of nerve fibers leads to a temporal separation in the recording trace between stimulation artefact and faster conducting Aδ fibers. Same statistics as b. **d.** Crosstalk mainly affects slowly conducting C fibers. Grouping by conduction velocity allows separate evaluation of conferred photosensitivity between slowly conducting C fibers and faster conducting Aδ fibers. Cut-off conduction velocity 2 m/s. Within injured nerve fibers Aδ fibers take up little photoswitch (PI=24±49%, n=22 signals) while C fibers experience significant permeability changes (PI=382±49%, n=78 signals) compared to contralateral control DRGs. For intact neurons a similar relationship is found: Aδ fibers PI=72±31%, n=40 signals; C fibers: PI=223±33%, n=112 signals.
Statistics: Kruskal-Wallis test for non-parametric distributions with Dunn's post hoc test: *** denotes a significance level of $p<0.001$, ** equals $p<0.01$, * equals $p<0.05$, n.s. describes not significant.

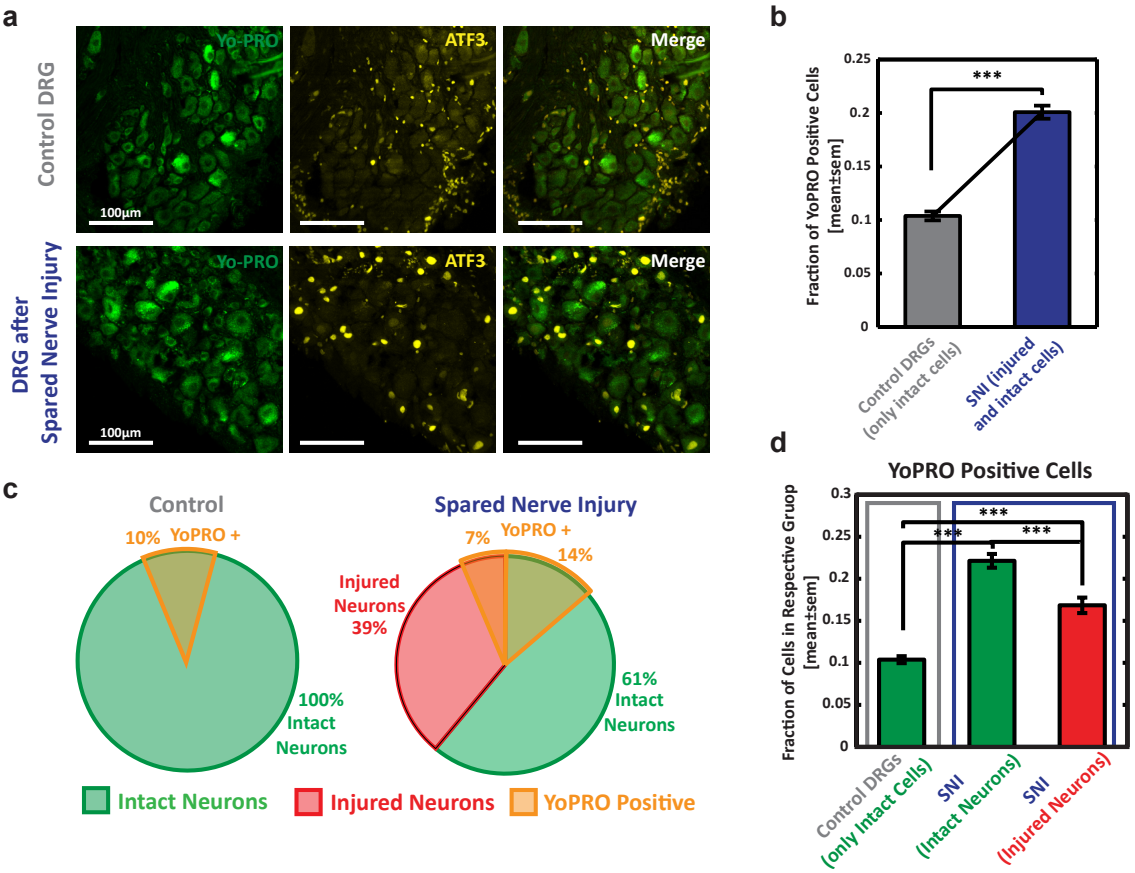

Figure 34.: Nerve Injury leads to Yo-PRO-1 Uptake in both Intact and Injured Neuronal Populations.

a. Example images of DRG cryo sections after Yo-PRO-1 loading and immunohistochemistry. Fluorescent dye was incubated with life DRG tissue before fixation and immunohistochemical labeling for ATF3 post sectioning allows for identification of axotomized cell bodies. **b.** Quantification of Yo-PRO-1 uptake. In analogy to Figure 32, the number of Yo-PRO-1 labelled cells was compared between control and SNI tissue and immunohistochemical preparation roughly preserves the difference in cell numbers (10.4±0.4% Control DRGs vs. 20.1±0.6% for SNI DRGs, Control: n=5414 cells, 31 images, SNI: n = 4234 cells, 28 images. **c.** Both intact and injured cells take up Yo-PRO-1 after SNI. Using ATF3 as marker we distinguished between intact and injured cells within SNI DRGs and found that both population take up Yo-PRO-1 dye. **d.** Not only injured but also intact cells take up Yo-PRO-1 after SNI. Normalizing the results of g. to the respective groups of intact or injured subpopulations reveals that intact sensory cells within DRGs exposed to SNI are twice as likely (22.1±0.8%, n=572/2584 cells) to take up Yo-PRO-1 than intact cells within control DRGs (10.4±0.4%, n=562/4852 cells). Injured cells as well take up elevated levels of dye (16.9±0.9%, n=278/1650 cells).
Statistics: Fisher's exact test, *** denotes $p<0.001$.

6. Injury Induced Increases in Photoswitch Permeability are Limited to Peptidergic, Non-myelinated C Fibers

Having established a method to identify cells undergoing permeability changes combined with immunohistochemical labelling, we next questioned which cell types are primarily contributing to the observed increase in cellular permeability. Staining for IB4 and N52 identifies non-petidergic and myelinated sensory fibers, respectively (Figure 35). We found that non-petidergic, IB4 positive sensory neurons do not significantly co-localize with Yo-PRO-1 dye both in control and SNI DRGs and we thus conclude that mainly petidergic sensory neurons shift their permeability and take up QAQ and Yo-PRO-1 (Figure 35b). Further, stained for N52 protein showed that more than 20% of myelianted, fast conducting neurons do take up dye in control tissue (Figure 35c). However, nerve injury does no recruit more myelinated cells to change permeability (Figure 35c).

Grouping Yo-PRO-1 positive cells by size shows that control DRGs show a significant number of larger cells taking up Yo-PRO-1 (Figure 36a) which is in agreement with the N52 staining results. However, it is unclear but what mechanism large diameter, myelianted cells take Yo-PRO-1 in the absence of injury.

More interestingly, nerve injury primarily recruits small diameter neurons, presumably C fibers to take up Yo-PRO-1 dye and this preference is sustained in both injured and intact subpopulation in DRG tissues after nerve damage (Figure36). Finally, co-staining for TRPV1 receptors indicates that TRPV1 expressing cells contribute to the population of dye positive cells after injury (Figure 36b and c). Again, both intact and injured sensory sub-population show increased uptake of Yo-PRO-1 (Figure 36c). This finding agrees with previous results since TRPV1 and TRPA1 are mainly expressed in C and Aδ delta fibers which show a small to medium cell diameter (up to about 30μm corresponding to a cell size of about 700μm^2). Since the number of TRPV1 positive, Yo-PRO-1 positive cells after injury does not account for all dye labelled cells after SNI, we hypothesize that other populations of small diameter nociceptors are involved. The existence of TRPA1 expressing, TRPV1 lacking cell populations (Braz et al., 2010) [23] could be one possible explanation. In summary, the effects of nerve injury are primarily focused on small, non myelinated, petidergic sensory neurons which are mostly comprised of C fiber nociceptors.

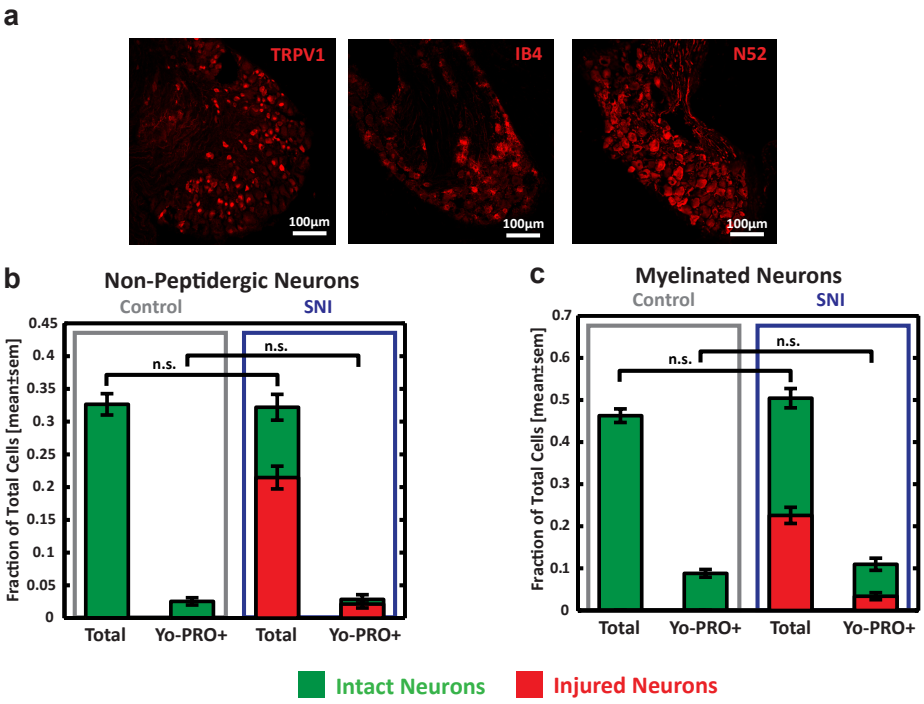

Figure 35.: Injury Induced Increases in Photoswitch Permeability are Limited to Peptidergic, Non-myelinated C Fibers.

a. Immunohistochemical labelling of TRPV1, IB4 and N52. Example images identifying peptidergic, myelinated and TRPV1 expressing sensory neurons in DRG tissues after SNI surgery. **b.** Nerve injury does not lead to increased uptake of dye in non-peptidergic cells. First, SNI surgery does not alter the number of IB4 positive cells in control (32.7±1.6%, n=269/824 cells) vs. SNI (32.2±2.0%, n=180/559 cells) overall. Moreover, nerve injury does not lead to increased uptake of Yo-PRO-1 in non-peptidergic cells (Control: 2.6±0.6%, n=21/824 cells; SNI: 2.9±0.7%, n=16/559 cells). However, IB4 positive cells are more often affected by nerve injured than average (67% compared to 39% overall) but this ratio is not significantly changed in Yo-PRO-1 positive cells. **c.** Peripheral nerve damage does not induce dye permeability shifts in myelinated neurons (Control: 8.8±0.9%, n=84/953 cells vs. SNI: 10.9±1.4%, n=52/474 cells). N52 positive cells are equally likely affected by nerve injured than cells on average (44% compared to 39% overall) and this ratio is not significantly changed in Yo-PRO-1 positive cells, thus there is not increased dye uptake by either injured or intact cells. In general, Nerve injury does not affect the overall fraction of N52 positive cells in control (46.3±1.6%, n=441/953 cells) or SNI (50.4±2.3%, n=239/474 cells) DRGs.

Statistics: Fisher's exact test, *** denotes $p<0.001$, ** denotes $p<0.01$, n.s. denotes not significant.

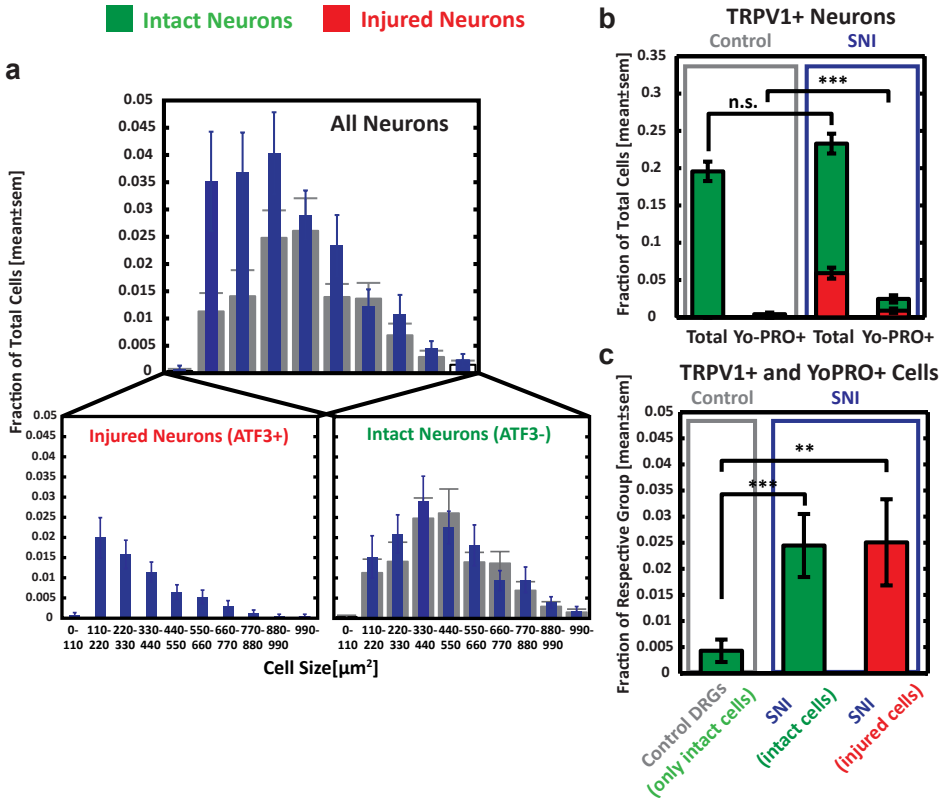

Figure 36.: Injury Induced Increases in Photoswitch Permeability are Limited to Small Diameter Fibers partly Expressing TRPV1.

a. Nerve injury recruits small diameter neurons to uptake dye. Yo-PRO-1 positive cells were grouped by cell size for control and SNI DRGs in 10 equally spaced bins. In control DRGs, mostly medium to large diameter neurons take up the dye. In DRGs ipsilateral to SNI, mostly small diameter, non-myelinated nociceptors contribute to the overall increase in Yo-PRO-1 positive cells. Separation of intact and injured subpopulations reveals that both axotomized and intact small diameter nociceptors take up Yo-PRO-1 after SNI surgery. **b.** Nerve injury changes dye permeability of TRPV1 expressing cells. In control DRGs, TRPV1 expressing cells do not take up Yo-PRO-1. However, nerve injury induces increased uptake of Yo-PRO-1 in TRPV1+ cells (Control: 0.4±0.2%, n=4/930 cells, SNI: 2.5±0.5%, n=25/1013 cells). Nerve injury in general does not affect the overall number of TRPV1 positive cells in control (19.6±1.3%, n=182/930 cells) compared to SNI (23.3±1.3%, n=236/1013 cells). **c.**. Both injured and intact TRPV1 expressing cells take up Yo-PRO-1 after injury. Cell numbers were normalized to the respective group of intact and injured neurons. Both intact (2.5±0.6%, n=16/654 cells) and injured (2.5±0.8%, n=9/259 cells) TRPV1 expressing cells show significantly increased permeability compared to uninjured control DRG (0.4±0.2%, n=4/930 cells).
Statistics: Fisher's exact test, *** denotes $p<0.001$, ** denotes $p<0.01$, n.s. denotes not significant.

7. Probing Temperature Induced Permeability Changes in Intact DRGs

7.1. Temperature Induced QAQ Uptake

After establishing that specific agonists for nociceptive ion channels can selectively change neuronal permeability, we studied the effects of more complex stimulation paradigms. Nerve injury and electrical activity presumably affect DRG permeability in a more sophisticated way. We were next wondering if changes in temperature alone are sufficient to shift cellular permeability. Temperature changes have many molecular effects on protein function as well as cellular metabolism and signaling. We know that several TRP channels are inherently temperature sensitive and open upon reaching a certain temperature threshold.

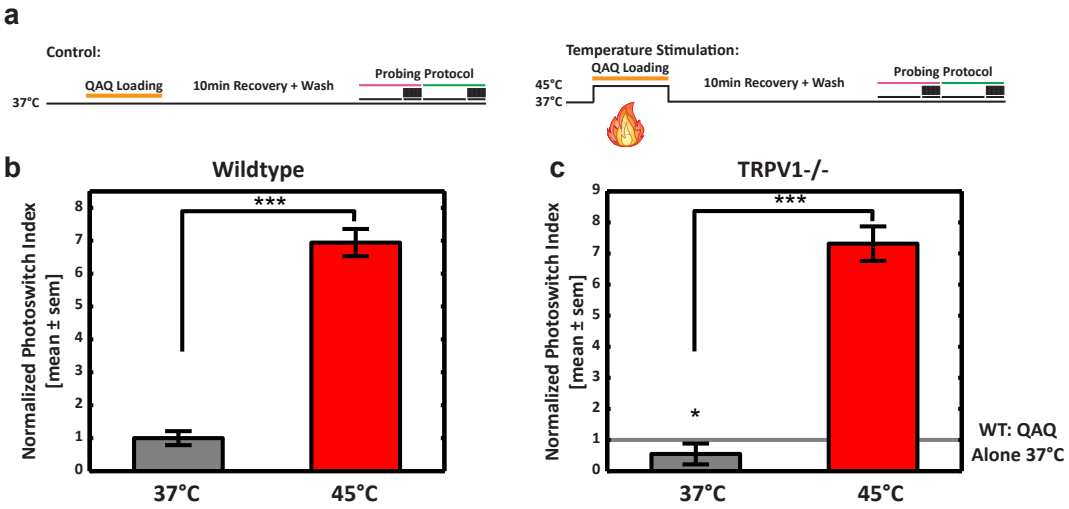

Figure 37.: A Temperature Stimulus induces Permeability Changes of Nociceptive Neurons. **a.** Experimental protocol schematics contrasting control and heat insult protocols. **b.** 5 min exposure to ACSF solution pre-heated to 45°C permealizes intact DRG tissue for QAQ uptake (694±41%, n=24 DRGs, 528 signals). **c.** The same procedure as b. in TRPV1-/- mice yields similar increase in permeability (732±56%, n=11 DRGs, 223 signals). Statistics: Wilcoxon ranksum test for non-parametric distributions: *** $p<0.001$, ** $p<0.01$, * $p<0.05$, n.s. describes not significant.

We briefly exposed DRG tissue of wildtype mice for 5 min to a temperature pulse of 45°C. We observed a very significant increase in QAQ uptake (Figure 37b) that seems to affect all recorded electrodes. This permeability shift is even more pronounced in tissue of mice lacking TRPV1 ion channels (Figure 37c). TRPV1 is therefore not necessary for the observed effects. We hypothesize that either other, not well-characterized TRP channel compensate for the lack of TRPV1 as heat sensor or that more unspecific cellular stress responses might be responsible for this significant shift in permeability.

7.2. Brief Exposure to Increased Temperatures Sensitizes DRG Tissue

In analogy to using electrical activity as conditioning stimulus, we next wondered whether temperature induced permeability changes also linger around for longer periods of time. We therefore separated the temperature conditioning stimulus from QAQ loading. We found that 2 minutes after a heat shock permeability levels are increased almost five-fold (Figure 38b). Even 10 minutes after conditioning, levels remain increased although they begin to approach baseline levels (Figure 38c). Again, identical experiments in TRPV1 knock-out animals confirm that TRPV1 is not necessary for the observed affect. In the contrary, lack of TRPV1 seems to potentiate temperature conditioning as permeability levels are more enhanced than in wildtype (Figure 38c). Whether compensation by other TRP channels in TRPV1-/- tissue or completely other molecular sensors mediate this effect, remains unclear. Unspecific stress response mechanisms independent of TRP channel signaling might also be responsible.

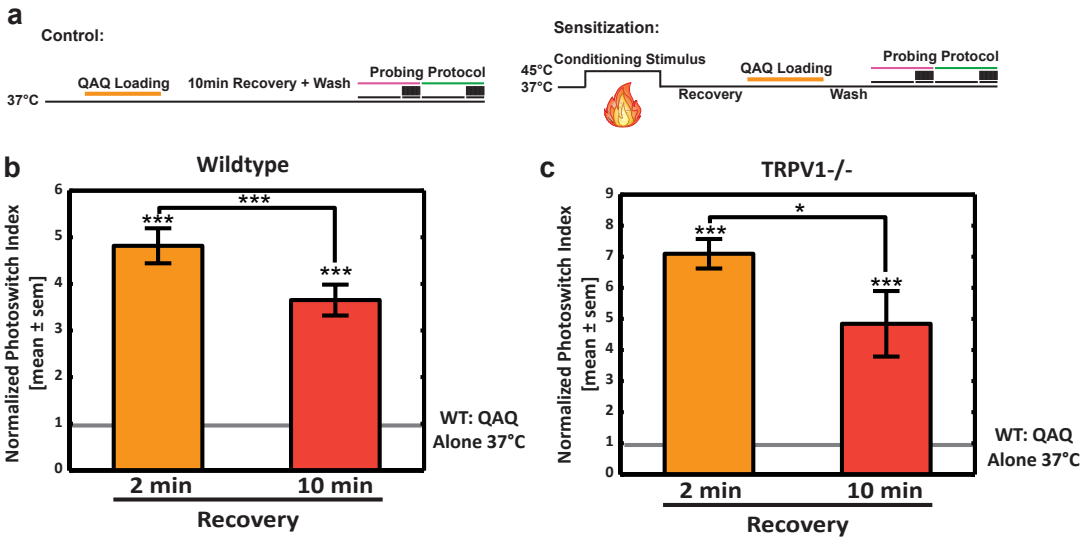

Figure 38.: Temperature conditions Permeability Changes in Intact DRGs.
a. Experimental protocol schematics contrasting control and heat sensitization protocols. **b.** In DRGs from wildtype mice, 2 min (482±38%, n=7 DRGs, 272 signals) and 10 min (365±33%, n=12 DRGs, 576 signals) after presenting a short temperature conditioning stimulus permeability levels are increased. **c.** In analogy to tissue from wildtype mice, permeability levels in DRGs from TRPV1-/- mice are also elevated 2 min (710±48%, n=17 DRGs, 343 signals) and 10 min (484±105%, n=3 DRGs, 81 signals) after conditioning.
Statistics: Wilcoxon ranksum test for non-parametric distributions: *** $p<0.001$, ** $p<0.01$, * $p<0.05$, n.s. describes not significant. Note: In collaboration with Jacob Simon.

8. QENAQ Functions like a Red-shifted QAQ

We tested whether red-shifted photoswitch compounds can be used in a similar way than QAQ. The QENAQ molecule (Figure 10) has an absorption maximum around 480nm and spontaneously relaxes back to its *trans* isomer. When using a dark-480nm probing protocol, QENAQ photosensitizes intact DRG tissue when co-applied with 1μM capsaicin (Figure 39). Also, baseline uptake of QENAQ is comparable to QAQ.

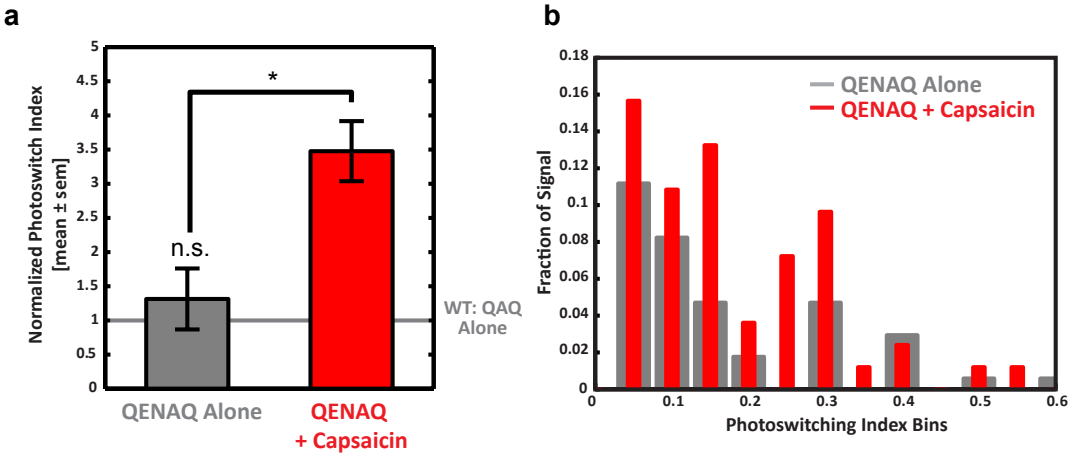

Figure 39.: QENAQ Functions like a Red-shifted QAQ.
a. QENAQ is a functional, red-shifted QAQ analogue which can be probed with 480nm light and shows similar baseline loading compared to QAQ controls (131±44%, n=10 DRGs, 170 signals). QENAQ uptake is facilitated by activation of TRPV1 receptors with 1μM capsaicin (348±44%, n=9 DRGs, 83 signals). **b.** Distribution diagram for the net contribution of positive PI correlating with permeability levels of QENAQ with and without capsaicin treatment.

In conclusion, QENAQ can potentially be used as a QAQ-like, red-shifted analog to probe cellular permeability or act as a silencer of electrical excitability in other neuronal preparations. But further studies are needed to establish QENAQ as a powerful new optopharmacological tool.

9. Interactions of QAQ with the K^+ Channel Shaker

Throughout the following set of experiments we chose to use a Shaker channel variant that has the ball-and-chain domain removed to delete the fast inactivation property. This inactivation-removed Shaker channel lacking residues δ 6 through 46 will be referred to as Shaker (IR) (Hoshi et al., 1990) [61].

9.1. Concentration Dependence of Shaker K^+ Current Block

We have shown before that QAQ reversibly photosensitizes Shaker potassium currents when Shaker is heterogeneously expressed in cell culture and QAQ is delivered to the cytosol by the patch pipette (Mourot at al., 2012) [104]. Shaker (IR) expressed in *Xenopus* oocytes can be modulated in a similar way. Perfusion of QAQ onto the cytosolic side of membrane inside-out patches from *Xenopus* oocytes imparts reversible photo block of K^+ currents (Figure 40b and c).

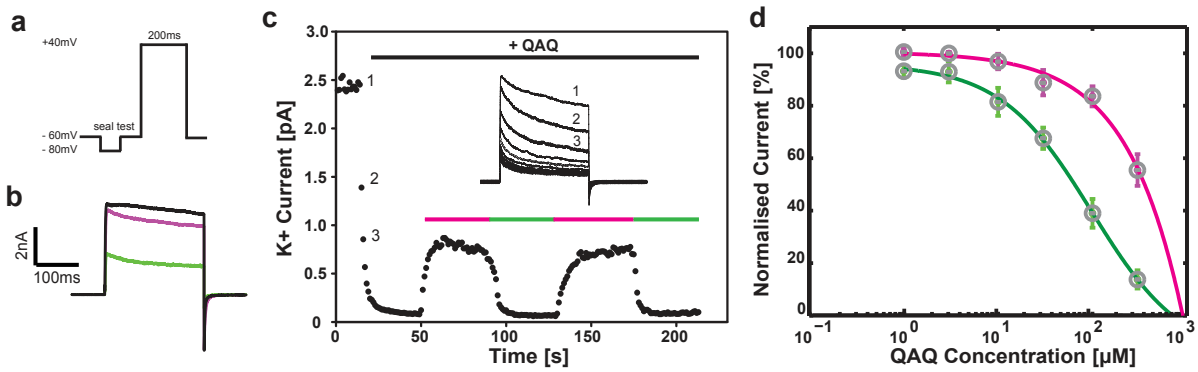

Figure 40.: QAQ is a Concentration-dependent Blocker of Shaker K^+ Currents.
a. Electrophysiological voltage-clamp protocol for probing Shaker K^+ currents. **b.** Example K^+ current trace before QAQ application (black trace), in the presence of unblocking *cis* (purple trace) and blocking *trans* QAQ isomer (green trace) at 100μM. **c.** Typical recording protocol probing Shaker currents at 1Hz frequency while perfusing on and photoswitching QAQ. **d.** Concentration dependence of QAQ block in *trans* and *cis* configuration, respectively. As described in Methods, the half maximal inhibitory concentration (IC50) of *trans* QAQ was calculated to 70-80μM, for *cis* QAQ 600μM. Note: In collaboration with Alexandre Mourot.

Potassium currents through Shaker (IR) channels can be rapidly probed by brief depolarization steps (Figure 40a) of the cell membrane. At a moderate probing frequency of 1Hz slow inactivation of Shaker is relatively limited. Repeated read-out of current amplitudes allows to observe the blocking actions of QAQ over time and under different light conditions (Figure 40c). Once QAQ is perfused onto the cytosolic side of Shaker (IR) in the dark QAQ rapidly blocks potassium currents but block can be readily and reversibly relieved under 380nm light illumination. The time course of block and unblock until steady state depends on light intensity and

the diffusion rate of QAQ isomers between the focal point of illumination and the surrounding solution which contains a reservoir of the respective other QAQ isomer. At the beginning, the rate of initial block is greatly limited by perfusion velocity and diffusion with the bath medium not containing QAQ. Although the patch is led into a plastic tube to speed up the exchange of solutions, a considerable dead volume slows down effective QAQ exposure.

We studied the concentration dependence of QAQ block in *trans* and *cis* over a range from 1μM to 300μM (Figure 40d) by exposing inside out patches to variable concentrations of QAQ. A Hill dose response analysis was conducted for Shaker steady state currents after stable block was achieved for illumination with both 380nm and 500nm light. Half maximal inhibitory concentration (IC50) analysis revealed an IC 50 for *cis* QAQ of about 600μM while *trans* QAQ blocks at half efficiency of around 70-80uμM. The Hill coefficient of the dose-response curve for both isomers is calculated to be around 1. This indicates that merely one QAQ molecule at a time can effectively block channel conductance and the recruitment of more QAQ molecules does not increase blocking efficacy. In other words, there is not cooperativity. However, there might still be physical space for more than one molecule in the lumen of the Shaker channel but presumably only one molecule at a time can be positioned in front of the mouth of the selectivity filter (see Modeling Results).

9.2. QAQ Block is Not Voltage-dependent

We next examined whether channel block by QAQ is voltage dependent. Specifically, is QAQ action increased at more depolarizing voltages? Answering this question can provide insights about how deep in the channel lumen QAQ binds. We recorded current-voltage-relationships (Figure 41a and b) to determine the ratio of blocked (*trans* QAQ) and unblocked (*cis* QAQ) currents to native Shaker currents before QAQ application (Figure 41). We found that block by QAQ shows almost no voltage dependence and conclude that a stronger electrical driving force presumably is not capable to pull the blocker molecule deeper into channel which could possibly enhance block.

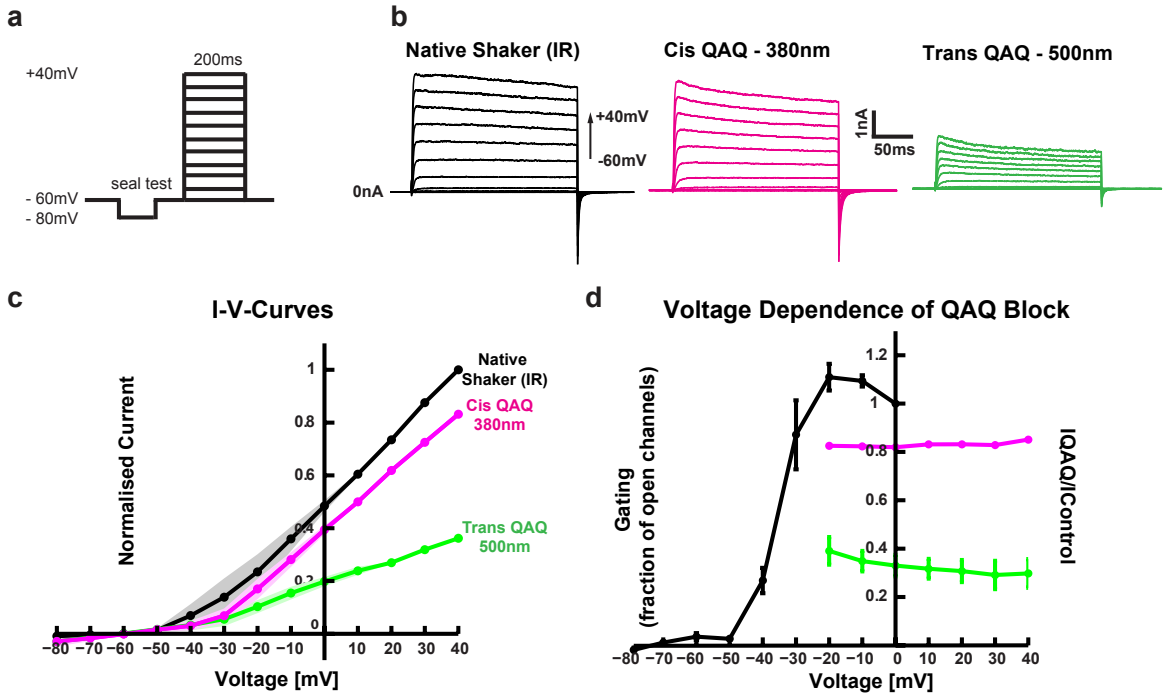

Figure 41.: QAQ Block of Shaker Currents is Not Voltage-dependent.
a. Electrophysiological voltage-clamp protocol for probing current-voltage relationships (IV curve). **b.** Example K^+ current traces at different holding voltages before QAQ application (black trace), in the presence of unblocking *cis* (purple trace) and blocking *trans* QAQ isomer (green trace) at 100μM. **c.** Current-voltage relationships of native Shaker (IR) compared to Shaker (IR) after application of *cis* or *trans* QAQ, currents were normalized to pool multiple patch recordings (n=3), means are represented by dotted line, s.e.m are represented by shaded areas. **d.** The ratio of native Shaker currents to respective currents in either wavelength were plotted over a voltage range where Shaker (IR) is fully opened (compare Shaker (IR) gating curve on the left), error bars represent s.e.m., n=3. Note: In collaboration with Alexandre Mourot.

However, QAQ action on Shaker could be voltage-dependent for the association phase of QAQ binding to the channel meaning block is more rapid at more depolarized potentials. To

examine this hypothesis, the kinetics of QAQ block during the initial probing pulse at various potentials would need to be analyzed.

9.3. QAQ Blocks Shaker Channels in a Use-dependent Fashion

We have shown before that QAQ is a potent silencer of electrical activity and effectively suppresses spiking. However, a first initial spike upon current injection in neuronal culture fails to be blocked even at high intracellular QAQ concentrations (Figure 5). This effect highlights QAQ's characteristic as an open channel blocker. In analogy to TEA and other open channel blockers, we hypothesize that QAQ is also use-dependent in the sense that increased opening time of the reporter channel leads to enhanced blocking efficiency. For applications of QAQ as a silencing tool a closer understanding of this process is crucial. The amount of block is not constant but rather depends on the electrical activity of a cell. Stronger electrical activity increases QAQ block resulting in more silencing. This effect needs to be considered when designing and evaluating experiments.

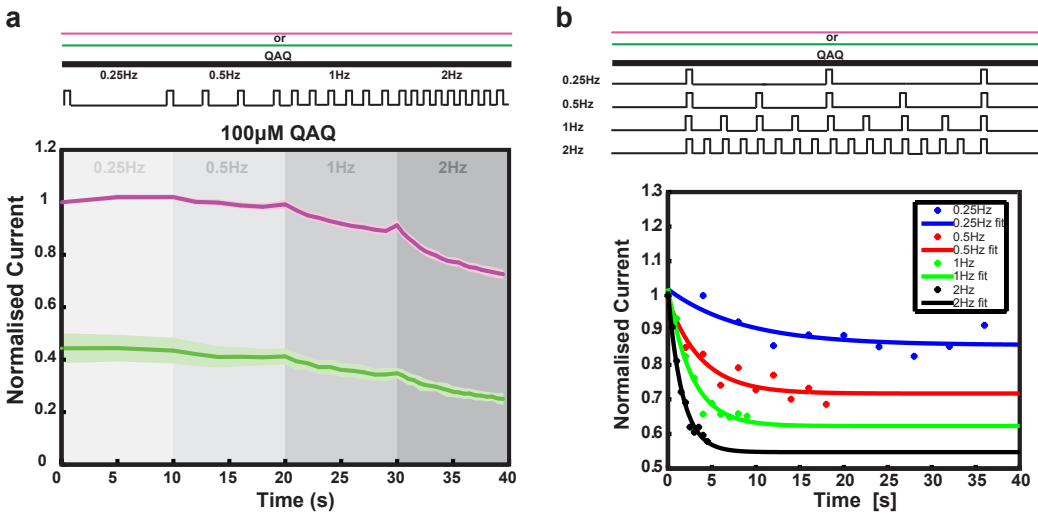

Figure 42.: QAQ Blocks Shaker Channels in a Use-dependent Fashion.
a. QAQ block is enhanced with increased mean channel open time. Schematics demonstrating the voltage clamp protocol used to probe the association of QAQ to the open Shaker channel with increasing probing frequency. At 0.25Hz probing and 200ms pulse length Shaker is open about 5% of the time, at 2Hz the mean open time is increased to 40%. Currents are normalized to initial amplitude under 380nm light. The shaded area represent s.e.m. with n=4. **b.** Equilibrium blocking efficiency is reached faster when channels open more often. Use-dependence does not only affect steady state block but also the time needed to reach stable block at given QAQ concentration and light intensity. An example recording is shown and currents are normalized to peak currents of each probing step. Note: In collaboration with Alexandre Mourot.

We tested use-dependence by probing Shaker currents with increasing frequency and hence increasing channel mean open time. Accelerating the probing frequency from 0.25Hz to 2Hz

increases proportional block for *trans* QAQ by 15% and for *cis* QAQ by 25% (Figure 42a). The mean channel open time changed from 5% to 40% over the course of the protocol indicating a non-linear correlation; the longer Shaker is open the more block can be exhibited.

There are multiple possible explanations for the observed effects. The affinity of QAQ to the open channel could change as channels are open longer. In contrast, if affinity remains constant changed kinetics of QAQ association and dissociation to and from open channels could be variable depending on channel open time.

9.4. Interaction of QAQ with Closed Channels

We next asked whether QAQ associates with closed channels to more readily block currents once probed. This property is not necessary mutually exclusive with functioning as an open channel blocker. Pre-exposure of closed channels could prime subsequent block once channels are opened. To test this hypothesis, we perfused closed Shaker channels with QAQ and asked if currents during the first probing step will be blocked more than during QAQ exposure to repeatedly opened channels. However, the first current steps shows almost no block but block develops fast once the channel is opened more often (Figure 43a). This result shows that QAQ does not associate with closed Shaker channels and does not prime blocking efficiency or kinetics in any way.

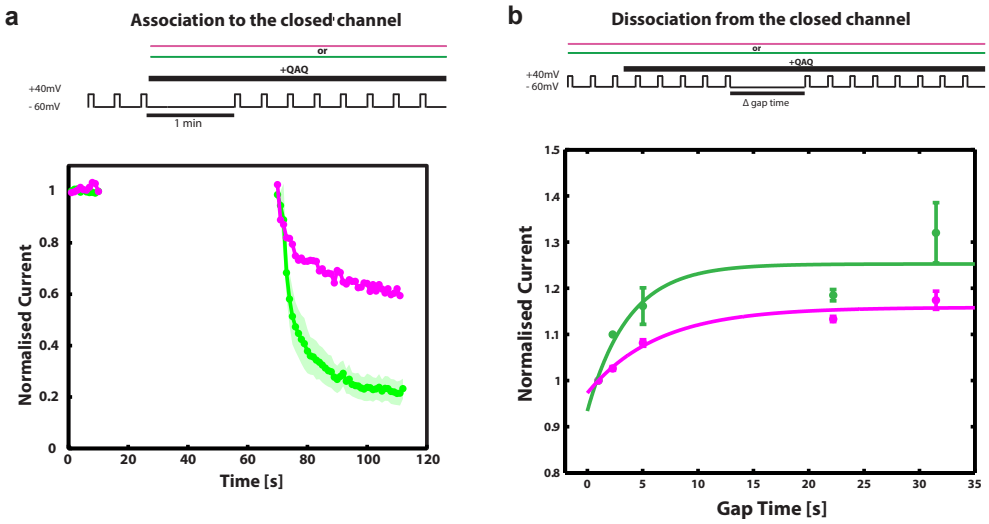

Figure 43.: Interaction of QAQ with Closed Channels.
a. QAQ does not associate with closed Shaker channels, QAQ is an open channel blocker. Exposure of closed Shaker channels to QAQ does not affect blocking properties after opening the channel. Shaded areas represent s.e.m with n=4. **b.** *Trans* QAQ dissociates slower from closed Shaker channels than *cis* QAQ. Currents are normalized to the last current step before the gap. Error bars represent s.e.m. with n=3. Note: In collaboration with Alexandre Mourot.

In the context of association to the closed channel, we next wondered if QAQ dissociates from close Shaker channels. We probed K^+ currents with QAQ present but stopped opening Shaker for variable periods of time before resuming probing. Initial block is reduced the longer the channels are kept closed until the point where block is as low as the first exposure to QAQ.

9.5. QAQ Stabilizes Conformational States

Studies using long-tail QAs, 4-AP and other open channels blockers entering the lumen of potassium channels have shown that the blocker molecules can interact with the protein in a way that stabilizes conformational states, e.g. the open channel state. This effect has been described as a foot-in-the-door mechanism as the blocker sterically hinders the channel gate to close until the blocker dissociates. If the gate closes with blocker still bound the molecule becomes trapped inside the lumen and dissociates even slower. TEA is too small to become trapped in native Shaker but certain Shaker mutants are able to trap TEA. The foot-in-the-door mechanism effectively slows down the off-kinetics of the channel. We wondered if QAQ in a similar way affects channel gating and measured tail currents kinetics in the presence of both QAQ isomers. Tail-currents describe ion flows through the channel after the membrane voltage returns to depolarized potentials. Tail-current kinetics are therefore a correlate to the rate of channel closing. Both *trans* and *cis* QAQ slow down closing of Shaker (Figure 44a). Surprisingly however, *cis* QAQ seems to effect gating more than *trans* QAQ. Further studies are needed to elucidate what molecular interactions are responsible for this effect.

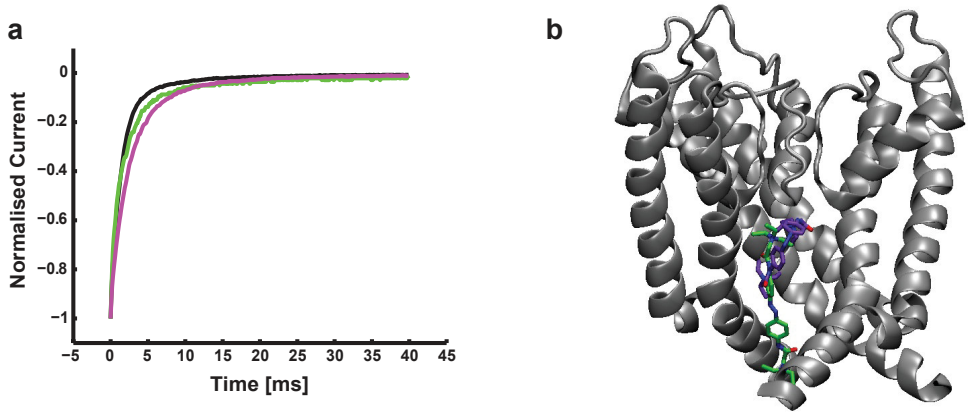

Figure 44.: QAQ Stabilizes the Conformational State of Shaker.
a. Closing kinetics of Shaker in the absence and presence of both QAQ isomers. Bound QAQ slows down off-gating and stabilizes the open conformational state. Exemplary tail currents are plotted after normalization to peak current. **b.** Molecular model of the open K_V1.2-2.1 chimera with docked QAQ isomers. For both *trans* QAQ (green) and *cis* QAQ (purple) the molecule position with the highest molecular docking score was plotted. Note: In collaboration with Alexandre Mourot.

Further, we docked the QAQ molecule into the three-dimensional x-ray structure of the open channel K_V1.2-2.1 chimera (Long et al., 2007) [87] to obtain indications on how the molecule could be positioned within the vestibule. *In silico* molecular docking minimizes free energies of binding (Ander et al., 2008) [3] to find most likely binding positions. All sterically possible and energetically favored docking states place one of the charged end groups of *trans* QAQ right at the entrance to the selectivity filter. In contrast, *cis* QAQ is sterically hindered to reach the mouth of the selectivity filter (Figure 44b). This result might indicate a reasonable explanation for efficient block of ion flow in *trans* versus *cis* QAQ. The charged end group in close vicinity to the selectivity filter presumably interferes with the molecular ion conduction process.

V. Discussion

1. Crosstalk between Nociceptive Neurons

We report permeability changes of nociceptive neurons after peripheral nerve injury in a TRPA1 dependent way. Furthermore, permeability shifts are not limited to axotomized neuronal populations but also affect intact sensory neurons. Injured neurons communicate with adjacent cells leading to increased permeability which is measured at the DRG cell bodies far away from the site of injury. We have also shown that electrical activity alone is sufficient to drive permeability changes in a TRPA1 dependent fashion.

Nerve injury and inflammation induced neuronal hyperexcitability underlie chronic and neuropathic pain. Further, hyperexitability has been shown to be correlated with TRPA1 activity which induces e.g. cold hyperalgesia (del Camino et al., 2010) [42]. TRPA1 activity in that context can be either cause or consequence of this hyperexcitability. Increased firing after injury might convey the signal leading to permeability changes at the cell bodies. Injured cells do not necessarily change their permeability itself but presumably release neuropeptides which in turn sensitize cells in the vicinity, both injured and intact. Our data suggests that TRPA1 is necessary for those adaptations of cellular permeability. However, TRPA1 might not be the nociceptive channel that actually mediates increased permeation. For instance, calcium influx through TRPA1 might initiate other signaling cascades eventually leading to opening of an unknown ion channel. Following that theory, TRPA1 does not even necessarily need to be expressed in injured, petidergic signaling cells but could mediate permeability changes at the receiving end. This notion is supported by our finding that Yo-PRO-1 co-localizes only to some extend with TRPV1 although TRPA1 expression is highly correlated with the presence of TRPV1. There is a small population of TRPA1 positive, TRPV1 negative neurons but the potential contribution of this group cannot account for all cells taking up Yo-PRO. Another point arguing that TRPA1 is not necessarily expressed in initiating cells is the lacking co-localization with IB4. TRPA1 and IB4 are highly correlated (Barabas et al., 2012) [11] and our data does not suggest much permeability change in non-peptidergic neurons.

The most important physiological impact of permeability changes is an increase in calcium conductance. Specifically, calcium might be key factor affecting either TRPA1 receptors or voltage-gated calcium channels in a self-propelling, feed forward way.

First, calcium influx could be triggered by frequent depolarization through voltage-gated calcium channels (Ca_V). Especially $Ca_V3.2$ has been linked with chronic pain states as increased

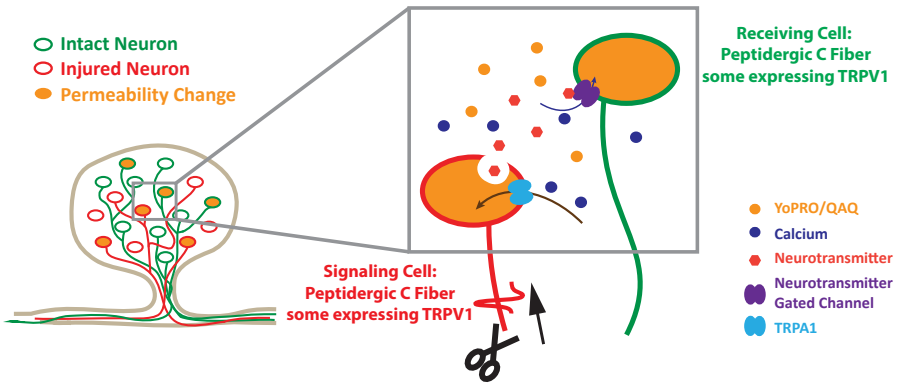

Figure 45.: Model for Crosstalk between Injured and Intact Nociceptive Populations.

expression is proalgesic and inhibiting of those channels mediates pain relief (Bourinet et al., 2005) [22]. Second, TRPA1 itself is regulated by calcium. Initial activation leading to calcium influx sensitizes TRPA1 to remain open even when initial stimuli have faded (Zurborg et al., 2007) [152]. Moreover, the dilated state of TRPA1 is highly modulated by calcium and increased calcium influx potentially depletes extracellular levels favoring a conversion to the dilated state (Banke, 2011) [10].

In the context of crosstalk manifested by permeability changes, there have been multiple studies arguing against a strict labelled line hypothesis and suggesting that complex pain signals are conveyed through interactions of different afferents (Prescott et al., 2014) [114]. Primary afferents are tuned to specific sensory modalities but complex environmental stimuli often impact many afferents. This co-activation can create more complex pain response patterns and communication between neurons enables more dynamic signal regulation. This principle of combinatorial coding is used, for example, in the retina where color coding of the entire visual spectrum is accomplished with merely three broadly tuned rhodopsins. Other crosstalk mechanisms in nociceptive systems have also been identified, e.g. interneuron mediated communication challenging the labelled line theory in the dorsal horn (Figure 12b, Prescott et al., 2014 [114]). Our results extend the level of crosstalk. Although the exact mechanism of communication is unknown, this signaling could contribute to the spread of receptive fields, extended pain perception, maladaptive plasticity and changes in sensory modalities. Also, nerve injury regulates gene expression and TRPV1 has been found to be down regulated in injured fibers after partial injury but upregulated in adjacent intact cells (Hudson et al., 2001) [63]. Other genes, e.g. TRPA1, could be modulated in a similar way.

Finally, we have shown before that bradykinin induces permeability changes in intact DRGs (Mourot et al., 2012) [104] and bradykinin release directly activates TRPA1 (Bautista et al., 2006; Bandell et al., 2004; Kwan et al., 2006) [14][6][74]. Further, peripheral nerve injury triggers bradykinin release in the periphery fostering pain hypersensitivity. Therefore, we speculate that

bradykinin might contribute to the observed permeability changes in the DRG in both injured and intact nociceptors.

In contrast to TRPV1, heterogeneous expression of TRPA1 channels cell culture and following stimulation with ally isothiocyanate did not lead to substantial QAQ entry (Mourot et al., 2012) [104]. However, in an intact DRGs similar stimulation leads to a more permeable TRPA1 activity state suggesting that additional factors present in DRG cells are required for TRPA1 activation.

2. Interactions of QAQ with Voltage-gated Ion Channels

QAQ's chemical structure is derived from two TEA groups linked together and therefore similar biophysical properties as TEA are expected. Extensive studies of TEA-Shaker interactions thus provide very helpful orientation on how to design and interpret experiments. However, QAQ's larger size and the ability to dramatically change geometry between isomers suggest qualitative differences.

For optimal application of QAQ block it is desirable to use a concentration where almost complete channel block is achieved in 500nm light while switching to 380nm light relieves block equally efficient. At current experimental conditions, there is no such optimal concentration since the dose-response curves of both isomers are not sufficiently separated. Photoisomerization is not complete and even at high UV light intensities a fraction of QAQ molecules with always remain in *trans* state. This would explain partial block even under 380nm light. However, it cannot be ruled out that *cis* QAQ does not have a low affinity for open channels and does exhibit some sort of blocking property. Further studies generating a light intensity dose response curve would be helpful to determine if partial block in 380nm at higher concentrations is indeed due to partial isomerization.

TEA block of Shaker is voltage-dependent. Surprisingly, we found that QAQ block does not seem to markedly increase with depolarizing voltage. This suggests that QAQ does not occupy different binding sites within the vestibule but rather remains in a given position which not necessarily needs to be coordinated with channel residues. Detailed mutation studies would be required to understand more the molecular basis of QAQ affinity to the open channel. Further, given a Hill coefficient of around 1 and based on the molecular docking results, we assume that only one QAQ molecule at a time can enter the verstibule and therefore cooperativity effects observed for TEA are not a factor for QAQ.

Like many other open channel blockers, we assumed that QAQ will also function in a use-dependent manner. Experiments silencing neuronal activity in cell culture already suggest use-dependence as an initial spike after current injection cannot be blocked even at high QAQ concentrations (Mourot et al., 2012) [104]. We probed use-dependence by increasing pulsing frequency simultaneously lengthening the mean open time of Shaker. Effective block is determined by the equilibrium of association and dissociation of QAQ to and from the channel. In analogy to

lidocaine, it has been proposed that extended open time could therefore increase affinity to the channel by forming of different channel open states (Cummins, 2007) [40]. Alternatively, QAQ could interfere with slow inactivation, accelerating current reduction. However, TEA has only been found to slow down inactivation which acts on the external channel. The kinetics reaching maximal block is also increased arguing for an affinity change.

We next studied the interactions of QAQ with the closed Shaker channel. As expected, QAQ does not associate with the closed channel and not prime block. The binding site lies within the mouth of the channel and is not accessible in the closed confirmation.

Some mutants of Shaker are capable to trap TEA within the vestibule, meaning the channel can closed with TEA still bound. We wondered if QAQ can be caught in a similar way. A possible experiment to test this would be equilibrating QAQ with frequently opened Shaker, then stop probing currents and wash away excess, unbound QAQ from the bath. Current amplitude after resuming to probe currents could give an indication about retained, trapped QAQ. However, this experimental design is very dependent on perfusion speed. The perfusion of QAQ and the exchange of external solution is rate limiting and cannot be perfectly controlled with our current setup. As a consequence, experiments involving kinetic consideration have to be designed at stable QAQ concentrations.

More studies are needed to better understand QAQ interactions with Shaker. For example, external application of QAQ could affect slow inactivation and block in similar ways as TEA. More interestingly, we found that QAQ entering cells through channel conduits like TRPV1 behaves differently than QAQ washed onto Shaker in excised patches. QAQ block remains active many minutes after establishing whole-cell configuration with a QAQ-free pipette reservoir. For some reason QAQ is not diluted into the pipette. Besides the possibility that QAQ diffusion is somehow hindered, recent structural studies have suggested the possibility of other entry routes for blocker compounds into the vestibule. Loading through TRPV1 could utilizes such a hydrophobic route and to test this hypothesis excised patches from previously QAQ loaded cells need to be examined.

Further studies are needed to better understand QAQ action but results will be translatable to similar photoswitch compounds, some of which even show potential drug applications.

VI. References

[1] Z. Ali, M. Ringkamp, T. V. Hartke, H. F. Chien, N. A. Flavahan, J. N. Campbell, and R. A. Meyer. Uninjured c-fiber nociceptors develop spontaneous activity and alpha-adrenergic sensitivity following l6 spinal nerve ligation in monkey. *J Neurophysiol*, 81(2):455–466, Feb 1999. 21

[2] Payam Andalib, Joseph F. Consiglio, Josef G. Trapani, and Stephen J. Korn. The external tea binding site and c-type inactivation in voltage-gated potassium channels. *Biophys J*, 87(5):3148–3161, Nov 2004. 16

[3] Martin Andér, Victor B. Luzhkov, and Johan Aqvist. Ligand binding to the voltage-gated kv1.5 potassium channel in the open state–docking and computer simulations of a homology model. *Biophys J*, 94(3):820–831, Feb 2008. 74

[4] C. M. Armstrong. Inactivation of the potassium conductance and related phenomena caused by quaternary ammonium ion injection in squid axons. *J Gen Physiol*, 54(5):553–575, Nov 1969. 16

[5] C. M. Armstrong. Interaction of tetraethylammonium ion derivatives with the potassium channels of giant axons. *J Gen Physiol*, 58(4):413–437, Oct 1971. 16

[6] Michael Bandell, Gina M. Story, Sun Wook Hwang, Veena Viswanath, Samer R. Eid, Matt J. Petrus, Taryn J. Earley, and Ardem Patapoutian. Noxious cold ion channel trpa1 is activated by pungent compounds and bradykinin. *Neuron*, 41(6):849–857, Mar 2004. 24, 76

[7] Matthew Banghart, Katharine Borges, Ehud Isacoff, Dirk Trauner, and Richard H. Kramer. Light-activated ion channels for remote control of neuronal firing. *Nat Neurosci*, 7(12):1381–1386, Dec 2004. 5

[8] Matthew R. Banghart, Alexandre Mourot, Doris L. Fortin, Jennifer Z. Yao, Richard H. Kramer, and Dirk Trauner. Photochromic blockers of voltage-gated potassium channels. *Angew Chem Int Ed Engl*, 48(48):9097–9101, 2009. 6, 7

[9] T. G. Banke, S. R. Chaplan, and A. D. Wickenden. Dynamic changes in the trpa1 selectivity filter lead to progressive but reversible pore dilation. *Am J Physiol Cell Physiol*, 298(6):C1457–C1468, Jun 2010. 26

[10] Tue G. Banke. The dilated trpa1 channel pore state is blocked by amiloride and analogues. *Brain Res*, 1381:21–30, Mar 2011. 35, 76

[11] Marie E. Barabas, Elena A. Kossyreva, and Cheryl L. Stucky. Trpa1 is functionally expressed primarily by ib4-binding, non-peptidergic mouse and rat sensory neurons. *PLoS One*, 7(10):e47988, 2012. 75

[12] Allan I. Basbaum, Diana M. Bautista, Grégory Scherrer, and David Julius. Cellular and molecular mechanisms of pain. *Cell*, 139(2):267–284, Oct 2009. 22

[13] Diana Bautista and David Julius. Fire in the hole: pore dilation of the capsaicin receptor trpv1. *Nat Neurosci*, 11(5):528–529, May 2008. 26

[14] Diana M. Bautista, Sven-Eric Jordt, Tetsuro Nikai, Pamela R. Tsuruda, Andrew J. Read, Jeannie Poblete, Ebenezer N. Yamoah, Allan I. Basbaum, and David Julius. Trpa1 mediates the inflammatory actions of environmental irritants and proalgesic agents. *Cell*, 124(6):1269–1282, Mar 2006. 24, 25, 76

[15] Diana M. Bautista, Pouya Movahed, Andrew Hinman, Helena E. Axelsson, Olov Sterner, Edward D. Högestätt, David Julius, Sven-Eric Jordt, and Peter M. Zygmunt. Pungent products from garlic activate the sensory ion channel trpa1. *Proc Natl Acad Sci U S A*, 102(34):12248–12252, Aug 2005. 24

[16] Andrew A. Beharry, Oleg Sadovski, and G Andrew Woolley. Azobenzene photoswitching without ultraviolet light. *J Am Chem Soc*, 133(49):19684–19687, Dec 2011. 12

[17] Andrew A. Beharry and G Andrew Woolley. Azobenzene photoswitches for biomolecules. *Chem Soc Rev*, 40(8):4422–4437, Aug 2011. 4

[18] Alexander M. Binshtok. Mechanisms of nociceptive transduction and transmission: a machinery for pain sensation and tools for selective analgesia. *Int Rev Neurobiol*, 97:143–177, 2011. 12

[19] Alexander M. Binshtok, Bruce P. Bean, and Clifford J. Woolf. Inhibition of nociceptors by trpv1-mediated entry of impermeant sodium channel blockers. *Nature*, 449(7162):607–610, Oct 2007. 12

[20] Alexander M. Binshtok, Peter Gerner, Seog Bae Oh, Michelino Puopolo, Suzuko Suzuki, David P. Roberson, Teri Herbert, Chi-Fei Wang, Donghoon Kim, Gehoon Chung, Aya A. Mitani, Ging Kuo Wang, Bruce P. Bean, and Clifford J. Woolf. Coapplication of lidocaine and the permanently charged sodium channel blocker qx-314 produces a long-lasting nociceptive blockade in rodents. *Anesthesiology*, 111(1):127–137, Jul 2009. 12

[21] T. J. Biscoe, S. M. Nickels, and C. A. Stirling. Numbers and sizes of nerve fibres in mouse spinal roots. *Q J Exp Physiol*, 67(3):473–494, Jul 1982. 20

[22] Emmanuel Bourinet, Abdelkrim Alloui, Arnaud Monteil, Christian Barrère, Brigitte Couette, Olivier Poirot, Anne Pages, John McRory, Terrance P. Snutch, Alain Eschalier, and Joël Nargeot. Silencing of the cav3.2 t-type calcium channel gene in sensory neurons demonstrates its major role in nociception. *EMBO J*, 24(2):315–324, Jan 2005. 76

[23] João M. Bráz and Allan I. Basbaum. Differential atf3 expression in dorsal root ganglion neurons reveals the profile of primary afferents engaged by diverse noxious chemical stimuli. *Pain*, 150(2):290–301, Aug 2010. 25, 54, 62

[24] Austin L. Brown, Brandon E. Johnson, and Miriam B. Goodman. Patch clamp recording of ion channels expressed in xenopus oocytes. *J Vis Exp*, (20), 2008. 42

[25] Iva Bruhova, Denis B. Tikhonov, and Boris S. Zhorov. Access and binding of local anesthetics in the closed sodium channel. *Mol Pharmacol*, 74(4):1033–1045, Oct 2008. 16

[26] Pablo Brumovsky, Marcelo J. Villar, and Tomas Hökfelt. Tyrosine hydroxylase is expressed in a subpopulation of small dorsal root ganglion neurons in the adult mouse. *Exp Neurol*, 200(1):153–165, Jul 2006. 19

[27] M Catherine Bushnell, Marta Ceko, and Lucie A. Low. Cognitive and emotional control of pain and its disruption in chronic pain. *Nat Rev Neurosci*, 14(7):502–511, Jul 2013. 21

[28] Erhu Cao, Maofu Liao, Yifan Cheng, and David Julius. Trpv1 structures in distinct conformations reveal activation mechanisms. *Nature*, 504(7478):113–118, Dec 2013. 25, 26

[29] Ombretta Caspani, Sandra Zurborg, Dominika Labuz, and Paul A. Heppenstall. The contribution of trpm8 and trpa1 channels to cold allodynia and neuropathic pain. *PLoS One*, 4(10):e7383, 2009. 25

[30] James J. Chambers, Matthew R. Banghart, Dirk Trauner, and Richard H. Kramer. Light-induced depolarization of neurons using a modified shaker k(+) channel and a molecular photoswitch. *J Neurophysiol*, 96(5):2792–2796, Nov 2006. 5

[31] Luis Puelles Charles Watson, George Paxinos, editor. *The Mouse Nervous System*. Elsevier Academic Press, 1st edition, 2012. 18, 21

[32] Jun Chen, Shailen K. Joshi, Stanley DiDomenico, Richard J. Perner, Joe P. Mikusa, Donna M. Gauvin, Jason A. Segreti, Ping Han, Xu-Feng Zhang, Wende Niforatos, Bruce R. Bianchi, Scott J. Baker, Chengmin Zhong, Gricelda H. Simler, Heath A. McDonald, Robert G. Schmidt, Steve P. McGaraughty, Katharine L. Chu, Connie R. Faltynek, Michael E. Kort, Regina M. Reilly, and Philip R. Kym. Selective blockade of trpa1 channel attenuates pathological pain without altering noxious cold sensation or body temperature regulation. *Pain*, 152(5):1165–1172, May 2011. 25

[33] Jun Chen, Donghee Kim, Bruce R. Bianchi, Eric J. Cavanaugh, Connie R. Faltynek, Philip R. Kym, and Regina M. Reilly. Pore dilation occurs in trpa1 but not in trpm8 channels. *Mol Pain*, 5:3, 2009. 26, 35

[34] B. A. Chizh and P. Illes. P2x receptors and nociception. *Pharmacol Rev*, 53(4):553–568, Dec 2001. 24

[35] K. L. Choi, C. Mossman, J. Aubé, and G. Yellen. The internal quaternary ammonium receptor site of shaker potassium channels. *Neuron*, 10(3):533–541, Mar 1993. 16

[36] Man-Kyo Chung, Ali D. Güler, and Michael J. Caterina. Trpv1 shows dynamic ionic selectivity during agonist stimulation. *Nat Neurosci*, 11(5):555–564, May 2008. 25, 26

[37] David E. Clapham. Trp channels as cellular sensors. *Nature*, 426(6966):517–524, Dec 2003. 24

[38] David E. Clapham, Craig Montell, Guenter Schultz, David Julius, and International Union of Pharmacology . International union of pharmacology. xliii. compendium of voltage-gated ion channels: transient receptor potential channels. *Pharmacol Rev*, 55(4):591–596, Dec 2003. 23

[39] D. A. Cockayne, S. G. Hamilton, Q. M. Zhu, P. M. Dunn, Y. Zhong, S. Novakovic, A. B. Malmberg, G. Cain, A. Berson, L. Kassotakis, L. Hedley, W. G. Lachnit, G. Burnstock, S. B. McMahon, and A. P. Ford. Urinary bladder hyporeflexia and reduced pain-related behaviour in p2x3-deficient mice. *Nature*, 407(6807):1011–1015, Oct 2000. 24

[40] Theodore R. Cummins. Setting up for the block: the mechanism underlying lidocaine's use-dependent inhibition of sodium channels. *J Physiol*, 582(Pt 1):11, Jul 2007. 78

[41] T. M. Cunha, WA Verri, Jr, J. S. Silva, S. Poole, F. Q. Cunha, and S. H. Ferreira. A cascade of cytokines mediates mechanical inflammatory hypernociception in mice. *Proc Natl Acad Sci U S A*, 102(5):1755–1760, Feb 2005. 22

[42] Donato del Camino, Sarah Murphy, Melissa Heiry, Lee B. Barrett, Taryn J. Earley, Colby A. Cook, Matt J. Petrus, Michael Zhao, Marc D'Amours, Nate Deering, Gary J. Brenner, Michael Costigan, Neil J. Hayward, Jayhong A. Chong, Christopher M. Fanger, Clifford J. Woolf, Ardem Patapoutian, and Magdalene M. Moran. Trpa1 contributes to cold hypersensitivity. *J Neurosci*, 30(45):15165–15174, Nov 2010. 75

[43] Ajay Dhaka, Taryn J. Earley, James Watson, and Ardem Patapoutian. Visualizing cold spots: Trpm8-expressing sensory neurons and their projections. *J Neurosci*, 28(3):566–575, Jan 2008. 24

[44] Ajay Dhaka, Amber N. Murray, Jayanti Mathur, Taryn J. Earley, Matt J. Petrus, and Ardem Patapoutian. Trpm8 is required for cold sensation in mice. *Neuron*, 54(3):371–378, May 2007. 24

[45] Ajay Dhaka, Valerie Uzzell, Adrienne E. Dubin, Jayanti Mathur, Matt Petrus, Michael Bandell, and Ardem Patapoutian. Trpv1 is activated by both acidic and basic ph. *J Neurosci*, 29(1):153–158, Jan 2009. 25

[46] Ajay Dhaka, Veena Viswanath, and Ardem Patapoutian. Trp ion channels and temperature sensation. *Annu Rev Neurosci*, 29:135–161, 2006. 24

[47] Mingxin Dong, Amirhossein Babalhavaeji, Subhas Samanta, Andrew A. Beharry, and G Andrew Woolley. Red-shifting azobenzene photoswitches for in vivo use. *Acc Chem Res*, 48(10):2662–2670, Oct 2015. 12

[48] Mirjam Eberhardt, Tal Hoffmann, Susanne K. Sauer, Karl Messlinger, Peter W. Reeh, and Michael J M. Fischer. Calcitonin gene-related peptide release from intact isolated dorsal root and trigeminal ganglia. *Neuropeptides*, 42(3):311–317, Jun 2008. 19

[49] Xin Fang, Laiche Djouhri, Simon McMullan, Carol Berry, Stephen G. Waxman, Kenji Okuse, and Sally N. Lawson. Intense isolectin-b4 binding in rat dorsal root ganglion neurons distinguishes c-fiber nociceptors with broad action potentials and high nav1.9 expression. *J Neurosci*, 26(27):7281–7292, Jul 2006. 19

[50] Timm Fehrentz, Christian A. Kuttruff, Florian M E. Huber, Michael A. Kienzler, Peter Mayer, and Dirk Trauner. Exploring the pharmacology and action spectra of photochromic open-channel blockers. *Chembiochem*, 13(12):1746–1749, Aug 2012. 5, 13

[51] Timm Fehrentz, Matthias Schönberger, and Dirk Trauner. Optochemical genetics. *Angew Chem Int Ed Engl*, 50(51):12156–12182, Dec 2011. 1

[52] Lief Fenno, Ofer Yizhar, and Karl Deisseroth. The development and application of optogenetics. *Annu Rev Neurosci*, 34:389–412, 2011. 2

[53] Doris L. Fortin, Matthew R. Banghart, Timothy W. Dunn, Katharine Borges, Daniel A. Wagenaar, Quentin Gaudry, Movses H. Karakossian, Thomas S. Otis, William B. Kristan, Dirk Trauner, and Richard H. Kramer. Photochemical control of endogenous ion channels and cellular excitability. *Nat Methods*, 5(4):331–338, Apr 2008. 6, 7

[54] Doris L. Fortin, Timothy W. Dunn, Alexis Fedorchak, Duane Allen, Rachel Montpetit, Matthew R. Banghart, Dirk Trauner, John P. Adelman, and Richard H. Kramer. Optogenetic photochemical control of designer k+ channels in mammalian neurons. *J Neurophysiol*, 106(1):488–496, Jul 2011. 5

[55] J. Frederick, M. E. Buck, D. J. Matson, and D. N. Cortright. Increased trpa1, trpm8, and trpv2 expression in dorsal root ganglia by nerve injury. *Biochem Biophys Res Commun*, 358(4):1058–1064, Jul 2007. 21

[56] E. L. Green. Genetic and non-genetic factors which influence the type of the skeleton in an inbred strain of mice. *Genetics*, 26(2):192–222, Mar 1941. 20

[57] Jessica H. Harvey and Dirk Trauner. Regulating enzymatic activity with a photoswitchable affinity label. *Chembiochem*, 9(2):191–193, Jan 2008. 4

[58] Bertil Hille. *Ion Channels of Excitable Membranes*. Sinauer Associates, third edition, 2001. 9

[59] Andrew Hinman, Huai-Hu Chuang, Diana M. Bautista, and David Julius. Trp channel activation by reversible covalent modification. *Proc Natl Acad Sci U S A*, 103(51):19564–19568, Dec 2006. 24

[60] M. Holmgren, P. L. Smith, and G. Yellen. Trapping of organic blockers by closing of voltage-dependent k+ channels: evidence for a trap door mechanism of activation gating. *J Gen Physiol*, 109(5):527–535, May 1997. 16

[61] T. Hoshi, W. N. Zagotta, and R. W. Aldrich. Biophysical and molecular mechanisms of shaker potassium channel inactivation. *Science*, 250(4980):533–538, Oct 1990. 68

[62] Tian-Ying Huang, Vitali Belzer, and Menachem Hanani. Gap junctions in dorsal root ganglia: possible contribution to visceral pain. *Eur J Pain*, 14(1):49.e1–49.11, Jan 2010. 21

[63] L. J. Hudson, S. Bevan, G. Wotherspoon, C. Gentry, A. Fox, and J. Winter. Vr1 protein expression increases in undamaged drg neurons after partial nerve injury. *Eur J Neurosci*, 13(11):2105–2114, Jun 2001. 21, 76

[64] Amteshwar Singh Jaggi, Vivek Jain, and Nirmal Singh. Animal models of neuropathic pain. *Fundam Clin Pharmacol*, 25(1):1–28, Feb 2011. 49

[65] Lily Yeh Jan and Yuh Nung Jan. Voltage-gated potassium channels and the diversity of electrical signalling. *J Physiol*, 590(Pt 11):2591–2599, Jun 2012. 14

[66] Sven-Eric Jordt, Diana M. Bautista, Huai-Hu Chuang, David D. McKemy, Peter M. Zygmunt, Edward D. Högestätt, Ian D. Meng, and David Julius. Mustard oils and cannabinoids excite sensory nerve fibres through the trp channel anktm1. *Nature*, 427(6971):260–265, Jan 2004. 24

[67] D. Julius and A. I. Basbaum. Molecular mechanisms of nociception. *Nature*, 413(6852):203–210, Sep 2001. 22

[68] Eric Kandel. *The Principles of Neuroscience*. McGraw-Hill Education, 2012. 19

[69] Yuji Karashima, Jean Prenen, Karel Talavera, Annelies Janssens, Thomas Voets, and Bernd Nilius. Agonist-induced changes in ca(2+) permeation through the nociceptor cation channel trpa1. *Biophys J*, 98(5):773–783, Mar 2010. 26

[70] Yuji Karashima, Karel Talavera, Wouter Everaerts, Annelies Janssens, Kelvin Y. Kwan, Rudi Vennekens, Bernd Nilius, and Thomas Voets. Trpa1 acts as a cold sensor in vitro and in vivo. *Proc Natl Acad Sci U S A*, 106(4):1273–1278, Jan 2009. 24

[71] Hirokazu Katsura, Koichi Obata, Toshiyuki Mizushima, Hiroki Yamanaka, Kimiko Kobayashi, Yi Dai, Tetsuo Fukuoka, Atsushi Tokunaga, Masafumi Sakagami, and Koichi Noguchi. Antisense knock down of trpa1, but not trpm8, alleviates cold hyperalgesia after spinal nerve ligation in rats. *Exp Neurol*, 200(1):112–123, Jul 2006. 25

[72] B. S. Khakh, X. R. Bao, C. Labarca, and H. A. Lester. Neuronal p2x transmitter-gated cation channels change their ion selectivity in seconds. *Nat Neurosci*, 2(4):322–330, Apr 1999. 25

[73] Richard H. Kramer, Alexandre Mourot, and Hillel Adesnik. Optogenetic pharmacology for control of native neuronal signaling proteins. *Nat Neurosci*, 16(7):816–823, Jul 2013. 3, 4, 5

[74] Kelvin Y. Kwan, Andrew J. Allchorne, Melissa A. Vollrath, Adam P. Christensen, Duan-Sun Zhang, Clifford J. Woolf, and David P. Corey. Trpa1 contributes to cold, mechanical, and chemical nociception but is not essential for hair-cell transduction. *Neuron*, 50(2):277–289, Apr 2006. 21, 24, 25, 76

[75] Kelvin Y. Kwan, Joshua M. Glazer, David P. Corey, Frank L. Rice, and Cheryl L. Stucky. Trpa1 modulates mechanotransduction in cutaneous sensory neurons. *J Neurosci*, 29(15):4808–4819, Apr 2009. 25

[76] Cédric J. Laedermann, Marie Pertin, Marc R. Suter, and Isabelle Decosterd. Voltage-gated sodium channel expression in mouse drg after sni leads to re-evaluation of projections of injured fibers. *Mol Pain*, 10:19, 2014. 20, 48

[77] M. Ledda, S. De Palo, and E. Pannese. Ratios between number of neuroglial cells and number and volume of nerve cells in the spinal ganglia of two species of reptiles and three species of mammals. *Tissue Cell*, 36(1):55–62, Feb 2004. 21

[78] Joshua Levitz, Carlos Pantoja, Benjamin Gaub, Harald Janovjak, Andreas Reiner, Adam Hoagland, David Schoppik, Brian Kane, Philipp Stawski, Alexander F. Schier, Dirk Trauner, and Ehud Y. Isacoff. Optical control of metabotropic glutamate receptors. *Nat Neurosci*, 16(4):507–516, Apr 2013. 5

[79] Mufeng Li, Gilman E S. Toombes, Shai D. Silberberg, and Kenton J. Swartz. Physical basis of apparent pore dilation of atp-activated p2x receptor channels. *Nat Neurosci*, 18(11):1577–1583, Nov 2015. 26

[80] Y. Li, M. J. Dorsi, R. A. Meyer, and A. J. Belzberg. Mechanical hyperalgesia after an l5 spinal nerve lesion in the rat is not dependent on input from injured nerve fibers. *Pain*, 85(3):493–502, Apr 2000. 21

[81] Yan Li, Sung Yon Um, and Thomas V. McDonald. Voltage-gated potassium channels: regulation by accessory subunits. *Neuroscientist*, 12(3):199–210, Jun 2006. 14

[82] Maofu Liao, Erhu Cao, David Julius, and Yifan Cheng. Structure of the trpv1 ion channel determined by electron cryo-microscopy. *Nature*, 504(7478):107–112, Dec 2013. 25, 26

[83] Wan-Chen Lin, Christopher M. Davenport, Alexandre Mourot, Devaiah Vytla, Caleb M. Smith, Kathryne A. Medeiros, James J. Chambers, and Richard H. Kramer. Engineering a light-regulated gabaa receptor for optical control of neural inhibition. *ACS Chem Biol*, 9(7):1414–1419, Jul 2014. 5

[84] Wan-Chen Lin, Ming-Chi Tsai, Christopher M. Davenport, Caleb M. Smith, Julia Veit, Neil M. Wilson, Hillel Adesnik, and Richard H. Kramer. A comprehensive optogenetic pharmacology toolkit for in vivo control of gabaa receptors and synaptic inhibition. *Neuron*, 88(5):879–891, Dec 2015. 5

[85] John D. Loeser and Rolf-Detlef Treede. The kyoto protocol of iasp basic pain terminology. *Pain*, 137(3):473–477, Jul 2008. 17

[86] Stephen B. Long, Ernest B. Campbell, and Roderick Mackinnon. Voltage sensor of kv1.2: structural basis of electromechanical coupling. *Science*, 309(5736):903–908, Aug 2005. 15

[87] Stephen B. Long, Xiao Tao, Ernest B. Campbell, and Roderick MacKinnon. Atomic structure of a voltage-dependent k+ channel in a lipid membrane-like environment. *Nature*, 450(7168):376–382, Nov 2007. 15, 43, 74

[88] Ellen A. Lumpkin and Michael J. Caterina. Mechanisms of sensory transduction in the skin. *Nature*, 445(7130):858–865, Feb 2007. 19

[89] Lindsey J. Macpherson, Adrienne E. Dubin, Michael J. Evans, Felix Marr, Peter G. Schultz, Benjamin F. Cravatt, and Ardem Patapoutian. Noxious compounds activate trpa1 ion channels through covalent modification of cysteines. *Nature*, 445(7127):541–545, Feb 2007. 24

[90] Lindsey J. Macpherson, Bernhard H. Geierstanger, Veena Viswanath, Michael Bandell, Samer R. Eid, SunWook Hwang, and Ardem Patapoutian. The pungency of garlic: activation of trpa1 and trpv1 in response to allicin. *Curr Biol*, 15(10):929–934, May 2005. 24

[91] Lindsey J. Macpherson, Bailong Xiao, Kelvin Y. Kwan, Matt J. Petrus, Adrienne E. Dubin, SunWook Hwang, Benjamin Cravatt, David P. Corey, and Ardem Patapoutian. An ion channel essential for sensing chemical damage. *J Neurosci*, 27(42):11412–11415, Oct 2007. 24

[92] Peggy Mason. Placing pain on the sensory map: classic papers by ed perl and colleagues. *J Neurophysiol*, 97(3):1871–1873, Mar 2007. 17

[93] E. Matthew. Neuropeptides in dissociated cell cultures of mammalian spinal cord and dorsal root ganglion. *Int J Dev Neurosci*, 11(6):721–729, Dec 1993. 19

[94] Colleen R. McNamara, Josh Mandel-Brehm, Diana M. Bautista, Jan Siemens, Kari L. Deranian, Michael Zhao, Neil J. Hayward, Jayhong A. Chong, David Julius, Magdalene M. Moran, and Christopher M. Fanger. Trpa1 mediates formalin-induced pain. *Proc Natl Acad Sci U S A*, 104(33):13525–13530, Aug 2007. 24

[95] Aertsen A. Meier R., Boven KH. and Egert U., editors. *An open-source analysis toolbox for multiple-neuron recordings and network simulations*, volume Proc 7th German Neurosci Meeting, p.1212, 2007. 34

[96] Jason R. Meyers, Richard B. MacDonald, Anne Duggan, David Lenzi, David G. Standaert, Jeffrey T. Corwin, and David P. Corey. Lighting up the senses: Fm1-43 loading of sensory cells through nonselective ion channels. *J Neurosci*, 23(10):4054–4065, May 2003. 11, 58

[97] Aaron D. Mickle, Andrew J. Shepherd, and Durga P. Mohapatra. Sensory trp channels: the key transducers of nociception and pain. *Prog Mol Biol Transl Sci*, 131:73–118, 2015. 23, 24

[98] Kendall Mitchell, Brian D. Bates, Jason M. Keller, Matthew Lopez, Lindsey Scholl, Julia Navarro, Nicholas Madian, Gal Haspel, Michael I. Nemenov, and Michael J. Iadarola. Ablation of rat trpv1-expressing adelta/c-fibers with resiniferatoxin: analysis of withdrawal behaviors, recovery of function and molecular correlates. *Mol Pain*, 6:94, 2010. 54

[99] A. Molina, A. G. Castellano, and J. López-Barneo. Pore mutations in shaker k+ channels distinguish between the sites of tetraethylammonium blockade and c-type inactivation. *J Physiol*, 499 (Pt 2):361–367, Mar 1997. 16

[100] A. Molina, P. Ortega-Sáenz, and J. Lopez-Barneo. Pore mutations alter closing and opening kinetics in shaker k+ channels. *J Physiol*, 509 (Pt 2):327–337, Jun 1998. 16

[101] M Luisa Molina, Francisco N. Barrera, José A. Encinar, M Lourdes Renart, Asia M. Fernández, José A. Poveda, Jorge Santoro, Marta Bruix, Francisco Gavilanes, Gregorio Fernández-Ballester, José L. Neira, and José M. González-Ros. N-type inactivation of the potassium channel kcsa by the shaker b "ball" peptide: mapping the inactivating peptide-binding epitope. *J Biol Chem*, 283(26):18076–18085, Jun 2008. 15

[102] Craig Montell. The trp superfamily of cation channels. *Sci STKE*, 2005(272):re3, Feb 2005. 24

[103] Alexandre Mourot, Timm Fehrentz, and Richard H. Kramer. Photochromic potassium channel blockers: design and electrophysiological characterization. *Methods Mol Biol*, 995:89–105, 2013. 14, 16

[104] Alexandre Mourot, Timm Fehrentz, Yves Le Feuvre, Caleb M. Smith, Christian Herold, Deniz Dalkara, Frédéric Nagy, Dirk Trauner, and Richard H. Kramer. Rapid optical control of nociception with an ion-channel photoswitch. *Nat Methods*, 9(4):396–402, Apr 2012. 7, 8, 9, 10, 11, 12, 14, 16, 47, 68, 76, 77

[105] Alexandre Mourot, Michael A. Kienzler, Matthew R. Banghart, Timm Fehrentz, Florian M E. Huber, Marco Stein, Richard H. Kramer, and Dirk Trauner. Tuning photochromic ion channel blockers. *ACS Chem Neurosci*, 2(9):536–543, Sep 2011. 12, 13, 14

[106] Alexandre Mourot, Ivan Tochitsky, and Richard H. Kramer. Light at the end of the channel: optical manipulation of intrinsic neuronal excitability with chemical photoswitches. *Front Mol Neurosci*, 6:5, 2013. 6

[107] Hiroshi Nakagawa and Akio Hiura. Comparison of the transport of qx-314 through trpa1, trpm8, and trpv1 channels. *J Pain Res*, 6:223–230, 2013. 26

[108] John K. Neubert, Andrew J. Mannes, Laszlo J. Karai, Alan C. Jenkins, Lanel Zawatski, Mones Abu-Asab, and Michael J. Iadarola. Perineural resiniferatoxin selectively inhibits inflammatory hyperalgesia. *Mol Pain*, 4:3, 2008. 54

[109] Koichi Obata, Hirokazu Katsura, Toshiyuki Mizushima, Hiroki Yamanaka, Kimiko Kobayashi, Yi Dai, Tetsuo Fukuoka, Atsushi Tokunaga, Makoto Tominaga, and Koichi Noguchi. Trpa1 induced in sensory neurons contributes to cold hyperalgesia after inflammation and nerve injury. *J Clin Invest*, 115(9):2393–2401, Sep 2005. 25

[110] I. Omana-Zapata, M. A. Khabbaz, J. C. Hunter, and K. R. Bley. Qx-314 inhibits ectopic nerve activity associated with neuropathic pain. *Brain Res*, 771(2):228–237, Oct 1997. 12

[111] László Pecze, Péter Pelsoczi, Miklós Kecskés, Zoltán Winter, András Papp, Krisztián Kaszás, Tamás Letoha, Csaba Vizler, and Zoltán Oláh. Resiniferatoxin mediated ablation of trpv1+ neurons removes trpa1 as well. *Can J Neurol Sci*, 36(2):234–241, Mar 2009. 54

[112] Marie Pertin, Romain-Daniel Gosselin, and Isabelle Decosterd. The spared nerve injury model of neuropathic pain. *Methods Mol Biol*, 851:205–212, 2012. 26, 36, 49

[113] Aleksandra Polosukhina, Jeffrey Litt, Ivan Tochitsky, Joseph Nemargut, Yivgeny Sychev, Ivan De Kouchkovsky, Tracy Huang, Katharine Borges, Dirk Trauner, Russell N. Van Gelder, and Richard H. Kramer. Photochemical restoration of visual responses in blind mice. *Neuron*, 75(2):271–282, Jul 2012. 6, 7

[114] Steven A. Prescott, Qiufu Ma, and Yves De Koninck. Normal and abnormal coding of somatosensory stimuli causing pain. *Nat Neurosci*, 17(2):183–191, Feb 2014. 19, 21, 76

[115] Andreas Reiner and Ehud Y. Isacoff. The brain prize 2013: the optogenetics revolution. *Trends Neurosci*, 36(10):557–560, Oct 2013. 2

[116] Marcel Rigaud, Geza Gemes, Marie-Elizabeth Barabas, Donna I. Chernoff, Stephen E. Abram, Cheryl L. Stucky, and Quinn H. Hogan. Species and strain differences in rodent sciatic nerve anatomy: implications for studies of neuropathic pain. *Pain*, 136(1-2):188–201, May 2008. 20, 48, 49

[117] D. P. Roberson, A. M. Binshtok, F. Blasl, B. P. Bean, and C. J. Woolf. Targeting of sodium channel blockers into nociceptors to produce long-duration analgesia: a systematic study and review. *Br J Pharmacol*, 164(1):48–58, Sep 2011. 12

[118] David P. Roberson, Sagi Gudes, Jared M. Sprague, Haley A W. Patoski, Victoria K. Robson, Felix Blasl, Bo Duan, Seog Bae Oh, Bruce P. Bean, Qiufu Ma, Alexander M. Binshtok, and Clifford J. Woolf. Activity-dependent silencing reveals functionally distinct itch-generating sensory neurons. *Nat Neurosci*, 16(7):910–918, Jul 2013. 12

[119] Gabriela M. Rozanski, Hyunhee Kim, Qi Li, Fiona K. Wong, and Elise F. Stanley. Slow chemical transmission between dorsal root ganglion neuron somata. *Eur J Neurosci*, 36(10):3314–3321, Nov 2012. 21

[120] Gabriela M. Rozanski, Qi Li, and Elise F. Stanley. Transglial transmission at the dorsal root ganglion sandwich synapse: glial cell to postsynaptic neuron communication. *Eur J Neurosci*, 37(8):1221–1228, Apr 2013. 21

[121] Gabriela M. Rozanski, Arup R. Nath, Michael E. Adams, and Elise F. Stanley. Low voltage-activated calcium channels gate transmitter release at the dorsal root ganglion sandwich synapse. *J Physiol*, 591(Pt 22):5575–5583, Nov 2013. 21

[122] Ruth Ruscheweyh, Liesbeth Forsthuber, Doris Schoffnegger, and Jürgen Sandkühler. Modification of classical neurochemical markers in identified primary afferent neurons with abeta-, adelta-, and c-fibers after chronic constriction injury in mice. *J Comp Neurol*, 502(2):325–336, May 2007. 19

[123] P. Renaud S. Metz, M. Heuschkel, editor. *Microelectrodes with three-dimensional structures for improved neural interfacing.*, volume Proceedings of the 23rd Annual International Conference of the IEEE. Vol 1, 2001. 32

[124] Subhas Samanta, Andrew A. Beharry, Oleg Sadovski, Theresa M. McCormick, Amirhossein Babalhavaeji, Vince Tropepe, and G Andrew Woolley. Photoswitching azo compounds in vivo with red light. *J Am Chem Soc*, 135(26):9777–9784, Jul 2013. 12

[125] A. Scholz. Mechanisms of (local) anaesthetics on voltage-gated sodium and other ion channels. *Br J Anaesth*, 89(1):52–61, Jul 2002. 9

[126] T. J. Shi, T. Tandrup, E. Bergman, Z. Q. Xu, B. Ulfhake, and T. Hökfelt. Effect of peripheral nerve injury on dorsal root ganglion neurons in the c57 bl/6j mouse: marked changes both in cell numbers and neuropeptide expression. *Neuroscience*, 105(1):249–263, 2001. 20

[127] T-J S. Shi, J. Li, A. Dahlström, E. Theodorsson, S. Ceccatelli, I. Decosterd, T. Pedrazzini, and T. Hökfelt. Deletion of the neuropeptide y y1 receptor affects pain sensitivity, neuropeptide transport and expression, and dorsal root ganglion neuron numbers. *Neuroscience*, 140(1):293–304, Jun 2006. 19

[128] O. Sokolova, L. Kolmakova-Partensky, and N. Grigorieff. Three-dimensional structure of a voltage-gated potassium channel at 2.5 nm resolution. *Structure*, 9(3):215–220, Mar 2001. 15

[129] Marco Stein, Andreas Breit, Timm Fehrentz, Thomas Gudermann, and Dirk Trauner. Optical control of trpv1 channels. *Angew Chem Int Ed Engl*, 52(37):9845–9848, Sep 2013. 4

[130] Gina M. Story, Andrea M. Peier, Alison J. Reeve, Samer R. Eid, Johannes Mosbacher, Todd R. Hricik, Taryn J. Earley, Anne C. Hergarden, David A. Andersson, Sun Wook Hwang, Peter McIntyre, Tim Jegla, Stuart Bevan, and Ardem Patapoutian. Anktm1, a trp-like channel expressed in nociceptive neurons, is activated by cold temperatures. *Cell*, 112(6):819–829, Mar 2003. 24, 25

[131] G. R. Strichartz. The inhibition of sodium currents in myelinated nerve by quaternary derivatives of lidocaine. *J Gen Physiol*, 62(1):37–57, Jul 1973. 9

[132] Stephanie Szobota, Pau Gorostiza, Filippo Del Bene, Claire Wyart, Doris L. Fortin, Kathleen D. Kolstad, Orapim Tulyathan, Matthew Volgraf, Rika Numano, Holly L. Aaron, Ethan K. Scott, Richard H. Kramer, John Flannery, Herwig Baier, Dirk Trauner, and Ehud Y. Isacoff. Remote control of neuronal activity with a light-gated glutamate receptor. *Neuron*, 54(4):535–545, May 2007. 5

[133] B.J. Krishek T.G. Smart. *Neuromethods: Xenopus Oocyte Microinjection and Ion Channel Expression*. Humana Press, 1995. 40, 41

[134] D. B. Tikhonov. Mechanisms of action of ligands of potential-dependent sodium channels. *Neurosci Behav Physiol*, 38(5):461–469, Jun 2008. 16

[135] Ivan Tochitsky, Matthew R. Banghart, Alexandre Mourot, Jennifer Z. Yao, Benjamin Gaub, Richard H. Kramer, and Dirk Trauner. Optochemical control of genetically engineered neuronal nicotinic acetylcholine receptors. *Nat Chem*, 4(2):105–111, Feb 2012. 5

[136] Ivan Tochitsky, Aleksandra Polosukhina, Vadim E. Degtyar, Nicholas Gallerani, Caleb M. Smith, Aaron Friedman, Russell N. Van Gelder, Dirk Trauner, Daniela Kaufer, and Richard H. Kramer. Restoring visual function to blind mice with a photoswitch that exploits electrophysiological remodeling of retinal ganglion cells. *Neuron*, 81(4):800–813, Feb 2014. 7

[137] Francesco Tombola, Medha M. Pathak, and Ehud Y. Isacoff. How does voltage open an ion channel? *Annu Rev Cell Dev Biol*, 22:23–52, 2006. 14, 15

[138] H. Tsujino, E. Kondo, T. Fukuoka, Y. Dai, A. Tokunaga, K. Miki, K. Yonenobu, T. Ochi, and K. Noguchi. Activating transcription factor 3 (atf3) induction by axotomy in sensory and motoneurons: A novel neuronal marker of nerve injury. *Mol Cell Neurosci*, 15(2):170–182, Feb 2000. 26, 59

[139] Pierluigi Valente, Nuria García-Sanz, Ana Gomis, Asia Fernández-Carvajal, Gregorio Fernández-Ballester, Félix Viana, Carlos Belmonte, and Antonio Ferrer-Montiel. Identification of molecular determinants of channel gating in the transient receptor potential box of vanilloid receptor i. *FASEB J*, 22(9):3298–3309, Sep 2008. 23

[140] Nicholas A. Veldhuis, Michael J. Lew, Fe C. Abogadie, Daniel P. Poole, Ernest A. Jennings, Jason J. Ivanusic, Helge Eilers, Nigel W. Bunnett, and Peter McIntyre. N-glycosylation determines ionic permeability and desensitization of the trpv1 capsaicin receptor. *J Biol Chem*, 287(26):21765–21772, Jun 2012. 26

[141] C. Virginio, A. MacKenzie, F. A. Rassendren, R. A. North, and A. Surprenant. Pore dilation of neuronal p2x receptor channels. *Nat Neurosci*, 2(4):315–321, Apr 1999. 25

[142] Matthew Volgraf, Pau Gorostiza, Rika Numano, Richard H. Kramer, Ehud Y. Isacoff, and Dirk Trauner. Allosteric control of an ionotropic glutamate receptor with an optical switch. *Nat Chem Biol*, 2(1):47–52, Jan 2006. 5

[143] Josef Wachtveitl and Andreas Zumbusch. Azobenzene: an optical switch for in vivo experiments. *Chembiochem*, 12(8):1169–1170, May 2011. 2, 4

[144] Stephen G. Waxman and Gerald W. Zamponi. Regulating excitability of peripheral afferents: emerging ion channel targets. *Nat Neurosci*, 17(2):153–163, Feb 2014. 19

[145] Hermann A. Wegner. Azobenzenes in a new light-switching in vivo. *Angew Chem Int Ed Engl*, 51(20):4787–4788, May 2012. 12

[146] Hao-Jui Weng, Kush N. Patel, Nathaniel A. Jeske, Sonya M. Bierbower, Wangyuan Zou, Vinod Tiwari, Qin Zheng, Zongxiang Tang, Gary C H. Mo, Yan Wang, Yixun Geng, Jin Zhang, Yun Guan, Armen N. Akopian, and Xinzhong Dong. Tmem100 is a regulator of trpa1-trpv1 complex and contributes to persistent pain. *Neuron*, 85(4):833–846, Feb 2015. 54

[147] Andy D. Weyer and Cheryl L. Stucky. Loosening pain's grip by tightening trpv1-trpa1 interactions. *Neuron*, 85(4):661–663, Feb 2015. 54

[148] Toshio Yamagishi, Wei Xiong, Andre Kondratiev, Patricio Vélez, Ailsa Méndez-Fitzwilliam, Jeffrey R. Balser, Eduardo Marbán, and Gordon F. Tomaselli. Novel molecular determinants in the pore region of sodium channels regulate local anesthetic binding. *Mol Pharmacol*, 76(4):861–871, Oct 2009. 16

[149] Hossain Md Zakir, Rahman Md Mostafeezur, Akiko Suzuki, Suzuro Hitomi, Ikuko Suzuki, Takeyasu Maeda, Kenji Seo, Yoshiaki Yamada, Kensuke Yamamura, Shaya Lev, Alexander M. Binshtok, Koichi Iwata, and Junichi Kitagawa. Expression of trpv1 channels after nerve injury provides an essential delivery tool for neuropathic pain attenuation. *PLoS One*, 7(9):e44023, 2012. 9

[150] Yi Zhao, Cheng Zhou, Jin Liu, Peng Liang, Daqing Liao, Yanfang Chen, and Xiangdong Chen. The quaternary lidocaine derivative qx-314 produces long-lasting intravenous regional anesthesia in rats. *PLoS One*, 9(6):e99704, 2014. 12

[151] Katharina Zimmermann, Alexander Hein, Ulrich Hager, Jan Stefan Kaczmarek, Brian P. Turnquist, David E. Clapham, and Peter W. Reeh. Phenotyping sensory nerve endings in vitro in the mouse. *Nat Protoc*, 4(2):174–196, 2009. 30

[152] Sandra Zurborg, Brian Yurgionas, Julia A. Jira, Ombretta Caspani, and Paul A. Heppenstall. Direct activation of the ion channel trpa1 by ca2+. *Nat Neurosci*, 10(3):277–279, Mar 2007. 76

[153] Melissa Zwick, Brian M. Davis, C Jeffrey Woodbury, John N. Burkett, H Richard Koerber, James F. Simpson, and Kathryn M. Albers. Glial cell line-derived neurotrophic factor is a survival factor for isolectin b4-positive, but not vanilloid receptor 1-positive, neurons in the mouse. *J Neurosci*, 22(10):4057–4065, May 2002. 19